COMPUTATIONAL MODELING ON CONVECTIVE FLOW OF NANOFLUIDS THROUGH A HEATED PIPE

IMAN BEHROYAN

FACULTY OF ENGINEERING
UNIVERSITY OF MALAYA
KUALA LUMPUR

2016

University of Malaya

COMPUTATIONAL MODELING ON CONVECTIVE FLOW OF NANOFLUIDS THROUGH A HEATED PIPE

IMAN BEHROYAN

THESIS SUBMITTED IN FULFILMENT OF THE REQUIREMENTS FOR THE DEGREE OF DOCTOR OF PHILOSOPHY

FACULTY OF ENGINEERING
UNIVERSITY OF MALAYA
KUALA LUMPUR

2016

University of Malaya

UNIVERSITI MALAYA
ORIGINAL LITERARY WORK DECLARATION

Name of Candidate: Iman Behroyan

Registration/Matric No: KHA130064

Name of Degree: PhD of Mechanical Engineering
Title of Thesis:

COMPUTATIONAL MODELING ON CONVECTIVE FLOW OF NANOFLUIDS THROUGH A HEATED PIPE

Field of Study: Heat transfer/ Nanofluid/ Computational Fluid Dynamics

I do solemnly and sincerely declare that:

(1) I am the sole author of this Work;
(2) This Work is original;
(3) Any use of any work in which copyright exists was done by way of fair dealing and for permitted purposes and any excerpt or extract from, or reference to or reproduction of any copyright work has been disclosed expressly and sufficiently and the title of the Work and its authorship have been acknowledged in this Work;
(4) I do not have any actual knowledge nor ought I reasonably to know that the making of this work constitutes an infringement of any copyright work;
(5) I hereby assign all and every rights in the copyright to this Work to the University of Malaya ("UM"), who henceforth shall be owner of the copyright in this Work and that any reproduction or use in any form or by any means whatsoever is prohibited without the written consent of UM having been first had and obtained;
(6) I am fully aware that if in the course of making this Work I have infringed any copyright whether intentionally or otherwise, I may be subject to legal action or any other action as may be determined by UM.

Candidate's Signature Date

Subscribed and solemnly declared before,

Witness's Signature Date

Name:

University of Malaya

ABSTRACT

This study is focused on the CFD modeling of nanofluid heat transfer during convective flows. Depending on the measure of the wall heat flux, the convective flows are categorized in two general regimes of forced convection and convective flow boiling. The both regimes are numerically investigated in this study. The commercial Ansys-Fluent CFD codes are employed for this purpose.

In case of the forced convection heat transfer, the research is limited to laminar and turbulent internal flows. Depending on whether the nanofluid is assumed as a homogeneous single-phase liquid or a colloidal mixture of nanoparticles and the base liquid, the nanofluid flows are simulated by either single-phase or two-phase approaches. The different single-phase models (i.e. Newtonian and non-Newtonian) and two-phase models (i.e. Eulerian-Eulerian, mixture and Eulerian-Lagrangian) are used in this study to simulate nanofluid forced convection through a heated pipe. Different fluid rheology, effective conductivity models and effective viscosity models are used in the single-phase approach to achieve the most accurate prediction of nanofluid heat transfer. Interphase interactions such as interphase heat transfer, Brownian motion, drag force, lift force, virtual mass force, thermophoretic force and nanoparticle migration, which exist between the nanoparticles and the base fluid, are considered in the different two-phase models to achieve the most accurate prediction of nanofluid heat transfer.

In case of the convective flow boiling, the research is focused on subcooled flow boiling. The Eulerian-Eulerian two-phase model is used to simulate the nanofluids heat transfer during subcooled flow boiling through a vertical heated tube. The effects of the nucleate boiling parameters (i.e. nucleate site density, bubble frequency, and bubble departure diameter) and the bubble dynamics (i.e. interfacial area concentration of bubbles, non-drag forces and turbulence interaction resource) on the CFD model prediction of the boiling heat transfer coefficient (BHTC) are investigated. The effect of

University of Malaya

interphase interactions (i.e. interactions of the nanoparticles and the base liquid) and nonhomogeneous nanoparticles distribution on heat transfer predictions are also investigated. For this purpose, the Eulerian-Lagrangian CFD model is incorporated with the Eulerian-Eulerian model to track the thermal and hydrodynamic effects of the nanoparticles. The surface wettability improvement induced by the nanoparticles deposition is considered in the CFD model to find out how the heat transfer predictions are affected by such wettability improvement.

Several User Define Function (UDF) programming codes are created and incorporated to Ansys-Fluent CFD software to define the thermal conductivity, the dynamic viscosity, the thermal dispersion models, the non-Newtonian rheology, the nucleate site density and the bubble departure diameter for the nanofluids. The UDF codes are incorporated with the commercial CFD codes of Ansys-Fluent. All the simulation results are benchmarked against the experimental ones from the literature.

The single phase model and the Eulerian-Lagrangian two-phase model, overall, are the recommended models. The single-phase CFD model can predict the nanofluid heat transfer, if the nanofluid rheology and thermo-physical properties are determined accurately. The Eulerian-Lagrangian two-phase model no needs to determine nanofluid rheology and thermo-physical properties but it needs more computational effort than the single-phase model.

University of Malaya

ABSTRAK

Oleh kerana krisis tenaga seperti kekurangan minyak dan kenaikan harga sumber tenaga semula jadi, para penyelidik dalam bidang kecekapan tenaga cuba untuk mencari beberapa teknik untuk meningkatkan kecekapan pemindahan haba. Sejak, kebelakangan ini, penggantungan pepejal nanopartikel dalam cecair telah menunjukkan peningkatan ciri-ciri cecair termo-fizikal dan adalah penting bagi penyelidik untuk mengkaji kesan nanofluids terhadap peningkatan pemindahan haba. Ramalan tepat mengenai pemindahan haba nanofluid juga merupakan keperluan asas untuk operasi yang selamat dan reka bentuk optimum sistem terma.

Kajian ini memberi tumpuan kepada pemodelan CFD pemindahan haba nanofluid semasa aliran olakan. Bergantung kepada ukuran dinding fluks haba aliran olakan dikategorikan kepada dua rejim umum iaitu olakan paksa dan olakan aliran mendidih. Kajian secara berangka akan dikendalikan keatas kedua-dua rejim ini dan. Komersial Kod Ansys-Fluent CFD digunakan untuk tujuan ini.

Dalam kes pemindahan haba olakan paksa, kajian adalah terhad kepada laminar dan aliran dalaman bergelora. Bergantung kepada sama ada nanofluid itu diandaikan sebagai cecair fasa tunggal homogen atau campuran koloid nanopartikel dan cecair asas, aliran nanofluid disimulasikan mengikut pendekatan fasa tunggal atau dua fasa dua. Model-model yang berbeza iaitu fasa tunggal (Newtonian dan bukan Newtonian) dan fasa dua (Eulerian-Eulerian, campuran dan Eulerian-Lagrangian) digunakan dalam kajian ini untuk mensimulasikan nanofluid perolakan secara paksaan melalui paip yang dipanaskan. Reologi cecair yang berbeza, model kekonduksian berkesan dan model kelikatan berkesan digunakan dalam pendekatan fasa tunggal untuk mencapai ramalan yang paling tepat bagi pemindahan haba nanofluid. Interfasa interaksi seperti interfasa pemindahan haba, gerakan Brownian, daya seret, daya angkat, daya massa maya, daya thermophoretic dan penghijrahan nanopartikel, yang wujud antara partikel nano dan

University of Malaya

cecair asas, dipertimbangkan dalam model fasa dua yang berbeza untuk mencapai ramalan yang tepat bagi pemindahan haba nanofluid.

Dalam kes mendidihnya aliran olakan mendidih, kajian ini memberi tumpuan kepada aliran subcooled mendidih. The Eulerian-Eulerian model fasa dua digunakan untuk mensimulasikan pemindahan haba nanofluids semasa aliran subcooled mendidih melalui tiub yang dipanaskan secara menegak. Kesan parameter mendidih nukleus (iaitu ketumpatan nukleus laman web, kekerapan gelembung, dan diameter gelembung berlepas) dan dinamik gelembung (iaitu ketumpatan buih di antara permukaan, kuasa bukan drag dan sumber pergolakan interaksi) dengan menggunakan model ramalan CFD daripada pekali pemindahan haba didih (BHTC) akan disiasat. Kesan interaksi interfasa (iaitu interaksi nanopartikel dan cecair asas) dan taburan nanopartikel tak homogen terhadap ramalan pemindahan haba juga akan disiasat. Untuk tujuan ini, model Eulerian-Lagrangian CFD digabungkan dengan model Eulerian-Eulerian digunakan untuk mengesan kesan haba dan hidrodinamik nanopartikel. Peningkatan kebolehbasahan permukaan yang disebabkan oleh pemendapan nanopartikel itu akan dipertimbangkan dalam model CFD untuk mengetahui bagaimana ramalan pemindahan haba dipengaruhi oleh peningkatan kebolehbasahan tersebut.

Disebabkan beberapa model termo-sifat-sifat fizikal, cecair reologi dan parameter mendidih nukleus tidak dimuatkan dalam Kod Ansys-Fluent CFD, beberapa Kod Fungsi Tentuan Pengguna (UDF) ditulis untuk menentukan kekonduksian haba, kelikatan dinamik, model penyebaran haba, reologi bukan Newtonian, ketumpatan kawasan nukleus dan diameter berlepas gelembung untuk nanofluids. Kod UDF digabungkan dengan Kod CFD komersial Ansys-Fluent. Eksperimen daripada kesusasteraan digunakan sebagai tanda aras bagi semua keputusan simulasi.

University of Malaya

ACKNOWLEDGEMENTS

First and above all, I praise God, the almighty for providing me this opportunity and granting me the capability to proceed successfully. This thesis appears in its current form due to the assistance and guidance of several people. I would therefore like to offer my sincere thanks to all of them.

I would like to express my sincere gratitude to my supervisor, Dr. Poo Balan Ganesan for the continuous support of my Ph.D. study and related research, for his patience, motivation, and immense knowledge. His guidance helped me in all the time of research and writing of this thesis. I could not have imagined having a better supervisor for my Ph.D. study. I am deeply grateful to Dr. Sivanandam Sivasankaran (applied mathematics department, University of Malaya) for his supports, encouragements and guidance during this project. I would like also to thank Prof. Shuisheng He (Mechanical engineering department, University of Sheffield) for reading my thesis and commenting on my views.

I gratefully acknowledge the funding received towards my PhD from Exploratory Research Grant Scheme (ERGS: ER013-2013A) and Ministry of Higher Education High Impact Research (UM.C/HIR/MOHE/ENG/20). I am also grateful to the staff of Mechanical Department at University of Malaya, for their various forms of support during my study.

A special thanks to my family. Words cannot express how grateful I am to my parents for all of the sacrifices that you've made on my behalf. Your prayer for me was what sustained me thus far. I would also like to thank all of my friends.

At the end I would like express appreciation to my beloved wife, Pooyeh, who spent sleepless nights with and was always my support in the moments when there was no one to answer my queries.

University of Malaya

TABLE OF CONTENTS

University of Malaya

University of Malaya

University of Malaya

University of Malaya

University of Malaya

LIST OF FIGURES

University of Malaya

University of Malaya

LIST OF TABLES

University of Malaya

University of Malaya

LIST OF SYMBOLS

Roman Symbols

a: Acceleration,$(\mathrm{m/s2})$

$a_{if:}$ Interfacial area concentration *(m^{-1})*

A_b: Bubble area *(m^2)*

A_q: Quenching area of heat transfer *(m^2)*

Bo: Boiling number

$\mathrm{C_C}$: Cunningham correction

$\mathrm{C_D}$: Drag coefficient

C_L: Lift coefficient

$\mathrm{C_p}$: Specific heat capacity at constant pressure,$(\mathrm{J/kg.\,K})$

d_b: Bubble mean diameter,(m)

d_{db}: Bubble departure diameter,(m)

$\mathrm{d_p}$: Nanoparticle diameter,(m)

D_{bd}: Bubble departure diameter,(m)

f: Bubble departure frequency,(Hz)

f: Drag friction factor

$\mathrm{F_B}$: Brownian force,(N)

$\mathrm{F_d}$: Drag force,(N)

$\mathrm{F_L}$: Lift force,(N)

F_{lg}: Action of interfacial forces from vapour on liquid,(N)

F_{lg}: Action of interfacial forces from liquid on vapour,(N)

$\mathrm{F_{Lub}}$: Lubrication force,(N)

$\mathrm{F_T}$: Thermophoreticforce,(N)

$\mathrm{F_{turb}}$: Turbulent dispersion force,(N)

$\mathrm{F_{vm}}$: Virtual mass force,(N)

G: Mass flux,$(kg\ /m^2\ s)$

g: Gravitational acceleration,$(\mathrm{m/s2})$

University of Malaya

h: Heat transfer coefficient,(w/m^2k)

h_{fg}: Latent heat of vaporization,(J/kg)

H: Enthalpy,(J/kg)

Ja: Jakob number

k: Thermal conductivity,$(W/m\ K)$

k: Turbulent kinetic energy,(m^2/s^2)

k_d: Dispersed thermal conductivity,$(W/m\ K)$

k_B: Boltzmann constant

Kn: Knudsen number

k_t: Turbulent conductivity,$(W/m\ K)$

m_p: Mass of a single nanoparticle (kg)

N_a: Active nucleation site density, (m^{-2})

Nu: Nusselt number,$(Nu = hD/k)$

Nu_p: Particle Nusselt number

p: Static pressure, (N/m^2)

Pr: Prandtl number

Pr_t: Turbulent Prandtl number

Q: Interphase heat transfer (w/m^2)

q'': Heat flux (w/m^2)

q_c: Heat transfer due to forced convection, (W/m^2)

q_e: Heat transfer due to evaporation, (W/m^2)

q_q: Quenching heat transfer, (W/m^2)

R: Tube radius,(m)

Re: Reynolds number,$Re = \frac{\rho V_0 D}{\mu}$

Re_{np}: Nanoparticle Reynolds number

S_{bk}: Breakup source term of interfacial area transfer (IAT) equation

S_{CO}: Coalescence source term of interfacial area transfer (IAT) equation

University of Malaya

S_e: Sink/source term of energy equation

S_m: Sink/source term of momentum equation

S_{ph}: Nucleation source term of interfacial area transfer (IAT) equation

S^k, S^ε: Sink/source term of k-ε equation

St: Stanton number

T: Temperature,(K)

T′: Temperature perturbation,(K)

T_{sat}: Saturated temperature,(K)

T_{sub}: Subcooled temperature,(K)

T_{sup}: Superheat temperature,(K)

T_w: Wall temperature,(K)

V: Velocity,(m/s)

V_B: Brownian velocity,(m/s)

V′: Velocity perturbation,(m/s)

$V_{dr,k}$: Drift velocity,(m/s)

V_{rel}: Nanoparticle and base fluid relative velocity,(m/s)

$\vec{\omega}$: Vorticity vector,(rad/s)

x, y: 2-D axisymmetric coordinates,(m)

X: Flow quality

Greek Symbols

α_g, α_l: Vapour or liquid volume fraction

σ: Surface tension,(N/m)

ε: Dissipation rate of turbulence kinetic energy,(m^2/s^3)

μ: Dynamic viscosity,$(kg/m\ s)$

μ_b: Bubble induced viscosity,$(kg/m\ s)$

μ_t: Turbulent viscosity,$(kg/m\ s)$

ρ: Density,(kg/m^3)

University of Malaya

Γ_{lg}: Interfacial mass transfer from vapour to liquid ($kg/m^3\ s$)

Γ_{gl}: Interfacial mass transfer from liquid to vapour ($kg/m^3\ s$)

λ: Molecular mean free path

θ: Droplet or vapour bubble contact angle

φ / ∅: Particle volume fraction

τ: Shear stress,(N/m^2)

δV: Cell volume,(m^3)

γ̇: Axisymmetric rate of deformation tensor

Subscripts

b: Bulk

bf: Base fluid

d: Dispersion

e /eff: Effective

f: Fluid

FC: Forced convection

g: Vapour

l: Liquid

NB: Nucleate boiling

NP: Nanoparticle

p: Particle phase

l: Liquid phase

m : Mixture

t : Turbulent

University of Malaya

1 CHAPTER 1: INTRODUCTION

1.1 Research background

Advances in thermal science and technology are continually focusing on heat exchangers optimization to enhance the heat transfer rate and minimize the surface of heat transfer simultaneously. Many studies (Edel & Mukherjee, 2011; Kandlikar, 2003; Qu & Mudawar, 2003; Siddique et al., 2010; Zhuan & Wang, 2012; Zu et al., 2011) have been done on the heat transfer enhancement by some passive methods, such as inserting extra components, swirl flow devices, treated surface, rough surfaces, extended surfaces, displaced enhancement devices, coiled tubes, surface tension devices and additives for fluids (S. Liu & Sakr, 2013).

In addition, improvement of thermal transport properties of heating fluids has been found to enhance the efficiency of heat exchangers, shrink the size of the systems and reduce the operational cost. Recently, suspension of the solid particles among the fluid has been shown to enhance thermal conductivity of the fluid. At first, suspending the mini and micro solid particles in fluids were offered. Although these particles improved the heat transfer characteristics of conventional fluids, some of problems, such as high pressure drop and instability of the particles, appeared due to the large size of the particles. The particles in the size of nano-meter have solved the problem of stability and sedimentation on one hand and have increased the heat transfer efficiency on the other. Nanofluids contain particles with dimensions smaller than 100 nm and are suspended in a base fluid, such as water, ethylene glycol, etc. The term nanofluid was for the first time used by Choi (1995) for such a suspension. It has been reported in a number of studies (E Abu-Nada et al., 2008; Roy et al., 2004; Xuan & Roetzel, 2000) that the dispersion of the solid nanoparticles in a base fluid significantly changes the thermo-physical properties of conventional fluids. Because the nanoparticles are so fine, gravity becomes less important and thus chances of sedimentation are also less, making

University of Malaya

nanofluids more stable. Nanofluids have been considered in many engineering applications, e.g., solar collectors (Allahyari et al., 2011), engine systems (Kakaç & Pramuanjaroenkij, 2009), micromechanics and instrumentation systems (Murshed et al., 2008). Since such suspension of nanoparticles in liquids has shown an improvement of the liquids thermo-physical–properties, it is important to further improve our understanding of heat transfer and fluid flow behaviour of nanofluids.

Accurate prediction of the nanofluid heat transfer is a fundamental requirement for safe operation and optimal design of thermal systems. In this study, the CFD modeling of nanofluid heat transfer is carried out for convective flows. Depending on the measure of the wall heat flux or the wall temperature, the convective flows are categorized in two general regimes of forced convection and convective flow boiling. The convective flow is known as forced convection as long as the temperature of the wall is lower than the saturation temperature. Increasing the wall heat flux, the temperature of the wall also increases. Once the wall temperature is higher than the saturation temperature, the convective flow boiling is happened (Cheung et al., 2014). The both regimes are numerically investigated in this study. Selection of these regimes covers a wide spectrum of heat exchangers with different values of heat flux. The forced convection heat transfer is a common case in heat exchangers with a low heat flux and without any phase-changes of working liquid, whereas the subcooled flow boiling is usually happened in heat exchangers with a high density heat flux and with a phase-change of the liquid to the vapour. Theses regimes are also important because of their significant potential in various empirical applications such as solar collectors, boilers and nuclear reactors (Allahyari et al., 2011). In case of the forced convection, the CFD modeling of nanofluid heat transfer is limited to the laminar and the turbulent internal flows. Regarding the convective flow boiling, this study is focused on the subcooled flow boiling where the wall and fluid bulk temperatures are higher and lower than the

University of Malaya

saturation temperature respectively. Depending on whether the nanofluid is assumed as a homogeneous single-phase liquid or a colloidal mixture of nanoparticles and the base liquid, the nanofluid flows can be simulated by either single-phase or multi-phase approaches . The CFD modeling is done based on the both approaches within this study. Once the models are validated, this can be beneficial as a reference for the selection of the proper CFD model in the similar cases for future studies or industrial research and development. One of the main aims of this study is the CFD model verification for the prediction of nanofluids convective heat transfer. Since the accuracy of the models' prediction is so dependent on the proper selection of thermo-physical properties of the nanofluids, two types of widely used nanofluids in literature, Al_2O_3/water and Cu/water, are selected for this study. This is beneficial not only for easily selecting the nanofluids thermo-physical properties but also for making more comparisons with the findings of the other studies.

1.2 Problem Statement

The use of nanofluids for heat transfer enhancement is a promising area for many researchers. In addition, accurate prediction of the nanofluid heat transfer is a fundamental requirement for safe operation and optimal design of thermal systems. Hence, this study is focused on heat transfer prediction of nanofluid flows during forced convection and subcooled boiling regimes. There are many CFD models to predict nanofluid heat transfer during forced convection regime. However, it is still unclear which models are able to predict the nanofluid heat transfer precisely. There are few numerical studies to model the heat transfer of nanofluid during subcooled flow boiling and conflicting results are found in the literature about boiling heat transfer enhancements and/or deteriorations of nanofluids. Boiling heat transfer by using nanofluid has not been fully understood yet. Further research has to be done in this field to improve our understanding of heat transfer of nanofluids. So, this study is focused on

University of Malaya

the numerical investigation of the nanofluids heat transfer for both forced convection and subcooled flow boiling in a heated pipe.

1.3 Research Objectives

The specific objectives of this research project are:

- To model and simulate the laminar flow of nanofluid through a heated pipe using the single-phase model and two-phase models of Eulerian-Eulerian (E-E), mixture and Eulerian-Lagrangian (E-L) models.
- To model and simulate the turbulent flow of nanofluid through a heated pipe using the single-phase model and two-phase models of Eulerian-Eulerian (E-E), mixture and Eulerian-Lagrangian (E-L) models; A correlation is also developed to describe the effective nanoparticle thermal conductivity of the nanoparticles to improve the heat transfer prediction of the E-E model.
- To model and simulate the nanofluid subcooled flow boiling through a heated pipe using the Eulerian-Eulerian two-phase model and the three-phase model (i.e. E-E model plus E-L model).

1.4 Scopes and Limitations

The scope of this study is limited to modeling of the nanofluid heat transfer during forced convection and subcooled flow boiling. Selection of these regimes covers a wide spectrum of heat exchangers with different values of heat flux. The forced convection heat transfer is a common case in heat exchangers with a low heat flux and without any phase-changes of working liquid, whereas the subcooled flow boiling is usually happened in heat exchangers with a high density heat flux and with a phase-change of the liquid to the vapour. Theses regimes are also important because of their significant potential in various empirical applications such as solar collectors, boilers and nuclear reactors. This study is a methodological work for the verification of a number of single- and multiphase CFD approaches in prediction of nanofluid heat

University of Malaya

transfer. Once a wide range of models are developed and validated, this can be beneficial as a reference for the selection of the proper CFD model in the similar cases. The turbulent model is limited to the commonly used *k-ε* model. The evaluation of different turbulent models is outside the scope of this thesis, and the reader is referred to the original publications. Horizontal and vertical tubes with internal diameters ranging from 4.5 to 15.4 mm have been considered in this study. The tubes are modeled as a two-dimensional (2D) axisymmetric geometry. This simplification is reasonable because the boundary condition around the pipe's centerline is thermally and hydro-dynamically symmetric. The effect of wall thickness is considered just for subcooled flow boiling. One of the main aims of this study is the CFD model verification for the prediction of nanofluids convective heat transfer. Since the accuracy of the models' prediction is so dependent on the proper selection of thermo-physical properties of the nanofluids, two types of widely used nanofluids in the literature, Al_2O_3/water and Cu/water, are selected for this study. This is beneficial not only for easily selecting the nanofluids thermo-physical properties but also for making more comparisons with the findings of the other studies. The Reynolds number differs from 745-1,600 and 10,000-25,000 for laminar and turbulent flow respectively. The inlet mass flux of 1,400-2,500 (kg/m^2s), inlet subcooled temperature of 10-20 (^oK) and wall heat flux of 50-110 (KW/m^2) are selected for subcooled flow boiling investigation. The nanoparticle volume fractions differ from 0% to 2%.

1.5 Thesis Outline

This thesis is composed of 6 chapters.

CHAPTER 1: INTRODUCTION.

CHAPTER 2: LITERATURE REVIEW. The background studies carried out in this research are presented, along with a review of previous work that is closely related to forced convection and subcooled flow boiling heat transfer of nanofluids.

University of Malaya

CHAPTER 3: MODELLING ON LAMINAR FORCED CONVECTION OF NANOFLUID. A comprehensive comparison of CFD analysis among various modelling approaches is presented in this chapter to investigate a laminar forced convection flow of Al_2O_3/water nanofluid in a heated tube. The results are benchmarked against the experimental data from literature. The deviation in Nusselt number is reported for each and every model which gives insight to strengths and weaknesses of each approach. The repeatability and the consistency of some of the most accurate CFD models are checked for other nanoparticle volume fractions and Reynolds numbers.

CHAPTER 4: MODELLING ON TURBULENT FORCED CONVECTION OF NANOFLUID. CFD analysis of various modeling approaches is presented in this chapter to investigate the turbulent forced convection flow of Cu-water nanofluid in a heated tube. The CFD results are benchmarked against the experimental investigations from literature for the same testing fluid and conditions. The deviation in Nusselt number is reported for each and every model which gives insight to strengths and weaknesses of each approach. This study is beneficial for selecting a suitable CFD model for modelling and simulation a similar type case study. Further investigations are also done to probe the accuracy improvement of the Eulerian two-phase CFD model in the prediction of the nanofluid heat transfer.

CHAPTER 5: MODELLING ON SUBCOOLED FLOW BOILING OF NANOFLUIDS. The subcooled flow boiling of two types of nanofluids (i.e. Al2O3/water and Cu/water nanofluids) in a vertical heated pipe is numerically investigated. For this purpose, the Eulerian-Eulerian (E-E) two-phase CFD model is used. Initially, for a strong validity of the CFD model, water subcooled flow boiling is modeled under different nucleate boiling parameters (i.e. nucleate site density, bubble frequency, and bubble departure diameter), boundary conditions (i.e. fluid mass flux,

University of Malaya

inlet subcooled temperature and wall heat flux) and bubble dynamic mechanisms (i.e. non-drag forces, turbulence interaction resource and interfacial area concentration). The predicted heat transfer coefficients are benchmarked against the experimental investigations from the literature. According to the findings of the validation tests, the most accurate combination of the boiling properties is used in the E-E approach to model the nanofluids subcooled flow boiling. The effect of interphase interactions (i.e. interactions of the nanoparticles and the base liquid) on heat transfer predictions is also investigated. For this purpose, the Eulerian-Lagrangian CFD model is incorporated with the E-E model. The surface wettability improvement induced by the nanoparticles deposition is considered in the CFD model to find out how the heat transfer predictions are affected by such wettability improvement.

CHAPTER 6: CONCLUSION AND FUTURE WORK. The conclusion and the contributions of this study are given in this chapter. Some recommendations are suggested for future studies.

University of Malaya

2 CHAPTER 2: LITERATURE REVIEW

2.1 Nanofluid Thermo-physical Properties

2.1.1 Effective Thermal Conductivity Models

A lot of models have been developed for prediction of effective thermal conductivity since the model that is offered by Maxwell (1881) for spherical particles at the first time. Among the all models, roughly most of them can be categorized in two general groups which are static and dynamic models. The former suppose the stationary nanoparticles in the base fluid and the thermal conductivity is calculated based on Maxwell correlation or its improvement whereas the latter are based on considering the random motion of nanoparticles known as Brownian motion. In this way the particle motion is considered to be in charge of heat transfer enhancement. In addition, a micro-convection effect, which is due to the fluid mixing around nanoparticles (thermal dispersion mechanism), is also proposed to be important (Mokmeli & Saffar-Avval, 2010; Xuan & Roetzel, 2000).

The classical static models such as those recommended by Maxwell (1881),and Hamilton and Crosser (1962), took into account the effective thermal conductivity of nanofluids based on a static continuum fluid in which the well-dispersed solid nanoparticles have been suspended. According to this assumption, thermal conductivity of nanofluids depends only on particle volume fraction, particle material, particle size, particle shape, base fluid material, and temperature (Özerinç et al., 2010).The Maxwell model was offered to calculate the effective thermal conductivity of liquids with low volumetric and spherical suspended solid particles.

$$k_{eff} = \frac{k_p + 2k_f + 2(k_p - k_f)\phi}{k_p + 2k_f - (k_p - k_f)\phi} k_f \tag{2.1}$$

where k_{eff}, k_p, and k_f are the thermal conductivity of the nanofluid, nanoparticles and base fluid, respectively. ϕ is the volume fraction of particles in the mixture. This model

University of Malaya

is applicable to statistically homogeneous and low volume fraction liquid–solid suspensions with randomly dispersed and uniformly sized spherical particles. The Maxwell model was modified by Hamilton and Crosser (1962) to consider the effect of particles shape on thermal conductivity.

$$k_{eff} = [\frac{k_p + (n-1)k_f - (n-1)(k_f - k_p)\phi}{k_p + (n-1)k_f + (k_f - k_p)\phi}].k_p \quad (2.2)$$

where n is the empirical shape factor given by:

$$n = \frac{3}{\psi},$$

where ψ is the particle sphericity defined as the ratio of the surface area of a sphere (with the same volume as the given particle) to the surface area of the particle. Based on experimental research, there is acceptable coincidence between the theoretical results and the experimental data captured for special particles in the range of volume fractions about 30%. As the size of particles is very small (~ 100 nm) in one hand and a so fine particle can be assumed as a sphere on the other, one can conclude the sphericity of nanoparticles equal to 3. For spherical particles, the Hamilton and Crosser (HC) model simplifies to the Maxwell model. These classical models are found to be unreliable in thermal conductivity prediction because of neglecting the effects of particle size, interfacial layer at the particle /liquid interface, clustering effect and Brownian motion of nanoparticles (Eastman et al., 2004; Jang & Choi, 2004; Keblinski et al., 2002; Wang et al., 1999; Xue, 2003; Yu & Choi, 2003).

It was reported by the experimental studies that the thermal conductivity of nanofluids increases with decreasing the size of nanoparticles. This trend is theoretically justified by two mechanisms having a crucial role in nanofluid thermal conductivity enhancement: Brownian motion of nanoparticles and liquid layering around nanoparticles (Özerinç et al., 2010). Due to the dependence of thermal conductivity of base liquid and solid particles on temperature, thermal conductivity of nanofluid

University of Malaya

depends on temperature. This is a rule that has already been considered for suspension of conventional solid particles (i.e. milli-particles or micro-particles) in liquids. However, in case of nanofluids, change of temperature also affects the Brownian motion of nanoparticles and clustering of nanoparticles which change the thermal conductivity of nanofluids (Calvin H Li et al., 2008). Koo and Kleinstreuer (2004) considered the thermal conductivity of nanofluids to be composed of two parts:

$$k_{eff} = k_{static} + k_{Brownian} \tag{2.3}$$

where k_{static} represents the thermal conductivity enhancement due to the higher thermal conductivity of the nanoparticles and $k_{Brownian}$ takes the effect of Brownian motion into account. For the static part, the classical Maxwell model was proposed while for $k_{Brownian}$ Brownian motion of particles was considered. As a result, the following expression was proposed:

$$k_{Brownian} = 5\times10^4 \beta\phi\rho_f c_{p,f} \sqrt{\frac{k_B T}{\rho_p d_p}}\, f \tag{2.4}$$

where ρ_f and k_B are the density of base fluid and Boltzmann constant, respectively, and T the temperature in k. $C_{p,f}$ is specific heat capacity of base fluid. In the analysis, the interactions between nanoparticles and fluid volumes moving around them were not considered and an additional term, β, was introduced in order to take that effect into account. Koo and Kleinstreuer (2004) indicated that this term becomes more effective with increasing volume fraction. Another parameter, f, was introduced to the model in order to increase the temperature dependency of the model. Both f and b were determined by utilizing available experimental data. Chon et al. (2005) investigated the thermal conductivity of Al_2O_3/water nanofluid experimentally for different sizes of the Al_2O_3 nanoparticle at different temperatures. It was reported that thermal conductivity increases with increasing temperature and decreasing particle size. Dependence on temperature becomes more pronounced at higher temperatures. Based on the

University of Malaya

experimental results, a correlation for calculation of the thermal conductivity of the nanofluid was suggested as follows:

$$k_{eff} / k_{bf} = 1 + 64.7(\phi)^{0.7460} \left(\frac{d_{bf}}{d_p} \right)^{0.3690} \left(\frac{k_{bf}}{k_p} \right)^{0.7476} Pr^{0.9955} Re_{np}^{1.2321} \quad (2.5)$$

where Re_{np} is nanoparticle Reynolds number based on Brownian motion of nanoparticles and it is given by

$$Re_{np} = \frac{\rho_{bf} K_B T}{3\pi \mu_{bf}^{2} \lambda} \quad (2.6)$$

where $\lambda = 0.17$ nm is the mean free path of water, K_B is the Boltzmann constant (1.3807 × 10-23 J/K) and μ_{bf} is the viscosity of water. Patel et al. (2006) investigated the Brownian motion (micro-convection) effect on thermal enhancement of nanofluids and presented a correlation for determination of nanofluids thermal conductivity based on the experimental data from literature as follows:

$$\frac{k_{eff}}{k_f} = 1 + \left(\frac{k_s A_p}{k_f A_f}\right)(1 + c.Pe) \quad (2.7)$$

where $\frac{A_p}{A_f} = \frac{d_f}{d_p} \frac{\phi}{(1-\phi)}$, $Pe = \frac{u_b d_p}{\alpha_f}$ and c =25,000. α_f is the thermal diffusivity of base fluid. u_b indicates the Brownian motion velocity of the nanoparticles which is given by

$$u_b = \frac{2k_b T}{\pi \mu_f d_p^{2}} \quad (2.8)$$

Some researchers have claimed that the use of temperature-dependent properties of nanofluid, especially the temperature-dependent model of thermal conductivity, in computational studies can result in more precise results (Namburu et al., 2009; Palm et al., 2006; Putra et al., 2003). The temperature-dependent conductivity based on experimental correlations of Putra et al. (2003) were employed by Palm et al. (2006) and Namburu et al. (2009). Finally, it was concluded that accounting temperature in

University of Malaya

relations for nanofluids properties led to more accurate prediction of heat transfer performance. However, contradictory results, which propose that Brownian motion is not very effective in thermal conductivity enhancement, are reported by Evans et al. (2006). It was theoretically shown that the thermal conductivity enhancement due to Brownian motion is a very small fraction of the thermal conductivity of the base fluid. This fact was also verified by molecular dynamics simulations. As a result, it was concluded that Brownian motion of nanoparticles could not be the main cause of high thermal conductivity enhancement with nanofluids.

Li and Peterson (2007) investigated the mixing effect of nanoparticles (nanoparticles dispersion) due to the Brownian motion of nanoparticles on the effective thermal conductivity of nanofluids numerically. Velocity, pressure, and temperature distribution around the nanoparticles were investigated for a single nanoparticle, for two nanoparticles, and for numerous nanoparticles. It was seen that improvement in thermal conduction capability of the nanofluid was induced by nanoparticles. As a result, it was concluded that the mixing effect created by the Brownian motion of the nanoparticles is an important reason of the large thermal conductivity enhancement of nanofluids (Özerinç et al., 2010). For mathematical modeling of dispersion phenomena, it is assumed that the irregular motion of nanoparticles with respect to the base fluid induces small perturbations of both temperature and velocity of the nanofluid. Thermal dispersion conductivity is defined to consider such temperature and velocity perturbations in nanoparticle conductivity enhancement. The thermal dispersion conductivity is added as a separate term to effective nanoparticle conductivity as follows:

$$k_{eff} = k_{nf} + k_d \tag{2.9}$$

where k_d is the dispersed thermal conductivity. There are various experimental and theoretical formulas for the dispersion thermal conductivity suggested by researchers

University of Malaya

(Mojarrad et al., 2013; Mokmeli & Saffar-Avval, 2010; Xuan & Li, 2000; Xuan & Roetzel, 2000). Xuan and Roetzel (2000) suggested two kinds of correlation to calculate thermal dispersion model are given as below:

$$k_d = C\left(\rho C_P\right)_{nf} Ru \tag{2.10}$$

$$k_d = C\left(\rho C_P\right)_{nf} Rud_p \tag{2.11}$$

where C is an unknown constant that should be calculated by matching the experimental data, R is the tube radius and u is local flow velocity. Equation (2.10) seems to be unreliable because it does not contain the main parameters of nanofluid namely volume fraction and nanoparticle size. The other weak point of the equation is that its two sides are not dimensionally compatible (Mokmeli & Saffar-Avval, 2010). Mokmeli and Saffar-Avval (2010) introduced a correlation to calculate the dispersed thermal conductivity in radial direction based on gradient of nanofluid axial velocity as below:

$$k_d = C_d\left(\rho C_P\right)_{nf} \frac{R\phi}{d_p}\left(\frac{\partial u_x}{\partial y}\right) \tag{2.12}$$

A correlation for the determination of radial dispersed thermal conductivity is suggested by Mojarrad et al.(2013) as:

$$k_d = C\left(\rho C_P\right)_{nf} \frac{R\phi}{d_p}\left(\frac{\partial T}{\partial y}\right) \tag{2.13}$$

This equation consists of the most important parameters on the thermal conductivity such as volume fraction of nanofluids, heat capacity of nanofluids, tube radius, particle diameter and temperature gradient in radial direction. It should be noted that the velocity field which influences the temperature gradient is also taken into account indirectly (Mojarrad et al., 2013).

University of Malaya

2.1.2 Effective Viscosity

Viscosity as one of the inherent properties of fluid effects on heat transfer phenomena significantly. The effective viscosity of nanofluids is claimed to be sensitive to temperature, base fluid material, nanoparticle size and concentration as reported by studies (Sarit K Das et al., 2003; Ding et al., 2006; Mooney, 1951; Tavman et al., 2008; Turgut et al., 2009; Wang et al., 1999). The effective viscosity increases by increasing particles concentration while it decreases with an increase in temperature. The effective dynamic viscosity of the nanofluid also increases as the size of nanoparticles decreases.

Some correlations, such as those suggested by Einstein (1956), Brinkman (1952), Lundgren (1972) and Batchelor (1977), have been originally developed for predicting the dynamic viscosity of the conventional colloid dispersions. The equations underestimate the actual values of the dynamic viscosity of nanofluids. This deviation is pronounced with decreasing the nanoparticle diameter and increasing the nanoparticle concentration.

According to Wang et al. (1999), a 20 to 30% increase in viscosity of water was observed when 3% volume fraction of γ-Al_2O_3 nanoparticles was added to water. Maiga et al. (2004) suggested a correlation based on the experimental results of Wang et al. (1999) as follows:

$$\mu_{nf} = (1 + 7.3\phi + 123\phi^2)\mu_f \tag{2.14}$$

The viscosities of the dispersed fluids with γ-Al_2O_3 and TiO_2 particles were measured by Pak and Cho (1998) at a 10% volume fraction of particles. The results showed roughly a three times higher viscosity than that of water. According to the results, a correlation was purposed as

$$\mu_{nf} = (1 + 39.11\phi + 533.9\phi^2)\mu_f \tag{2.15}$$

University of Malaya

A correlation for calculation of nanofluids dynamic viscosity is purposed by Corcione et al. (Corcione, 2011; Corcione et al., 2012) based on a wide range of experimental data from the literature.

$$\frac{\mu_{nf}}{\mu_f} = \frac{1}{1-34.87\left(d_p / d_f\right)^{-0.3}\phi^{1.03}} \tag{2.16}$$

where d_f is the equivalent diameter of a base fluid molecule, given by

$$d_f = 0.1\left(\frac{6M}{N\pi\rho_{f0}}\right)^{1/3} \tag{2.17}$$

In which, M is the molecular weight of the base fluid, N is the Avogadro number, and ρ_{f0} is the mass density of the base fluid calculated at temperature T_0 = 293 K. Although the size of nanoparticle is considered by the correlation, the correlation is not valid at far from room temperature. The experimentally measured nanofluid viscosity deviates from the classical models, which consider viscosity as a function of volume concentration only, and there is no consideration of temperature dependence (P. Namburu et al., 2007). For example, Zhu and Wang (2009) measured the viscosity of cu-water nanofluid by using capillary viscometers. They found that the temperature is the main factor influencing the viscosity of the cu-water nanofluid. Recently, the new model of effective viscosity by considering the Brownian motion was offered by Masoumi et al. (2009):

$$\mu_{nf} = \mu_f + \frac{\rho_p V_B d_p^2}{72C\delta} \tag{2.18}$$

where V_B , δ and C are Brownian velocity, distance between the nanoparticles and correction factor respectively. In addition V_B , C and δ are defined as follows:

$$C = \mu_{bf}^{-1}[(c_1 d_p + c_2)\varphi + (c_3 d_p + c_4)] \tag{2.19}$$

$$c_1 = -0.000001133,\ c_2 = -0.000002771$$
$$c_3 = 0.00000009,\quad c_4 = -0.000000393$$

University of Malaya

$$V_B = \frac{1}{d_p}\sqrt{\frac{18k_BT}{\pi\rho_p d_p}} \quad (2.20)$$

$$\delta = \sqrt[3]{\frac{\pi}{6\phi}}d_p \quad (2.21)$$

where k_B represents Boltzmann constant. The nanofluid viscosity is predicted by this model as a function of temperature, mean particle diameter, particle volume fraction, density of particle and the base fluid physical properties.

After adding the nanoparticles to fluid, depending on the particles volume fraction, temperature and methods of particle suspension, the Newtonian or non-Newtonian behaviors are appeared by the fluid (Sarit K Das et al., 2003; Ding et al., 2006; Kulkarni et al., 2006; P. Namburu et al., 2007). Das et al. (2008) showed the increase of viscosity with particles volume fraction. In addition to this, they found that after particles addition the fluid keeps its typical Newtonian nature. Similarly, Namburu et al. (2009) found that ethylene glycol and water mixture loaded by nano Sio_2 particles show the non-Newtonian behavior at a temperature below -10^{o}C whereas Newtonian properties are appeared at above -10^{o}C. Heris et al. (2006) have carried experiment with Al_2O_3–water and CuO–water nanofluid up to ϕ=3% and have shown that up to this limit the nanofluid behaves like Newtonian fluid. Above that, the viscosity increases rapidly as shear rate decreases. At a high shear rate, the viscosity becomes constant, indicating shear thinning behavior of nanofluid.

University of Malaya

2.2 Nanofluid Forced Convection

2.2.1 Experimental Studies

Significant improvements of heat transfer of nanofluids have been demonstrated experimentally (Anoop et al., 2009; Q. Li & Xuan, 2002; Pak & Cho, 1998). For example, Anoop et al. (2009) experimentally investigated the effect of suspended alumina nanoparticles, in sizes of 45 nm and 150 nm, in water on the heat transfer coefficient in a fully developed laminar flow. The heat transfer was found to be augmented as a result of dispersing nano-solid particles into the water. It was also observed that the heat transfer enhancement of the nanofluid is higher when the particle size is smaller. A similar study was done by Wen and Ding (2004) for 27-56 nm alumina nanoparticles suspended in deionized water and significant enhancement was reported in the entrance region of laminar flow. Xuan and Li (2002) experimentally studied the average heat transfer coefficient of Cu-water nanofluid with volume fractions of 0.3-2 vol.% in laminar and turbulent flow regimes. It was seen that the Nusselt number of Cu-water nanofluid enhances to 60% by using 2% Cu volume concentration. Pak and Cho (1998) performed viscosity, pressure loss and heat transfer measurements on titanium dioxide nanofluids up to 3% volume fraction experimentally. It was shown that the convective heat transfer coefficient increases with the increase of the particle volume fraction and Reynolds number; Nusselt numbers is reported to increase by over 30% that was calculated using Dittus–Boelter equation (Bergman et al., 2011).

Yang et al. (2005) have carried out experimental investigations on the convective heat transfer using graphite-water nanofluid in a horizontal pipe. The effects of the Reynolds number, the nanoparticles' volume concentration and the temperature on the heat transfer coefficient were studied. The heat transfer coefficient was found to increase with the increase of the Reynolds number and the particle concentration.

University of Malaya

Experimental analysis of the oxide nanofluid (CuO and Al_2O_3 in water) by Zeinali et al. (2006) using a constant pipe wall temperature and based on laminar flow regime showed the heat transfer enhancement in both kinds of nanofluids with the increase in volume fraction of particles as well as the Peclet number. It was found that the heat transfer enhancement of the Al_2O_3-water nanofluid is higher than that of the CuO-water for a higher nanoparticle concentration but remains about the same at a low concentration.

2.2.2 Numerical Studies

There are a number of studies focusing on modeling of nanofluid convective flows. Several methods are utilized by the different researchers to perform the simulations. All these methods can be categorized into two general types: single-phase and two-phase methods. The details of the investigations are reviewed in the following subsections (2.2.2.1 and 2.2.2.2)

2.2.2.1 Single-phase Models

Single phase (homogenous) model is very popular for numerical studies of nanofluids because of its simplicity. In the single-phase model, nanoparticles are assumed to be uniformly distributed in the base fluid (Niu et al., 2012), and moreover, the effective thermo-physical properties, including conductivity, viscosity, heat capacity and density, are based on the mixture of nanoparticles and the base fluid. Further, in this model, it is considered that both the liquid and particle phases are in chemical and thermal equilibrium, and the relative velocity between the phases is equal to zero (Corcione et al., 2012; Q. Li et al., 2003; Namburu et al., 2009). This assumption may be realistic because the relative velocity decreases with the decrease of the particle size, and the nanoparticles are much smaller than the microparticles (Namburu et al., 2009). The easy fluidization of nanoparticles in the base fluid is also assumed, and therefore, the effective mixture behaves similar to a single-phase fluid (Q. Li et al., 2003;

University of Malaya

Namburu et al., 2009). The accuracy of the numerical results of single model approach is very much dependent on the proper selection of the effective thermo-physical properties.

2.2.2.1.1 Newtonian and non-Newtonian rheology

One simplified view which has been considered in many works (J Koo & Kleinstreuer, 2005; Maïga et al., 2004; Moraveji & Ardehali, 2013; Moraveji et al., 2011) is to treat nanofluid as a Newtonian fluid with modified properties (Niu et al., 2012). For example, Maiga et al. (2004) numerically investigated the laminar and turbulent forced convective heat transfer of Al_2O_3−water and Al_2O_3−ethylene glycol nanofluids inside a heated tube. They used the single-phase model with constant dynamic viscosity (i.e. Newtonian fluid behaviour) and constant thermal conductivity which were selected from the experimental data for the each nanoparticle volume fraction. The obtained numerical results in terms of heat transfer coefficient were in a satisfactory agreement compared to the experimental data with a maximum error of 10%. Moraveji et al. (2011) used the similar model to investigate the heat transfer enhancement of Al_2O_3-water nanofluid under laminar forced convection. It was reported that the simulation results get closer to the experimental data as the Re number increases and the size of particle decreases. The Nusselt numbers predicted by the model showed a maximum 10% deviation from the experimental data. On the contrary, some studies suggested that the rheology of nanofluid is more likely as a shear-thinning fluid rather than of a Newtonian fluid (Chang et al., 2005; Niu et al., 2012; Pak & Cho, 1998; Putra et al., 2003; Santra et al., 2009). For example, Chang et al. (2005) found the non-Newtonian fluid behaviour for CuO-water nanofluid during their experimental study. The non-Newtonian rheology can be described by the power-law model with the flow index less than 1 (Niu et al., 2012). Putra et al. (2003) have reported experimentally the relation between the shear stress and shear strain for Al_2O_3−water nanofluid. According

University of Malaya

to the data given by Putra et al. (2003), the constants of power-law model have been extracted by several researchers (Niu et al., 2012; Santra et al., 2008, 2009) to be used in numerical investigations. Santra et al. (2009) investigated numerically the laminar forced convection of Cu-water nanofluid through two isothermally heated parallel plates using both Newtonian and the power-law rheology. It was found that the difference in the predicted Nusselt numbers between the two models becomes significant as the Re number increases. So, the need of consideration of the non-Newtonian effect for nanofluids has been suggested in this study.

2.2.2.1.2 Brownian motion and dispersion model

Increase in the Brownian motion (microconvection effect) is supposed to be one of the main reasons for nanofluids thermal conductivity enhancement. This has led to the development of a number of new theoretical models (Corcione, 2011; Jang & Choi, 2004, 2007; Junemoo Koo & Kleinstreuer, 2004; Murshed et al., 2009; Patel et al., 2006; Prakash & Giannelis, 2007; Prasher et al., 2006; Xie et al., 2005; Xue, 2003; Yu & Choi, 2003) which are dependent upon temperature for the evaluation of the effective thermal conductivity of nanofluids. These models were already used in the single-phase computational fluid dynamics (CFD) approach by many studies (Akbari et al., 2012; Bianco et al., 2009; Corcione et al., 2012; Namburu et al., 2009; Yarmand, Ahmadi, et al., 2014; Yarmand, Gharehkhani, et al., 2014). Namburu et al. (2009) used the single-phase model with temperature dependent effective conductivity to investigate the turbulent forced convection of the three kinds of nanofluid (Al_2O_3, CuO and SiO_2 in mixture of ethylene glycol and water) numerically. The results showed a good agreement between the Nusselt number prediction for the nanofluids and Gnielinski correlation.

It should be noted that the chaotic movement of nanoparticles also causes a thermal dispersion in nanofluid, and it may be considered as one of the main reasons for

University of Malaya

the thermal conductivity enhancement of nanofluids. A few number of authors applied the dispersion model, and it was seen that the model predicts the nanofluid heat transfer behaviour more reliably as compared to experimental data. Heris et al. (2007) numerically investigated laminar-flow convective heat transfer of nanofluid in a circular tube with the constant wall temperature boundary condition. It was concluded that dispersion and random movement of nanoparticles inside the fluid change the structure of the flow field and lead to heat transfer enhancement. To assess the accuracy of the dispersion model in predicting heat transfer coefficients of nanofluids, a comparison between numerical and experimental results for Al_2O_3/water, CuO/water, and Cu/water nanofluids was carried out, and the model predictions showed good agreement. Mokmeli and Saffar-avval (2010) introduced a new dispersed thermal conductivity relation in radial direction to study the laminar convective heat transfer behaviour of nanofluids in straight pipes. It was seen that the dispersion model predicts the nanofluid heat transfer behaviour more reliably as compared to experimental data. The discrepancy in regard to volume fraction variations was reported at less than 2.5%, and the variations of Reynolds number were less than 4%. While the homogenous model predictions generally resulted in a discrepancy in the range of 14–30%. Mojarrad et al. (2013) carried out both experimental and numerical investigations to analyse the heat transfer performance of Al_2O_3 (30nm)–water nanofluids flowing in the entrance region of a circular tube with a constant surface temperature on the walls. In this work, a new correlation for the determination of the radial dispersed thermal conductivity was suggested and assessed. Finally, it was reported that the new dispersion model gives accurate prediction of the experimental results.

University of Malaya

2.2.2.2 Two-phase Models

Due to the findings reported by Ding and Wen (2005), in which the nanoparticle concentration can be lower near the wall region than that in the core region, the assumption of homogeneous distribution of nanoparticles in base fluid may not always remain true for a nanofluid (Kamyar et al., 2012; Moraveji & Ardehali, 2013). In addition, factors such as gravity, Brownian motion, Brownian diffusion, friction force between the fluid and nanoparticles, sedimentation, dispersion, layering at the solid-liquid interface, ballistic phonon transport, thermophoresis, etc., may affect a nanofluid flow (Bahiraei & Hosseinalipour, 2013a; Hejazian et al., 2014b; Moghari, 2011). These factors may be caused to the nanoparticle migration, slip velocity between nanoparticle and base fluid and non-homogeneous distribution of nanoparticles among the base fluid (Aminfar & Motallebzadeh, 2011; Moraveji & Ardehali, 2013). This fact has motivated researchers to use the two-phase models for numerical investigation of nanofluids.

In the two-phase model, the nanoparticles and the based fluid can be distinguished as two separated phases with different thermo-physical properties. The multiphase can be solved either using Eulerian or Lagrangian frameworks. In the Eulerian/Eulerian framework, each phase is treated as a continuum having separate transport equations, while in the Eulerian/Lagrangian framework, particle phases are traced as a discrete phase. The inter-phase interactions of particles, and fluid are accounted in the both frameworks (Fluent, 2009). There are two different Eulerian two-phase models which are commonly used for the simulation of nanofluid flows:(i) mixture model and (ii) Eulerian-Eulerian (two-fluid) model. While the mixture model solves only the governing equations for the mixture phase and prescribes relative velocities to describe the dispersed phases, the Eulerian-Eulerian model solves the equations for each phase. So, more time and computational efforts are required for the Eulerian-Eulerian method in comparison with the mixture model (Fluent, 2009).

University of Malaya

Lotfi et al. (Lotfi et al., 2010) numerically investigated the laminar forced convection of Al_2O_3/water in horizontal pipes using the single-phase model, Eulerian-Eulerian and mixture two-phase models. According to the results, the mixture model gives the closer predictions to experimental data than the others. It was also found that the single-phase and Eulerian-Eulerian models under-predict the Nusselt number. The laminar forced convection of three types of nanofluid (Cu/water, CuO/water and Al_2O_3/water) in a circular tube with constant wall temperature was studied experimentally and numerically by Haghshenas Fard et al. (2010). They compared the single-phase model versus the Eulerian two-phase model and reported that the two-phase model gives the better agreement with the experimental data than the single-phase model. Mojarrad et al. (2013) analysed numerically the laminar convective heat transfer of α-Al_2O_3/water using the homogenous single-phase (using temperature dependent conductivity), Eulerian-Lagrangian and mixture models. It was shown that the homogenous single-phase model underestimates the thermal behaviour of the nanofluid and the mixture model overestimates. However, the Eulerian-Lagrangian model shows a reasonable agreement with the experimental data. Saberi et al. (2013) examined laminar forced convective heat transfer of nanofluids contained alumina/water and zirconia/water through a vertical heated tube using both single-phase approach and two-phase mixture model. The comparison of their results with experimental data showed that the mixture model have better prediction for the convective heat transfer coefficient with 8% and 5% average relative error for alumina/water and zirconia/water nanofluids, respectively, while these figures were 13% and 8% for single-phase model. Bianco et al. (2009) and Moraveji and Esmaeili (2012) performed single- and two-phase CFD modelling of developing laminar forced convection flow of alumina nanofluid inside a circular tube under constant heat flux. In the both studies, the Lagrangian-Eulerian model was employed with either constant or temperature-dependent properties,

University of Malaya

and the maximum difference of 11% was detected for the average heat transfer coefficient by comparing the single-phase and the two-phase models.

Akbari et al. (2012) numerically investigated turbulent forced convection of Al_2O_3/water and Cu/water nanofluid in a straight pipe with constant wall heat flux. They used the single-phase model (using temperature dependent properties) and the three different two-phase models (volume of fluid, mixture and Eulerian-Eulerian). It was found that the all three two-phase models give the same thermal field predictions. However, the predictions of the two-phase models are very far from the experimental data and the single-phase model results. The two-phase models show higher difference from the experimental data as the nanoparticle volume fraction increases. But regarding the single-phase model, the results are close to the experimental data in almost all the conditions. It was also found that the predicted Nusselt number by the CFD methods shows lower dependency on Re number than those obtained by the experiments. The authors believe that this is due to the clustering phenomena and the Re number effect on it, which changes the thermal and hydrodynamic properties of the nanofluids. Behzadmehr et al. (2007) utilized a two-phase mixture model to investigate turbulent forced convection of nanofluid inside a pipe based on thermal equilibrium assumption (the same temperatures for both nanoparticle and fluid). The results of the two-phase model in their study were found to be closer to the experimental data than those of the single-phase (homogeneous) model.

University of Malaya

2.3 Nanofluid Subcooled Flow Boiling

2.3.1 General Background

Among different heat transfer mechanisms, flow boiling shows a significant enhancement of heat transfer coefficient because of bubble motions. Heat transfer in flow boiling is determined by both transfer of heat accumulated by the vapour production mechanism on the surface (pool boiling heat transfer) and by liquid convection (forced convection heat transfer) (Zou, 2011).

In some applications the fluid bulk temperature is lower than the saturation temperature. Subcooled flow boiling is a phenomenon that could be used in such an application. In particular, subcooled flow boiling has been known to be a very efficient mode of heat transfer where it can be utilized in energy conversion system, such as a heat exchanger and cooling of high-energy-density electronic hardware. Subcooled flow boiling is also known to be of considerable importance in the design, operation and thermal–hydraulic safety analysis of a nuclear reactor. Such a regime may occur in narrow flow passages between the heated fuel rods of a pressurized nuclear reactor core. Here vapour bubbles are generated in the micro cavities commonly designated as nucleation sites, which are randomly distributed over the heated surface. The vapour bubble is generated on a nucleation site when the surface temperature sufficiently exceeds the liquid saturation temperature at the local pressure. Bubbles may slide along the heated surface, eventually depart from it and migrate further into the subcooled liquid flow, where they are subjected to condensation (E Abedini et al., 2013; Cheung et al., 2014; Rzehak & Krepper, 2013).

Figure 2.1 depicts a description of a subcooled flow boiling which is accompanied by a boiling curve describing the void fraction distribution along the heated wall. Two general flow patterns are seen during subcooled flow boiling heat transfer; single-phase forced convection and two-phase subcooled flow boiling (Končar

University of Malaya

& Mavko, 2003). At a point designated as the onset of nucleate boiling (ONB), boiling occurs and bubbles remain attached to the heating surface. As the bulk liquid temperature increases further downstream, vapour bubbles on the wall grow larger and begin to detach from the heating surface. A rapid increase of the void fraction commences at a location called the net vapour generation (NVG) or the onset of significant void (OSV), which indicates the transitional point between the low void fraction region followed by another region in which the void fraction increases sharply thereafter (Cheung et al., 2014).

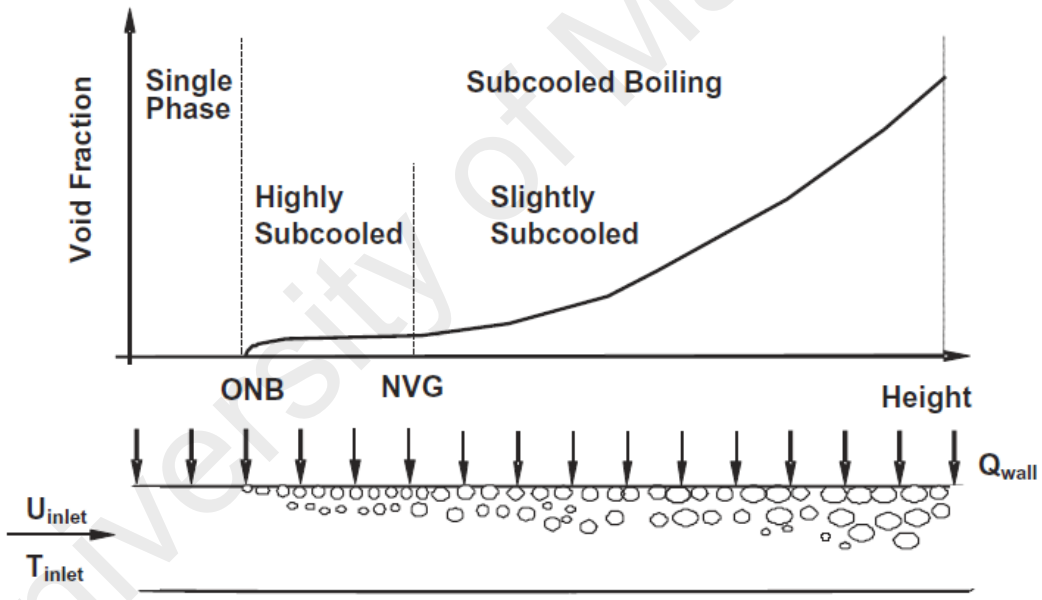

Figure 2.1: A schematic illustration of a subcooled flow boiling in a heated pipe (Cheung et al., 2014)

University of Malaya

2.3.2 Experimental Studies

In addition to investigate the heat transfer of nanofluids single-phase flow, many experimental works (Ehsan Abedini et al., 2013; S. J. Kim et al., 2010; M. Sarafraz & Hormozi, 2014; M. Sarafraz et al., 2014; M. M. Sarafraz & Hormozi, 2013; Setoodeh et al., 2015) were dedicated to the nanofluids' multiphase regime.

According to the literature, some inconsistent results were reported about the boiling heat transfer coefficient (BHTC) of nanofluids. Some studies report no change of heat transfer in the nucleate boiling regime (S. J. Kim et al., 2010; Vassallo et al., 2004; You et al., 2003); some report heat transfer deterioration (Bang & Chang, 2004; Sarit K Das et al., 2003; S. J. Kim, 2007) and others heat transfer enhancement (Lun-Chun & Zhen-Hua, 2008; JP Tu et al., 2004; Wen & Ding, 2005). For example, Liu et al. (2010) carried out the pool boiling experiment using carbon nanotube/water nanofluid, and they showed a heat transfer enhancement. Kwark et al. (2010) investigated pool boiling of Al_2O_3, CuO, and diamond nanoparticles in water. They reported that the boiling heat transfer coefficient remains unchanged. Kim et al. (2010) studied subcooled flow boiling heat transfer of dilute alumina, zinc oxide, and diamond water base nanofluids at atmospheric pressure. It was reported that the heat transfer coefficients are similar for both the nanofluids and water. However, Suriyawong and Wongwises (2010) investigated pool boiling of TiO_2 /water nanofluid on Cu and Al plates with two surface roughness measurements (0.2 and 4 mm). They found degradation of boiling heat transfer coefficient for all nanoparticle concentrations and the surface roughnesses. Li et al. (2003) also found the deterioration of the pool boiling heat transfer using CuO/water nanofluid. Abedini et al. (2013) investigated subcooled flow boiling of TiO_2/water nanofluid in vertical and horizontal tubes. They found the decrease of the heat transfer coefficient by increasing the nanoparticle volume fraction

University of Malaya

for both inclinations of the tube. Further investigations are needed to find out how the BHTC is changed using nanofluids.

Some experimental investigations (Barber et al., 2011; S. Kim et al., 2006, 2007) have been focused on nanoparticles' deposition during nanofluid boiling. It is claimed that the nanoparticles' deposition fills the micro-cavities on the heating surface (Vafaei & Borca-Tasciuc, 2014). This is followed by a decrease in the number of nanoparticles available to interact with the bubbles, an increase of the bubble departure diameter, wettability improvement and also a loss of nucleation sites at the heater surface (Bang & Chang, 2004; Sarit K Das et al., 2003; X. Li et al., 2014). For example, Kim et al. (2007) reported the wettability improvement of the heater surface during pool boiling of alumina/water, zirconia/water and silica/water nanofluids. The contact angles of pure water and 0.01% vol. alumina/water on a clean stainless steel (SS) surface and nanofluid boiled SS surface have been measured by Kim et al. (2006). It was found that the suspension of the nanoparticle in the base liquid showed no effect on the base liquid contact angle on a clean surface. However, the layer of deposited nanoparticles decreased the base liquid contact angle (see Figure 2.2). It was claimed that the nanoparticles deposited on the heater surface during nanofluid boiling create a nanoparticle coating formation. In other words, the nanoparticle coating was formed by nucleated vapour bubbles and the evaporating liquid remained a concentrated microlayer of nanoparticles at the bubble base (Barber et al., 2011) (as illustrated in Figure 2.3). According to the literature, it is obvious that the nanoparticle deposition affects nucleate boiling parameters. However, the effect of nanoparticle deposition on the BHTC is still unclear.

University of Malaya

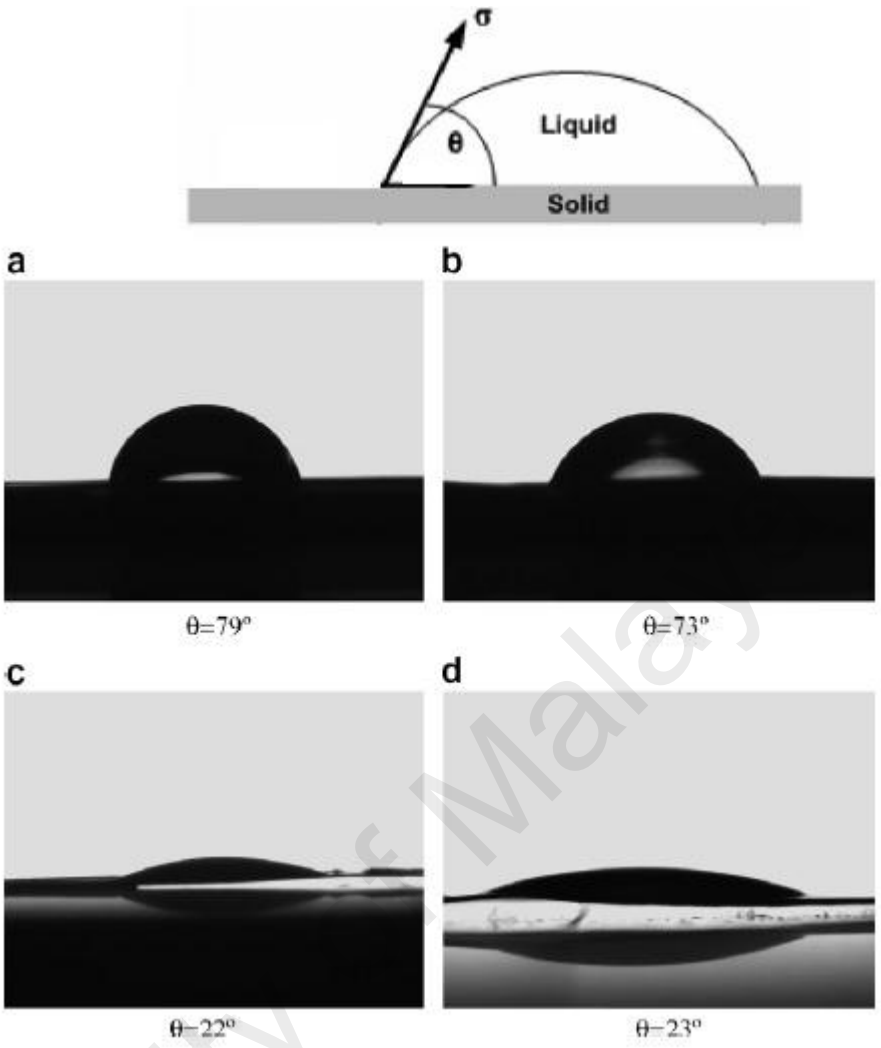

Figure 2.2: Contact angles of droplets on stainless steel surfaces, (a) Pure water droplet on surface boiled in pure water, (b) 0.01%vol. alumina nanofluid droplet on surface boiled in pure water, (c) pure water droplet on surface boiled in 0.01%vol. alumina nanofluid, (d) 0.01%vol. alumina nanofluid droplet on surface boiled in 0.01%vol. alumina nanofluid (Kim et al., 2007).

University of Malaya

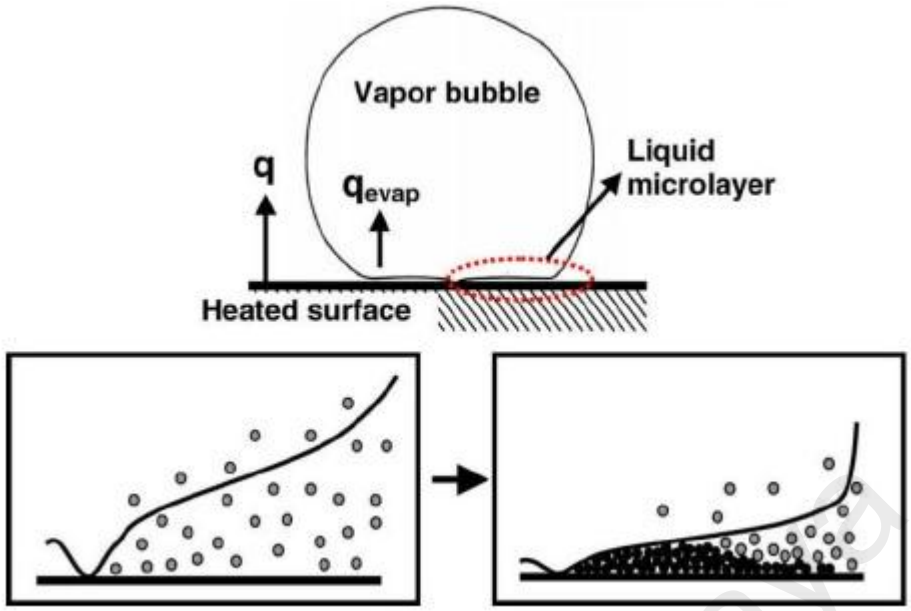

Figure 2.3: Mechanism of nanoparticle deposition during the boiling process (micro-layer evaporation) (Barber et al., 2011)

2.3.3 Numerical Studies

In case of numerical studies, many numerical investigations (Chen et al., 2009; Cheung et al., 2014; Končar et al., 2004; Končar & Mavko, 2003; JY Tu & Yeoh, 2002) have been focused on conventional fluids like water. Almost all these studies investigate the accurate prediction of bubble dynamics. For example, Tu & Yeoh (2002) carried out numerical modelling of low-pressure subcooled boiling flows. They found that the closure relationships (i.e. partition of the wall heat flux, bubble size distribution, interfacial area concentration, bubble departure diameter and frequency) play crucial role in an accurate prediction of void fraction distributions. Sensitivity tests were made using different closure models. Predictions of the proposed model agreed closely with the experimental results from the literature. Similarly, Koncar et al. (2004) investigated the same case study to predict the vapor void fraction, and they found that lateral hydrodynamic mechanisms (i.e. lift force, wall lubrication force and mixing due to bubble-induced turbulence) and variation of bubble diameter according to local flow conditions are important for modelling subcooled flow boiling. The importance of non-

University of Malaya

drag forces in vapor void fraction distribution were pronounced by Chen et al. (2009) again. They applied a three-dimensional two-fluid model coupled with a homogeneous multiple size group (MUSIG) approach for the numerical simulations of upward subcooled boiling flow of water at a low pressure. Cheung et al. (2014) numerically investigated the distribution of vapor void fraction during subcooled flow boiling of water in vertical channels at a low pressure. They carried out sensitivity tests on different combinations of the empirical boiling models (e.g. active nucleation site density models, bubble departure diameter models and bubble departure frequency models) covering a wide range of subcooled flow conditions and imposed wall heat fluxes. Some of the model combinations were proposed to be able to predict the distribution of the vapor void fraction comparing with the experimental data from the literature. According to the literature, a comprehensive sensitivity test is needed to assess the effect of bubble dynamics on accurate prediction of the boiling heat transfer coefficient (BHTC).

There are a few numerical studies (E Abedini et al., 2013; X. Li et al., 2014) considering nanofluids boiling. For example, Abedini et al. (2013) studied subcooled flow boiling of Al_2O_3/water nanofluid using the two-phase mixture model. They neglected the effect of drag and non-drag forces in the study. It was observed that the convective heat transfer coefficient for Al_2O_3/water nanofluid in subcooled flow boiling is higher than that of the base fluid and the heat transfer coefficient increases with increasing of nanoparticles volume fraction. Li et al. (2014) investigated the nucleate pool boiling of dilute water-silica nanofluid using the Eulerian-Eulerian two-phase model. They recommended that the morphology modification induced by nanoparticle deposition needs to be taken into account. They developed correlations for active nucleate site density and bubble departure diameter in which the effect of such nanoparticle deposition has been considered. It was also found that the modified liquid

University of Malaya

property induced by the existence of the nanoparticles has a negligible effect on the boiling heat transfer in dilute nanofluids. In the both studies ((Abedini et al., 2013) and (Li et al., 2014)), the liquid-nanoparticle suspension was supposed to treat as a single-phase and not to treat as a two-phase in which the liquid phase, and the particle phase are treated separately. Further numerical studies should be done to assess the effects of interphase interactions between the base liquid and the nanoparticles on CFD model prediction of the BHTC.

University of Malaya

2.4 Research Gaps

2.4.1 Nanofluid Forced Convection

As discussed in the literature, there are a number of CFD models for modelling of nanofluids forced convection. Figure 2.4 illustrates these models. The following sections explain the gaps, the weak points of some CFD models and the results inconsistency are found through the literature.

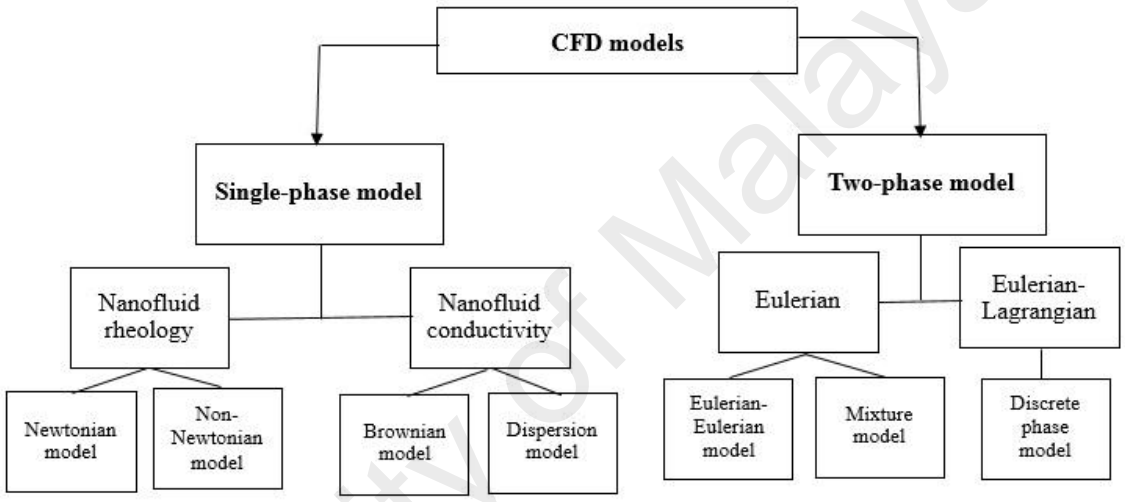

Figure 2.4: Different CFD models for simulation of nanofluids forced convection

2.4.1.1 Laminar flow

According to the discussion in Section 2.2.2, there are some inconsistencies among the results of different numerical solutions (Behroyan et al., 2015). There are various models that have been incorporated in numerical studies in order to improve the prediction of heat transfer of various nanofluids. Totally, each CFD approach is capable to consider some of the factors which play role in the nanoparticle migration and nanoparticle distribution (Behroyan et al., 2015). For example, the single-phase model is able to take into account only the effect of Brownian motion (micro-convection between base fluid and nanoparticles by calculation of interphase heat transfer) and thermal dispersion. The Eulerian model considers only the drag force and Brownian

University of Malaya

motion. Although the mixture model cannot calculate the interphase heat transfer, the factor of Brownian motion can be considered in effective nanofluid conductivity (similar to the single-phase model). The Lagrangian-Eulerian model considers Brownian motion, Brownian force and thermophoresis and the drag force. In different numerical studies, some of these factors are taken into account and some are overlooked (Bahiraei & Hosseinalipour, 2013a). Theoretically, although the two-phase models could provide more accurate results in comparison to the single phase model, but there are number studies which have reported otherwise (J Koo & Kleinstreuer, 2005; Maïga et al., 2004; Moraveji & Ardehali, 2013; Moraveji et al., 2011). Some of the numerical studies do not provide sufficient benchmarking with experimental investigations making it difficult to evaluate the accuracy of the model used (Kalteh et al., 2011). It is still very much unclear an appropriate use of the models and the quantitative error involved in the prediction of heat transfer of various nanofluids. Therefore, a comprehensive numerical investigation is needed to evaluate the accuracy of each model in heat transfer prediction of laminar nanofluids forced convection.

2.4.1.2 Turbulent flow

Based on comparisons by various studies in the literature (see Section 2.2.2), it is difficult at present, to make any conclusions in terms of accuracy between the single-phase and two-phase models. This is because of various limitations that have been adopted in both models and in the prediction of results; some studies have not directly made comparisons with experimental work (Bianco et al., 2009; Kalteh et al., 2011; Moraveji et al., 2012; Santra et al., 2009); various inconsistencies in selections of effective properties, such as viscosity, conductivity, solidus viscosity etc. have resulted in an inappropriate prediction of heat transfer (Behzadmehr et al., 2007; Göktepe et al., 2014; Shahriar et al.). Most studies are limited to a particular volume fraction and Reynolds number (Akbari et al., 2012; Behzadmehr et al., 2007; Lotfi et al., 2010), and

University of Malaya

they do not cover a range of these elements. There are a number of contradictory findings from one study to other in terms of accuracy in result predictions between the single-phase and two phase-models; for example, Salman et al. (2014) used the Eulerian, mixture and single-phase models for the simulation of laminar and turbulent forced convective flow of SiO_2-EG nanofluid in a microtube, and it was reported that the single-phase model gave accurate results. On the contrary, the numerical investigation by Hejazian et al. (2014a) on TiO_2/water nanofluid flow showed that the mixture the two-phase model (maximum error of 11%) was slightly better than the single-phase model (maximum error of 12.41%). Likewise, Behzadmehr et al. (2007) investigated the turbulent flow of Cu-water nanofluid and the mixture two-phase model was found to be more accurate in the prediction of the Nusselt number than that of the single-phase model. On the contrary, Bianco et al. (2009) investigated the single- and mixture two-phase models for turbulent Al_2O_3/water nanofluid flow and found the same accuracy between them. Therefore, a comprehensive numerical investigation is needed to evaluate the accuracy of each model in heat transfer prediction of turbulent nanofluids forced convection.

For the single-phase model, various sophisticated effective conductivity and viscosity correlations have been suggested by researchers (Corcione, 2011; Kumar et al., 2010; Masoumi et al., 2009; Özerinç et al., 2010) to improve the accuracy of the prediction of the Nusselt number. For example, Akbari et al. (2012) tested different combinations of effective conductivity and viscosity correlations suggested in the literature, to numerically investigate the turbulent forced convection of Al_2O_3/water and Cu/water nanofluid in a straight pipe with a constant wall heat flux. The best correlations were selected for further investigations. Unlike the single-phase model, not much work has been done to improve the accuracy of the two-phase model. The Eulerian two-phase models, i.e. mixture and the Eulerian-Eulerian (two-fluid) models

University of Malaya

are based on the concept of interpenetrating continua. This also means that all of the thermal and hydrodynamic properties, such as viscosity and thermal conductivity of the phases (i.e., liquid and solidus phases), must be calculated. It is often not that straightforward to describe the thermo-physical properties of the solidus phase. For example, there are no specific correlations for the calculations of the properties of the solidus phase (solid nanoparticles) of nanofluids for the use in the Eulerian two-phase models, and this can be regarded as the main drawback. Consequently, researchers normally adopt any other correlations from the literature to best describe the properties of the solidus phase. For example, Behzadmehr et al. (2007) have carried out CFD investigations of a forced convection of nanofluid in a tube and used the experimental correlations suggested by Miller and Gidaspow (1992) for the calculation of the viscosity of the solidus phase representing 1% volume fraction of Cu nanoparticle of 42 nm particle size. This is despite the fact that Miller and Gidaspow's correlations were originally developed for the calculation of the solidus viscosity in a dense gas-solid flow inside a vertical tube. In addition, the calculations of the thermal conductivity of the solidus phase are simply done by proportioning the volume fractions of nanoparticles and the thermal conductivity of the material of the solid particle. Behzadmehr et al. (2007) showed that a maximum error found by using his mixture model was about 6%, but the authors' study was only limited to 1% volume fraction of the nanoparticle. In other words, the accuracy of the two-phase mixture model has not been tested on other nanoparticle volume fractions. Kalteh et al. (2011), who adopted the Eulerian-Eulerian model for a CFD investigation of nanofluid flow through a microchannel, used Kuipers et al. (1992) equations to calculate the effective conductivity of the solidus phase representing 100 nm Cu nanoparticle, consisting of 1% to 5% volume fractions. However, the equations were originally developed to estimate the effective radial thermal conductivity in pack beds. The effectiveness of using the equations for the two-

University of Malaya

phase modelling of the nanofluid was not conclusive since no validation was made. Hence, further investigations are needed to improve the accuracy of the Eulerian CFD model in prediction of the nanofluid heat transfer.

2.4.2 Subcooled Flow Boiling

According to the review of the literature has been done in Section 2.3, there are a number of investigations in which the effect of the different boiling properties, such as the nucleate boiling parameters and the bubble dynamics, have been considered. Figure 2.5 illustrates these boiling properties. Almost all studies reported the effects of boiling properties on bubble void fraction or bubble distribution. However, the effects of the nucleate boiling parameters (i.e. nucleate site density, bubble frequency, and bubble departure diameter) and the bubble dynamics (i.e. interfacial area concentration of bubbles, non-drag forces and turbulence interaction resource) on the CFD model prediction of the boiling heat transfer coefficient (BHTC) are still unclear. Despite the investigations have been done by the researchers about nanofluid boiling heat transfer, the BHTC enhancements and/or deteriorations by using nanofluid are not so clear. All numerical studies also considered the liquid-nanoparticle suspension as a homogenous single-phase. Further studies are needed to assess the effects of interphase interactions between the nanoparticles and the base fluid on the heat transfer prediction of nanofluid subcooled flow boiling. Moreover, there is not any numerical investigation to assess how the heat transfer prediction of nanofluid subcooled flow boiling are effected by nanoparticles deposition. Further numerical studies are needed to investigate the effect of such nanoparticle deposition on the heat transfer prediction of nanofluid subcooled flow boiling.

University of Malaya

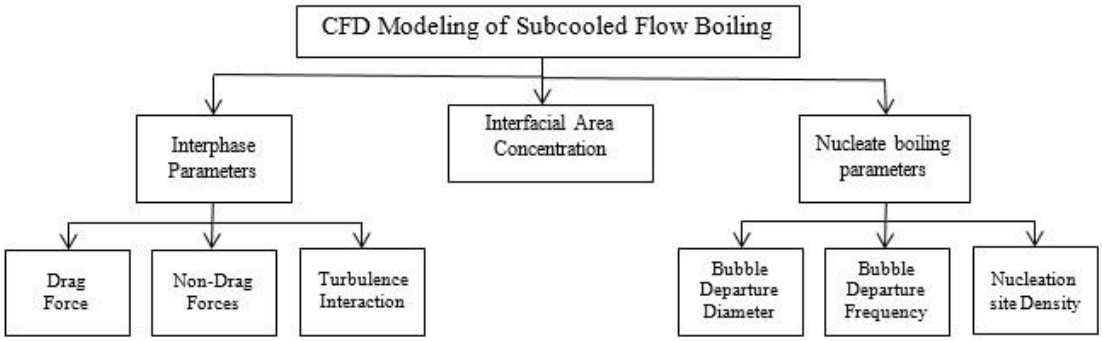

Figure 2.5: Boiling properties for modeling of subcooled flow boiling

University of Malaya

3 CHAPTER 3: MODELLING ON LAMINAR FORCED CONVECTION OF NANOFLUID

3.1 Introduction

A comprehensive comparison of CFD analysis among various modelling approaches is presented in this chapter to investigate a laminar forced convection flow of Al_2O_3/water nanofluid in a heated tube. The results are benchmarked against that calculated using Velagapudi' s correlation (Velagapudi et al., 2008) for the Nusselt number. The deviation in the Nusselt number will be reported for each and every model which gives insights to strengths and weaknesses of each approach. The repeatability and the consistency of some of the most accurate CFD models will be checked for 0–2% nanoparticle volume fraction and also for Re ranging from 745 to 1600. This study benefits when selecting a suitable model for a similar type case study.

3.2 Methodology

3.2.1 Geometry Structure

A horizontal tube with length (L) of 1.0 m and circular cross section with the diameter (D) of 4.5mm is considered in the current study (Figure 3.1). The considered nanofluid is a mixture containing 30 nm average size Al_2O_3 nanoparticles dispersed in water as a base fluid. The flow and the thermal field are assumed to be two-dimensional axisymmetric with respect to the tube main axis, in order to save computational time without compromising accuracy. As a result, a rectangular domain with dimensions of 2.25 mm × 1 m is created.

University of Malaya

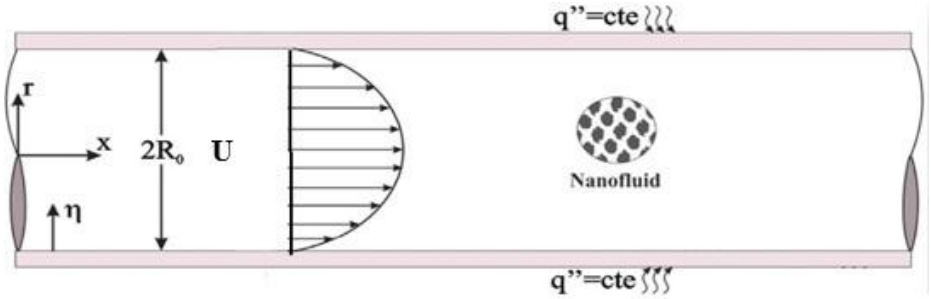

Figure 3.1: The geometry structure of the physical model

3.2.2 Nanofluids Thermophysical Properties

The working fluid is a mixture of water andAl_2O_3 particles with a diameter of 30 nm, at volume concentration (φ) ranging from 0 to 2%. Thermophysical properties of alumina and water are listed in Table 3.1.

Table 3.1: Thermophysical properties of alumina nanoparticle and water as a base at T=295 ^{o}K (Moraveji et al., 2011)

Thermophysical properties	Al_2O_3	Water
$\rho(\mathrm{kg/m^3})$	3600	998
$\mathrm{Cp(J/kg.K)}$	765	4181
$\mathrm{K\ (W/m.K)}$	36	0.606
$\mu\ (\mathrm{Ns/m^2})$	−	0.000959

Many researchers have used the solid–liquid mixture equations for estimating the density and specific heat capacity (Leong et al., 2006; Maïga et al., 2004; Mokmeli & Saffar-Avval, 2010; Moraveji et al., 2011; Yarmand et al., 2014) of nanofluids from the following equations:

$$\rho_{nf} = (1-\varphi)\rho_{bf} + \varphi\rho_p \quad (3.1)$$

$$(\rho C_p)_{nf} = (1-\varphi)(\rho C_p)_{bf} + \varphi(\rho C_p)_p \quad (3.2)$$

It is noted that the density, specific heat and thermal expansion coefficient of the nanofluids are assumed to be a linear function of volume fraction due to lack of experimental data on their temperature dependence.

University of Malaya

The Brownian motion is supposed to be one of the main reasons for nanofluids' thermal conductivity enhancement and changing the effective viscosity by temperature. This has led to the development of a number of new theoretical models (Corcione, 2011; Jang & Choi, 2004, 2007; Junemoo Koo & Kleinstreuer, 2004; Masoumi et al., 2009; Murshed et al., 2009; P. K. Namburu et al., 2007; Patel et al., 2006; Prakash & Giannelis, 2007; Prasher et al., 2006; Xie et al., 2005; Xue, 2003; Yu & Choi, 2003) which are dependent upon temperature for the evaluation of the effective thermal conductivity and dynamic viscosity of nanofluids. These models were already used in the single-phase computational fluid dynamics (CFD) approach by many studies (Akbari et al., 2012; Bianco et al., 2009; Corcione et al., 2012; Namburu et al., 2009) and improve the prediction of the Nusselt number. Chon's correlation (Chon et al., 2005) is chosen to calculate the thermal conductivity which is an empirical correlation for water-Al_2O_3 nanofluids and takes into account the Brownian motion and the mean diameter of nanoparticles. The model has been used by many studies (E Abedini et al., 2013; Eiyad Abu-Nada, 2009; Lai & Yang, 2011; Mojarrad et al., 2013) and is given as follows:

$$k_{eff}/k_{bf} = 1+64.7(\varphi)^{0.7640}\left(\frac{d_{bf}}{d_p}\right)^{0.3690}\left(\frac{k_{bf}}{k_p}\right)^{0.7476} Pr^{0.9955} Re_{np}{}^{1.2321} \quad (3.3)$$

where Re_{np} is given by

$$Re_{np} = \frac{\rho_{bf} K_B T}{3\pi\mu_{bf}{}^2\lambda} \quad (3.4)$$

where $\lambda = 0.17$ nm is the mean free path of water, K_B is the Boltzmann constant (1.3807×10^{-23} J/K) and μ_{bf} is the viscosity of water. The thermal conductivity calculated by the above correlations at ambient temperature shows ±0.5 % deviation from the experimental data from literature (Anoop et al., 2009). User Define Function (UDF) codes are written to define Equations (3.3) – (3.4) for the effective thermal conductivity of the nanofluid. The UDF codes are incorporated with the commercial CFD codes of Ansys-Fluent.

University of Malaya

In the single-phase model, the effective dynamic viscosity of Al_2O_3-water nanofluid is calculated based on two general fluid behaviours, i.e. Newtonian and non-Newtonian models, which are considered for the nanofluid. The details of each rheology will be described in the next section.

3.2.3 Governing Equations

To analyse the thermal behaviour of the considered nanofluid, Newtonian and non-Newtonian single phase models with and without thermal dispersion effect, and also two phase models including Eulerian, mixture, and the discrete phase model are employed.

3.2.3.1 Single-phase Model

The general forms of governing equations for steady state nanofluid using conventional single-phase approach are as follows:

Conservation of mass:

$$\nabla.\left(\rho_{nf}\vec{V}\right) = 0 \tag{3.5}$$

Conservation of momentum:

$$\nabla.\left(\rho_{nf}\vec{V}\vec{V}\right) = -\nabla P + \mu_{nf}\nabla^2\vec{V} \tag{3.6}$$

Conservation of energy:

$$\nabla.\left((\rho C_P)_{nf}\vec{V}T\right) = \nabla.\left(k_{nf}\nabla T\right) \tag{3.7}$$

3.2.3.1.1 Newtonian Single-phase Model

For an incompressible Newtonian fluid, the relationships between the shear stress and shear rate in the case of two-dimensional axisymmetric coordinates are as follows (Bird et al., 2007; Santra et al., 2009):

$$\tau_{xx} = -2\mu_{eff}\left(\frac{\partial u}{\partial x}\right) \tag{3.8}$$

$$\tau_{yx} = \tau_{xy} = -\mu_{eff}\left(\frac{\partial u}{\partial y} + \frac{\partial v}{\partial x}\right) \tag{3.9}$$

University of Malaya

$$\tau_{yy} = -2\mu_{eff}\left(\frac{\partial v}{\partial y}\right) \quad (3.10)$$

For calculation of effective viscosity of Al_2O_3-water nanofluid, the model proposed by Pak and Cho (1998) has been used in this study. This model is as follows:

$$\mu_{nf} = (1 + 39.11\varphi + 533.9\varphi^2)\mu_{bf} \quad (3.11)$$

where $\mu_{bf}$is recommended by Chon et al. (2005) as follows

$$\mu_{bf} = A10^{\left(\frac{B}{T-C}\right)} \quad (3.12)$$

A = 2.414 ×10^{-5}, B = 247.8, and C = 140.

This model, in general, has been determined for calculation of the effective viscosity of the Al_2O_3/water nanofluid. The dynamic viscosity calculated by the above correlation at ambient temperature shows ±1 % deviation from the experimental data from literature (Anoop et al., 2009). UDF codes are written to define Equations (3.11) – (3.12) for effective dynamic viscosity of the nanofluid. The UDF codes are incorporated with the commercial CFD codes of Ansys-Fluent.

3.2.3.1.2 Non-Newtonian Single-phase Model

For a non-Newtonian fluid, the relationships between the shear stress and shear rate in the case of two-dimensional axisymmetric coordinate according to the Ostwald–de Waele model (two-parameter power law model) are as follows (Bird et al., 2007; Santra et al., 2008, 2009):

$$\tau = -m\left[\left|\sqrt{\frac{1}{2}(\dot{\gamma}.\dot{\gamma})}\right|\right]^{(n-1)}\dot{\gamma} \quad (3.13)$$

where

$$\frac{1}{2}(\dot{\gamma}.\dot{\gamma}) = 2\left\{\left(\frac{\partial u}{\partial x}\right)^2 + \left(\frac{\partial v}{\partial y}\right)^2\right\} + \left(\frac{\partial v}{\partial x} + \frac{\partial u}{\partial y}\right)^2 \quad (3.14)$$

Thus the stress tensors take the following forms:

University of Malaya

$$\tau_{xx} = -2\left\{m\left|\left[2\left\{\left(\frac{\partial u}{\partial x}\right)^2 + \left(\frac{\partial v}{\partial y}\right)^2\right\} + \left(\frac{\partial v}{\partial x} + \frac{\partial u}{\partial y}\right)^2\right]^{1/2}\right|^{(n-1)}\right\}\left(\frac{\partial u}{\partial x}\right) \quad (3.15)$$

$$\tau_{yx} = \tau_{xy} = -\left\{m\left|\left[2\left\{\left(\frac{\partial u}{\partial x}\right)^2 + \left(\frac{\partial v}{\partial y}\right)^2\right\} + \left(\frac{\partial v}{\partial x} + \frac{\partial u}{\partial y}\right)^2\right]^{1/2}\right|^{(n-1)}\right\}\left(\frac{\partial u}{\partial y} + \frac{\partial v}{\partial x}\right) \quad (3.16)$$

$$\tau_{yy} = -2\left\{m\left|\left[2\left\{\left(\frac{\partial u}{\partial x}\right)^2 + \left(\frac{\partial v}{\partial y}\right)^2\right\} + \left(\frac{\partial v}{\partial x} + \frac{\partial u}{\partial y}\right)^2\right]^{1/2}\right|^{(n-1)}\right\}\left(\frac{\partial v}{\partial y}\right) \quad (3.17)$$

Here *m* and *n* are two empirical constants, which depend on the type of nanofluid used. Putra et al. (2003) have shown experimentally the relation between the shear stress and shear strain for Al_2O_3/water nanofluid. Using this data, the values of m and n have been calculated for 1% and 4% solid volume fraction. These values are suitably interpolated and extrapolated keeping in mind that the shear stress decreases with increase in φ for a particular shear rate in the mixture. The values of *m* and *n* for different φ have been given in Table 3.2. It is to be noted that for a shear thinning fluid, the value of n is less than 1 (Bird et al., 2007). UDF codes are written to define the non-Newtonian rheology (Equations (3.13) – (3.17)). The UDF codes are incorporated with the commercial CFD codes of Ansys-Fluent.

Table 3.2: Values of the fluid consistency coefficient m and flow behaviour index n for different φ (Niu et al., 2012)

φ (%)	m ($Nsec^n m^{-2}$)	n
0	0.001	1
1	0.0023	0.830
2	0.00347	0.730

University of Malaya

3.2.3.1.3 Dispersion Model

In this model, it is assumed that the relative motion of nanoparticles with respect to the base fluid introduces a perturbation ($\acute{T}$and$\acute{V}$, respectively) to both temperature and velocity of the nanofluid. Therefore, the intrinsic phase averages considering analogy with turbulence are given as:

$$T = \overline{T} + \acute{T} \tag{3.18}$$

$$\vec{V} = \overline{\vec{V}} + \vec{\acute{V}}$$

where $\overline{T} = \frac{1}{V}\int_V T dV$, $\overline{\vec{V}} = \frac{1}{V}\int_V \vec{V} dV$, $\frac{1}{V}\int_V \acute{T} dV = 0$. By neglecting boundary surface between the fluid and the nanoparticles which are very small and substituting the above values of $\vec{V}$and$T$ in Equation (3.7) and rearranging,

$$\nabla.\left((\rho C_P)_{nf}\overline{\vec{V}}\overline{T}\right) = fa(k_{nf}\nabla\overline{T}) - \nabla.\left((\rho C_P)_{nf}\overline{\acute{V}\acute{T}}\right) \tag{3.19}$$

The second term on the right side of Equation (3.19) indicates the effect of the thermal dispersion in an energy equation. The heat flux induced by the thermal dispersion in nanofluid flow can be represented as:

$$q_d = (\rho C_P)_{nf}\overline{\acute{V}\acute{T}} = -k_d\nabla\overline{T} \tag{3.20}$$

Finally, Equation (3.19) can be rewritten as below:

$$\nabla.\left((\rho C_P)_{nf}\overline{\vec{V}}\overline{T}\right) = \nabla.(k_{nf} + k_d)\nabla\overline{T} \tag{3.21}$$

where k_d is the coefficient of the dispersed thermal conductivity, and it can be calculated based on either velocity gradient or temperature gradient suggested by (Mokmeli & Saffar-Avval, 2010) and (Mojarrad et al., 2013) respectively as follows:

$$k_d = C_d(\rho C_P)_{nf}\frac{R\varphi}{d_p}\left(\frac{\partial u_x}{\partial y}\right) \tag{3.22}$$

$$k_d = C_d(\rho C_P)_{nf}\frac{R\varphi}{d_p}\left(\frac{\partial T}{\partial y}\right) \tag{3.23}$$

UDF codes are written to define the dispersion models. The UDF codes are incorporated with the commercial CFD codes of Ansys-Fluent.

University of Malaya

3.2.3.2 Two-Phase Model

3.2.3.2.1 Eulerian Model

In the Eulerian model, there are different kinds of coupling between phases. The pressure is shared by all the phases, while separate continuity, momentum, and energy equations are employed for different phases, including primary and secondary phases. The volume of each phase is calculated by integrating its volume fraction throughout the domain, while the summation of all the volume fractions is equal to unity (Behroyan et al., 2015; Ganesan et al., 2015). The governing mass, momentum and energy equations for the particle and base liquid phases can be written as follows (Behroyan et al., 2015):

Conservation of mass:

$$\nabla.\left(\varphi_q \rho_q \vec{V}_q\right) = 0 \tag{3.24}$$

where $\vec{V}_q = \int_V \varphi_q \, dV$, and $\sum_{q=1}^{2} \varphi_q = 1$and q indicates the phase.

Conservation of momentum (q^{th} phase):

$$\nabla.\left(\varphi_q \rho_q \vec{V}_q \vec{V}_q\right) = -\varphi_q \nabla P + \varphi_q \mu_q \nabla^2 \vec{V} + \sum_{p=1}^{n} \vec{R}_{pq} + \left(\vec{F}_{collision} + \vec{F}_{lift,q} + \vec{F}_{vm,q}\right) \tag{3.25}$$

where $\sum_{p=1}^{2} \vec{R}_{pq} = \sum_{p=1}^{2} S_{pq}\left(\vec{V}_p - \vec{V}_q\right)$ stands for the interaction drag forces from phase p^{th} to phase q^{th} (the nanoparticles and the base fluid), $S_{pq} = (\varphi_q \varphi_p \rho_q f)/\tau_p$, $\tau_p = \left(\rho_p d_p^2\right)/\left(18\mu_q\right)$ and f indicates the drag friction, which is calculated according to Schiller and Naumann (1935) as:

$$f = \frac{C_D Re_p}{24} \tag{3.26}$$

$$C_D = \begin{cases} \frac{24\left(1+0.15 Re_p^{0.687}\right)}{Re_p} & Re_p \le 1000 \\ 0.44 & Re_p > 1000 \end{cases} \tag{3.27}$$

$$Re_p = \frac{\rho_q \left|\vec{V}_p - \vec{V}_q\right| d_p}{\mu_q} \tag{3.28}$$

where q and p indicates the base fluid and the nanoparticles phases respectively. For nanofluids, the virtual mass effect ($\vec{F}_{vm,q}$) can be neglected because the secondary

University of Malaya

phase (nanoparticles) density is much greater than the primary phase (base fluid) density. Moreover, the inclusion of lift force ($\vec{F}_{lift,q}$) is not appropriate for nano-sized particles. It was shown that particle–particle interaction force ($\vec{F}_{collision}$) does not have any effect on the average Nusselt number (Kalteh et al., 2011). Therefore, it is possible to ignore the particle–particle interaction force for nanofluid in the mathematical modelling.

Conservation of energy:

$$\nabla.\left(\rho_q \varphi_q c_{p,q} T_q \vec{V}_q\right) = \nabla.\left(\varphi_q k_{eff,q} \nabla T_q\right) + \sum_{p=1}^{2} Q_{pq} \quad (3.29)$$

where $Q_{pq} = h\left(T_p - T_q\right)$ and the heat exchange coefficient is $h = \frac{6 k_q \varphi_q \varphi_p Nu_p}{d_p^2}$. Nu_p is calculated from the Ranz and Marshall model (Ranz & Marshall, 1952):

$$Nu_p = 2 + 0.6 Re_p^{0.5} Pr_q^{0.333} \quad (3.30)$$

where $Pr_q = \left(C_{p,q}\mu_q\right)/k_q$

The effective thermal conductivity ($k_{eff,q}$) is estimated for liquid and particle phases as:

$$k_{eff,l} = \frac{k_{b,l}}{\varphi_l}, \quad (3.31)$$

$$k_{eff,p} = \frac{k_{b,p}}{\varphi_p}, \quad (3.32)$$

where

$$k_{b,l} = \left(1 - \sqrt{(1-\varphi_l)}\right) k_l, \quad (3.33)$$

$$k_{b,p} = \sqrt{(1-\varphi_l)}(\omega A + [1-\omega]\Gamma) k_l\,, \quad (3.34)$$

and

$$\Gamma = \frac{2}{\left(1-\frac{B}{A}\right)}\left\{\frac{B(A-1)}{A\left(1-\frac{B}{A}\right)^2}\ln\left(\frac{A}{B}\right) - \frac{(B-1)}{\left(1-\frac{B}{A}\right)} - \frac{B+1}{2}\right\} \quad (3.35)$$

with

$$B = 1.25\left(\frac{|1-\varphi_l|}{\varphi_l}\right)^{10/9} \quad (3.36)$$

For spherical particles we have

University of Malaya

$$A = \frac{k_p}{k_l} \text{ and } \omega = 7.26 \times 10^{-3} \quad (3.37)$$

3.2.3.2.2 Mixture Model

The mixture model is employed in the simulation by assuming that the coupling between phases is strong, and the particles closely follow the flow. Each phase has its own velocity vector field, and within any control volume there is a volume fraction of primary phase and also a volume fraction of the secondary phase. Instead of utilizing the governing equations of each separately, the continuity, momentum and energy equations for the mixture are employed. A nanofluid composed of water and Cu nanoparticles flowing in a long tube with uniform heating at the wall boundary is considered. Therefore, the dimensional equations for steady state mean conditions are (Behroyan et al., 2015):

Conservation of mass:

$$\nabla.\left(\rho_m \vec{V}_m\right) = 0 \quad (3.38)$$

Conservation of momentum:

$$\nabla.\left(\rho_m \vec{V}_m \vec{V}_m\right) = -\nabla P_m + \mu_m \nabla^2 \vec{V} + \nabla.\left(\sum_{k=1}^{n} \varphi_k \rho_k \vec{V}_{dr,k} \vec{V}_{dr,k}\right) \quad (3.39)$$

where $\vec{V}_{dr,k}$ is the drift velocity of the kth phase.

Volume fraction:

$$\nabla.\left(\varphi_p \rho_p \vec{V}_m\right) = -\nabla.\left(\varphi_p \rho_p \vec{V}_{dr,p}\right) \quad (3.40)$$

Conservation of energy:

$$\nabla.\left(\sum_{k=1}^{n} \rho_k \phi_k c_{p,k} T_k \vec{V}_k\right) = \nabla.\left(k_{eff} \nabla T\right) \quad (3.41)$$

In the momentum conservation Equation (3.39) $\vec{V}_{dr,k}$ is the drift velocity for secondary phase k (i.e., the nanoparticles) defined as:

$$\vec{V}_{dr,k} = \vec{V}_k - \vec{V}_m \quad (3.42)$$

The slip velocity (relative velocity) is defined as the velocity of secondary phase (*p*) relative to the velocity of the primary phase (*f*):

University of Malaya

$$\vec{V}_{pf} = \vec{V}_p - \vec{V}_f \quad (3.43)$$

The drift velocity is related to the relative velocity:

$$\vec{V}_{dr,p} = \vec{V}_{pf} - \sum_{k=1}^{n} \frac{\varphi_k \rho_k}{\rho_m} \vec{V}_{fk} \quad (3.44)$$

The relative velocity is determined from Equation (3.44) proposed by Manninen et al. (1996).

$$\vec{V}_{pf} = \frac{\rho_p d_p^2}{18 \mu_f f_{drag}} \frac{(\rho_p - \rho_m)}{\rho_p} a \quad (3.45)$$

The acceleration in Equation (3.45) is:

$$a = g - (\vec{V}_m . \nabla)\vec{V}_m \quad (3.46)$$

In two-phase models with the Eulerian-Eulerian points of view, the viscosity of the second phase, i.e., solid viscosity is required. A value of 1.38×10^{-3} Pa.s suggested by Kalteh et al. (2011) is adopted in this study for the Eulerian model and mixture model1.

For mixture model 1, the effective viscosity and conductivity are calculated using simply volume weighted summation by referring to the references of (Akbari et al., 2012; Behzadmehr et al., 2007; Lotfi et al., 2010) and (Mojarrad et al., 2013; Nuim Labib et al., 2013) respectively. Whereas, in mixture model 2, Equations (3.3) − (3.4) and Equations (3.11) − (3.12) are respectively implemented in the calculation of effective conductivity and viscosity.

3.2.3.2.3 Discrete Phase (Eulerian-Lagrangian) Model

The two-way coupling Eulerian-Lagrangian model has been used in this study. This two-way coupling is accomplished by alternately solving the discrete phase (nanoparticles) and continuous phase (base fluid) equations until the solutions in both phases have stopped changing. The governing equations of the continuous phase are the same as Equations (3.5) − (3.7). Considering the momentum and heat exchanges between the nanoparticle phase and the continuous phase, the sink/source terms S_m and

University of Malaya

S_e are added to the conservation of momentum and energy equations respectively (Bianco et al., 2009; Fluent, 2009). The momentum transfer between the particles and base fluid is calculated as:

$$S_m = \frac{1}{\delta V}\sum_{np}\vec{F} \tag{3.47}$$

In the Lagrangian frame of reference, the equation of motion of the particles is given by Equation (3.48) as (Mirzaei et al., 2014):

$$m_p\frac{d\vec{V}_p}{dt} = \vec{F}_d + \vec{F}_L + \vec{F}_T + \vec{F}_B + \frac{g(\rho_p-\rho_l)}{\rho_p} \tag{3.48}$$

The left hand side of Equation (3.48) $\vec{V}_p$ is the velocity of the particle and the right hand side of that represents the forces acting on the particle which are drag, Saffman's lift, thermophoretic and Brownian forces, respectively.

Because of low nanoparticle Reynolds number ($Re_{np} < 1$), the viscous drag force is relevant which can be calculated by the Stokes law (Mirzaei et al., 2014):

$$\vec{F}_d = \frac{\pi}{8}\rho_{bf}d_p^2\frac{C_D}{C_C}V_{rel}\vec{V}_{rel} \tag{3.49}$$

where C_D is calculated from Equation.(3.27) and $C_C$is the Cunningham factor which should be considered for submicron particles as (Bahiraei & Hosseinalipour, 2013b):

$$C_C = 1 + \frac{2\lambda}{d_p}\left(1.257 + 0.4e^{1.1d_p/2\lambda}\right) \tag{3.50}$$

Saffman's lift force is important near walls because of the vorticity vector $\vec{\omega}$. The following equation is provided by Saffman (Mirzaei et al., 2014) to calculate this force in shear fields:

$$\vec{F}_L = \frac{6.46}{4}\rho_{bf}d_p^2\sqrt{\frac{\mu_{bf}}{\rho_{bf}}}\frac{1}{\sqrt{\omega}}\left(\vec{V}_{rel}\times\vec{\omega}\right) \tag{3.51}$$

The thermophoretic force can be calculated as:

$$\vec{F}_T = -6\pi\mu_{bf}^2 d_p C_s \frac{1}{\rho_{bf}(1+6C_mKn)}\frac{k_{bf}/k_p+2C_tKn}{1+2k_{bf}/k_p+4C_tKn}\frac{\nabla T}{m_p T} \tag{3.52}$$

where $C_s = 1.17$, $C_m = 2.28$, $C_t = 4.36$, and Kn is Knudsen number is calculated from the following correlation:

University of Malaya

$$Kn = \frac{\lambda}{d_p} \tag{3.53}$$

For a nanofluid with suspended nanoparticles of 1 to 100 *nm*, the Knudsen number would be obtained smaller than 0.3, thus the fluid phase surrounding the nanoparticles could be taken as continuum in an Eulerian frame. Brownian force can be modelled by a Gaussian white noise random process with intensity of S_0 (Mirzaei et al., 2014).

$$S_0 = \frac{216\nu k_B T}{\pi^2 \rho_{bf} d_p^5 (\rho_p/\rho_{bf})^2 C_C} \tag{3.54}$$

So:

$$\vec{F}_B = G\sqrt{\frac{\pi S_0}{\Delta t}} \tag{3.55}$$

where, G is the zero mean, unit variance independent Gaussian random number. The same approach used for momentum equation can be employed for the energy equation and for spherical particles the following equation is obtained as (Mirzaei et al., 2014):

$$\rho_p C_{p,p} \frac{dT_p}{dt} = \frac{6h_p}{d_p}(T - T_p) \tag{3.56}$$

The energy source term would be the heat transfer between the phases as:

$$S_e = \frac{1}{\delta V}\sum_{np} Nu_p \pi d_p k_p (T - T_p) \tag{3.57}$$

where h_p or Nu_p are calculated from the Ranz and Marshall's correlation (Ranz & Marshall, 1952).

3.2.4 Boundary Conditions

At the tube inlet section, a uniform axial velocity (V_0) based on the Reynolds number and the profile temperature of $T_0 = 295$ K, are assumed. Moreover, for the two-phase flow, the velocity of particles is assumed the same as that of the base fluid at the pipe inlet. At the tube exit section, velocity components and temperature derivatives are considered equal to zero. On the tube wall, non-slip conditions and uniform heat flux of $2000\ W/m^2$ are imposed.

University of Malaya

3.2.5 Numerical Method and Validation

The numerical methods available in the commercial CFD package of Ansys Fluent, V14 (Fluent, 2009) have been used for the current study. Fluent uses a finite volume approach to convert the governing partial differential equations into a system of discrete algebraic equations (Fluent, 2009). As discretization methods, a second-order upwind scheme is selected for the momentum and the energy equations. All these conditions are the same for governing equations of both single and two-phase models. For conductivity, viscosity and dispersion conductivity models, codes are developed to incorporate the Ansys-Fluent case file using User Defined Function (UDF) (Fluent, 2009).

The SIMPLE coupling algorithm is selected for the single phase in order to couple pressure and velocity. For Eulerian two-phase calculations, the phase momentum equations with the shared pressure are solved in a coupled and segregated fashion. The phase coupled SIMPLE (PC-SIMPLE) algorithm is employed for the pressure-velocity coupling. PC-SIMPLE is an extension of the SIMPLE algorithm to multiphase flows. The velocities are solved coupled by phases but in a segregated fashion. The scaled residuals for the velocity components and energy are set equal to10^{-8} and 10^{-9}, respectively.

The meshing tool available in Ansys is used to construct the computational mesh. A structured mesh based on a rectangular grid is used throughout the domain (Figure 3.2). A grid independence test was performed for the tube using water as working fluid to analyse the effects of grid size on the results. Four sets of mesh are considered, which are 35,553 nodes, 45,378 nodes, 69,876 nodes, and 74,705 nodes with a Reynolds number of 1600. By comparing the fourth and third mesh configurations, in terms of the average Nusselt number, the corresponding percentage

University of Malaya

relative error is 0.02%. Therefore, the third grid case has been adopted to obtain an acceptable compromise between the computational time and the results accuracy.

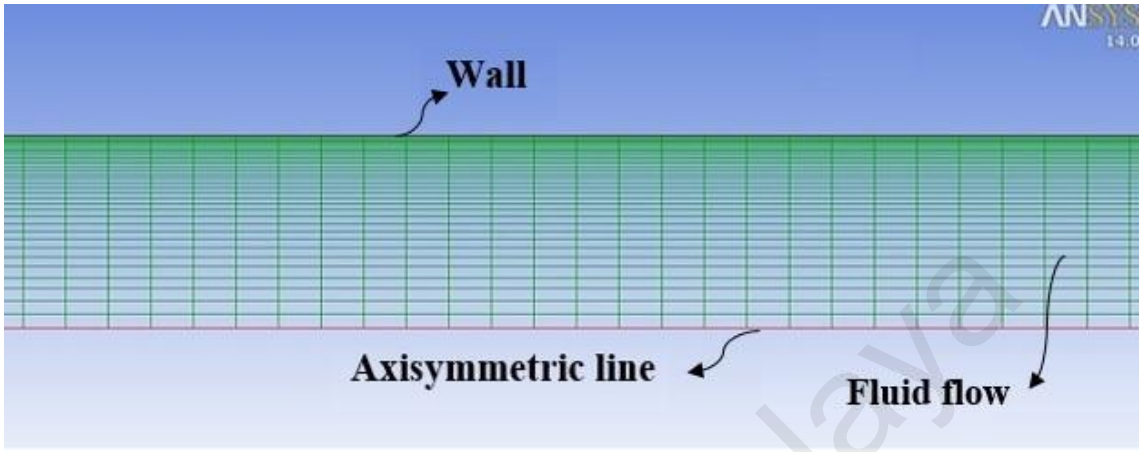

Figure 3.2: A sample mesh structure for modelling of laminar forced convection

In order to establish accuracy and reliability of the numerical model, the predicted local Nusselt number for laminar forced convection of distilled water flow inside a tube with constant wall heat flux has been benchmarked against Shah Correlation (Bejan & Kraus, 2003). The correlation is as follows:

$$\mathrm{Nu} = \begin{cases} 1.953\left(\mathrm{RePr}\frac{\mathrm{D}}{\mathrm{x}}\right)^{1/3} & \left(\mathrm{RePr}\frac{\mathrm{D}}{\mathrm{x}}\right) \geq 33.3 \\ 4.364 + 0.0722\mathrm{RePr}\frac{\mathrm{D}}{\mathrm{x}} & \left(\mathrm{RePr}\frac{\mathrm{D}}{\mathrm{x}}\right) < 33.3 \end{cases} \tag{3.58}$$

The axial variation of the Nusselt number along the tube are shown in Figure 3.3 at Re=1600. The predicted Nusselt number by the CFD model shows a good agreement with Shah Equation with a maximum error of 8%. This seems presumably good because Shah Equation was derived for large channels (Bejan & Kraus, 2003; Rashidi & Nezamabad, 2011; Shah, 1979).

University of Malaya

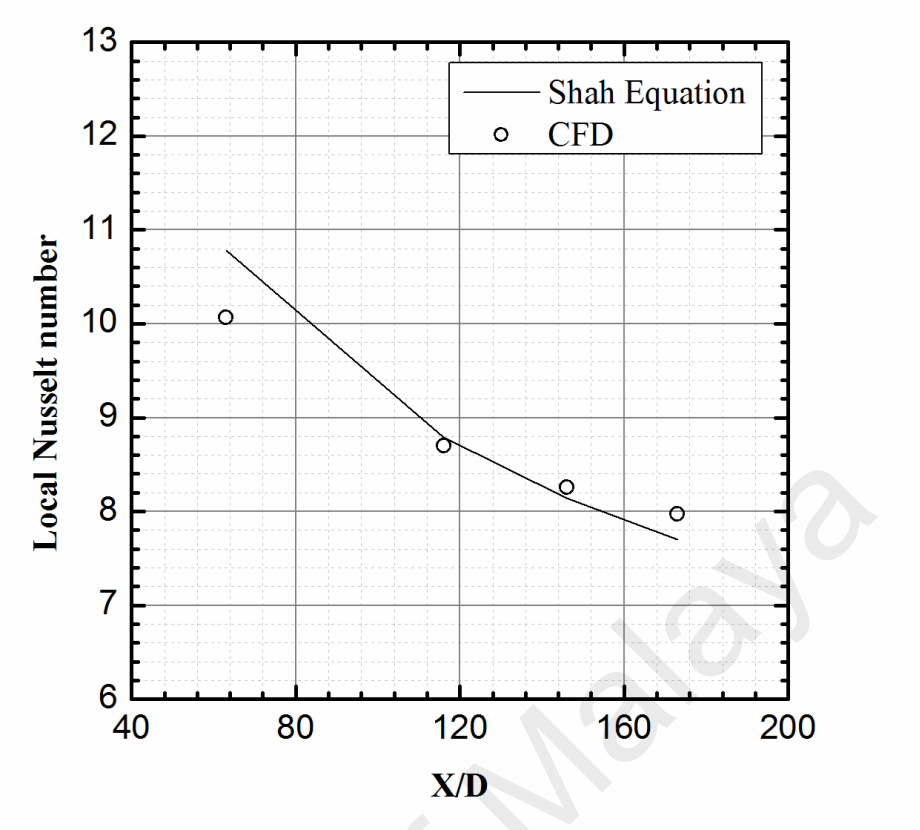

Figure 3.3: Validation of the simulation results of the local Nusselt number with Shah Equation (Bejan & Kraus, 2003) along axial direction for water at Re=1600.

3.2.6 Simulation Cases

Table 3.3 shows different simulation cases which have been investigated in the present study. Initially, the laminar forced convection of Al_2O_3-water nanofluid is simulated by use of different single- and two-phase models for Re=1600 and φ=1.6% (cases 1–8). The Newtonian single-phase (NSP) and non-Newtonian single-phase (non-NSP) models are employed for the first two cases. Next, dispersion model 1(DM 1) and dispersion model2 (DM 2) are considered for non-NSP model (cases 3 and 4). A similar simulation is done using the two-phase approaches of mixture 1, mixture 2, Eulerian and discrete phase model (DPM) for cases 5–8. Simulation cases 1–8 are carried out to find the error of each model in prediction of the local Nu number. The influence of nanoparticle volume fraction (0.6–2%) on Nu number prediction and temperature profiles in axial and radial directions are investigated in cases 9–14, using the non-NSP

University of Malaya

(DM1) model and the DPM at Re=1600. Finally, the effect of Re number, ranging from 745 to1600, is assessed to evaluate the local Nu number at the fixed value of 1.6% volume fraction in cases 15–20.

Table 3.3: The simulation table for different cases changing in CFD model, Re number and φ

Cases		Model	Changing Parameters	Purpose
$1-4$	Single-Phase	• NSP • Non-NSP • Non-NSP(DM1) • Non-NSP(DM2)	Re=1600 $\varphi = 1.6\%$	Different models validation
$5-8$	Two-Phase	• Mixture 1 • Mixture 2 • Eulerian • DPM	$x/D = 63-173$	
$9-14$		• Non-NSP(DM1) • DPM	Re=1600 $\varphi = 0.6\%-2\%$ $x/D = 63-173$	Volume fraction influence
$15-20$		• Non-NSP(DM1) • DPM	$Re = 745-1600$ $\varphi = 1.6\%$ $x/D = 63-173$	Re number influence

NSP=Newtonian Single-Phase, Non-NSP=Non-Newtonian Single-Phase, DM1=Dispersion Model1 (Equation (3.22)), DM2=Dispersion Model2 (Equation (3.23)), DPM=Discrete Phase Model

University of Malaya

3.3 Results and Discussion

There are two correlations available in the literature which have been proposed based on the experimental data for developing laminar forced convection of nanofluid throughout a horizontal tube with a constant heat flux on the walls, namely Anoop's correlation (Anoop et al., 2009) and Velagapudi's correlation (Velagapudi et al., 2008). It was shown that the first correlation falls in the region of ±20% deviation compared to the corresponding experimental data. The second correlation showed a maximum average deviation of 2% and standard deviation of 4% from the experiment and was built with greater amount of experimental data. Thus, the accuracy of four single- and five two-phase models in prediction of the Nusselt number are benchmarked against the correlation given by Velagapudi et al (2008). Equation (3.59) shows the proposed correlations by Velagapudi et al. (2008) as below:

$$\mathrm{Nu} = 1.98\left(\mathrm{Re}_{\mathrm{nf}}\mathrm{Pr}_{\mathrm{nf}}\frac{\mathrm{D}}{\mathrm{x}}\right)^{1/3} \tag{3.59}$$

Referring to Figure 3.4, the local Nusselt number prediction of different single-phase models is benchmarked against Velagapudi et al. correlation for 1.6% Al_2O_3-water at Re=1600. Besides, for better comparison, the error of each model at different axial positions is highlighted in Table 3.4.

University of Malaya

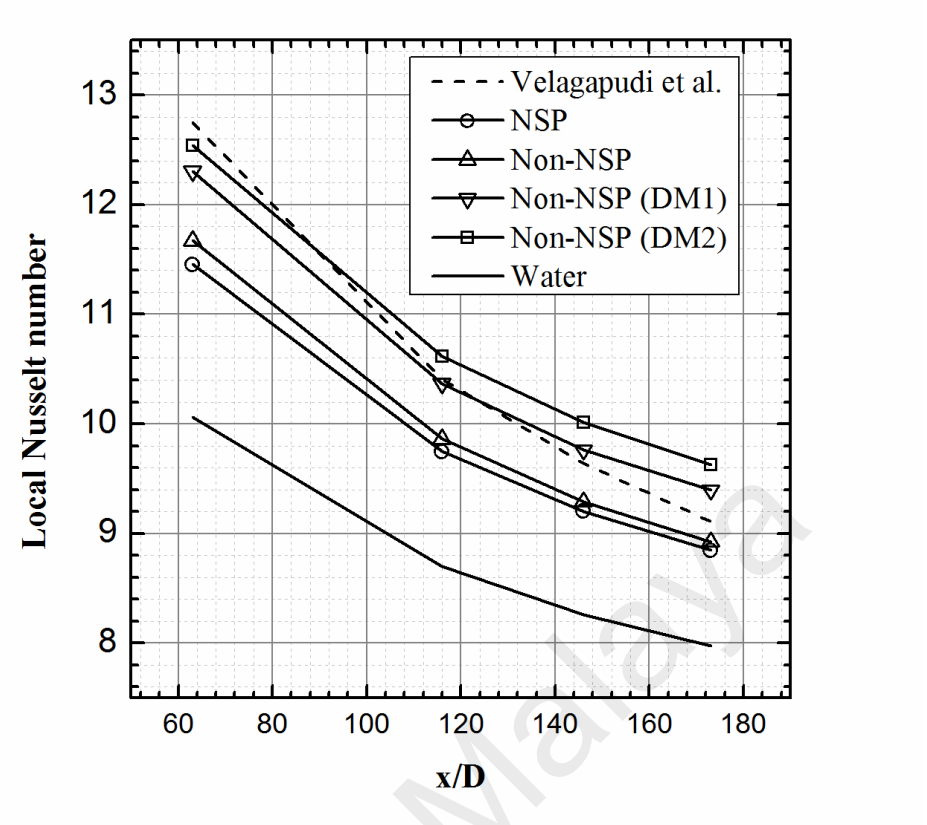

Figure 3.4: Comparison of single-phase models with Velagapudi et al. (Velagapudi et al., 2008) for 1.6%Al_2O_3/water nanofluid at Re=1600.

Table 3.4: Error in local Nusselt number use of various single-phase models for 1.6% Al_2O_3/water at Re=1600.

Model	X/D=63	X/D=116	X/D=146	X/D=173	Min_Error	Max_Error	Ave_Error
NSP	-10.19	-6.33	-4.54	-2.87	2.87	10.19	5.98
Non-NSP	-8.48	-5.21	-3.61	-2.04	2.04	8.48	4.84
Non-NSP(DM1)	-3.52	-0.37	1.28	3.13	0.37	3.52	2.07
Non-NSP(DM2)	-1.68	2.03	3.91	5.71	1.68	5.71	3.33

All single-phase models predict a significant improvement of Nu number in comparison to pure water. Comparing NSP and non-NSP, similarly both models underestimate the Nusselt number and the error decreases with the increase of axial location. The underestimation of single-phase modelling is caused by neglecting the slip

University of Malaya

mechanisms between ultrafine nanoparticles and the base fluid. Non-Newtonian rheology shows less average error than that of the Newtonian, decreasing from 5.98 % to 4.84%. Since the non-NSP model shows better prediction, this rheology is considered for the nanofluid for further investigations of the single-phase model. Underestimation of non-NSP model in prediction of the Nusselt number may be improved by considering the dispersion effect of nanoparticles among the host fluid. Employing the dispersion models, the average error decreased from 4.84% to 2.07% and 3.33%, for DM1 and DM2 respectively. Therefore, DM1, which uses dispersion conductivity formulation given by Equation (3.22), is more accurate in predicting Nu number compared to DM2, which uses formulation given by Equation (3.23).

The local Nusselt number predictions using various two-phase models along with their corresponding errors for 1.6% Al_2O_3/water at Re=1600 are shown in Figure 3.5 and Table 3.5 respectively. Mixture1 and mixture2 underestimate Nusselt number values, and the errors of the models decrease with increase of axial location. Mixture model 1 shows the largest prediction error among the other two-phase models as well as the single-phase models. Anomalously, the local Nusselt number which is predicted by this model is even less than that of water. It may be caused by simply using a volume weighted summation model for the calculation of effective conductivity and viscosity. Using Equations (3.3) − (3.4) and (3.11) − (3.12) to calculate the effective conductivity and viscosity for mixture model 2, the average error decreases from 17.57% in model1 to 5.87% in model2. It should be noted that mixture model 2 shows nearly the same error as NSP model in all positions along the tube. This mixture model considers only the drag force as a slip mechanism, resulting in a very small value of drift velocity ($V_{dr} \approx 0$) between the fluid and the nanoparticles. Thus, the governing equations based on the both CFD modelling give similar results. In the other words, once the value of the drift velocity tends to zero, mixture model behaves the same as the NSP model.

University of Malaya

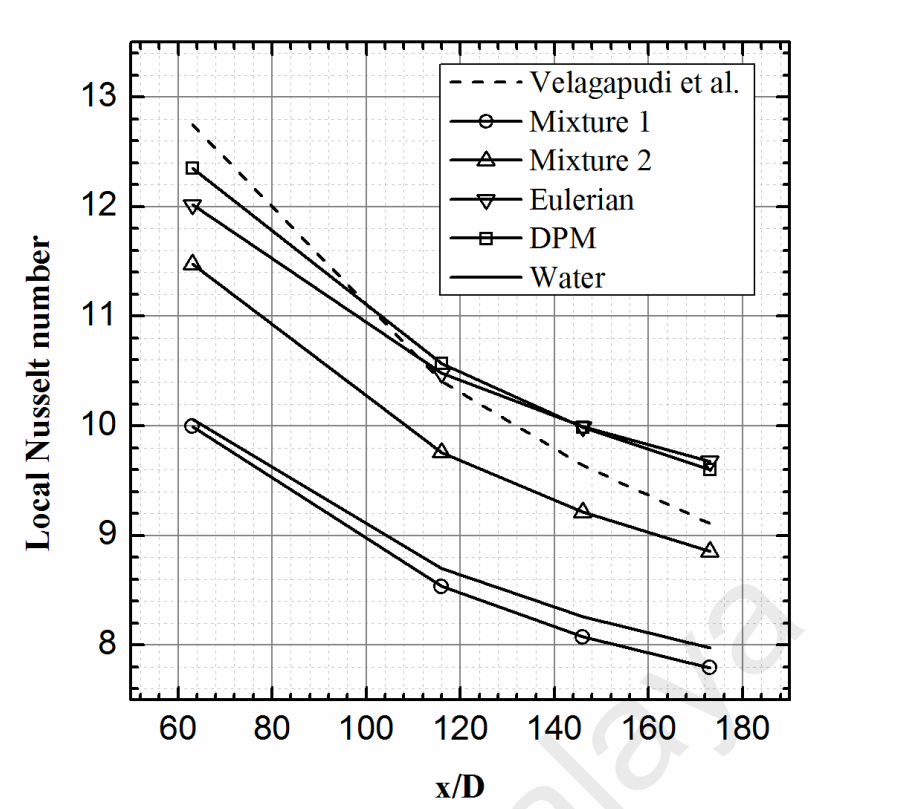

Figure 3.5: Comparison of two-phase models with Velagapudi et al. (Velagapudi et al., 2008) for 1.6%Al_2O_3/water nanofluid at Re=1600.

Table 3.5: Error in local Nusselt number use of various two-phase models for 1.6% Al_2O_3/water at Re=1600.

Model	X/D=63	X/D=116	X/D=146	X/D=173	Min_Error	Max_Error	Ave_Error
Mixture1	-21.62	-17.99	-16.23	-14.45	14.45	21.62	17.57
Mixture2	-10.01	-6.24	-4.41	-2.81	2.81	10.01	5.87
Eulerian	-0.58	0.69	3.66	6.22	0.58	6.22	2.79
DPM	-0.32	1.57	3.63	5.41	0.32	5.41	2.73

The Eulerian model shows the average error of 2.79%, less than mixture model 2 with the error of 5.87%. The error of the Eulerian model may be caused by adoption of the improper effective nanoparticle conductivity used in the model. Since there is no specific correlation to calculate the effective nanoparticle conductivity, Equations (3.31)−(3.37) which were originally developed to estimate the effective radial thermal conductivity in pack beds (Kuipers et al., 1992) and employed by many researchers for nanofluids (Akbari et al., 2012; Hejazian et al., 2014b; Kalteh et al., 2012; Kalteh et al., 2011) have been used in this study. Table 3.6 shows the values of effective nanoparticle

University of Malaya

conductivity for fraction of 0.6%, 1% and 1.6%. Unexpectedly, the solidus conductivity decreases with increasing the nanoparticle conductivity. The DPM model has the least error in comparison to the other two-phase models (average error of 2.73%). The error of both Eulerian and DPM models increases with position along the tube in most of the cases.

Table 3.6: The values of effective nanoparticle conductivity based on Kuipers et al. (Kuipers et al., 1992) correlations.

Φ	$K_{eff,p}$(W/m.^{0}C)
0.6%	11.67
1%	9.30
1.6%	7.66

According to the above comparisons, the non-NSP model using dispersion model 1 (DM 1) and DPM can be selected as the most accurate approaches. Some additional investigations are needed to check the models accuracy in the other Re numbers and volume fractions of the nanofluid. Table 3.7 shows the error of local Nusselt number predicted by non-NSP DM 1 and DPM models at different axial positions and Re= 1600 for the nanofluid volume fraction of 0.6%, 1.6% and 2%. Generally, both models underestimate Nu number (negative error) at the initial position (x/D=63) and the error either tends to zero or positive with increasing the axial position. Once the error becomes positive, the error increases with increasing X/D. Non-NSP DM 1 shows greater average error than DPM for 0.6% Al_2O_3-water nanofluid (4% compared to 2.87%). On the contrary the average errors of non-NSP (DM 1) are less than DPM for the other fractions.

University of Malaya

Table 3.7: Error in local Nusselt number using Non-NSP (DM1) and DPM at Re=1600 for different volume fractions (φ=0.6%, 1.6% and 2%).

Φ	Model	X/D=63	X/D=116	X/D=146	X/D=173	Ave_Error
0.6%	Non-NSP(DM1)	-2.04	2.55	4.74	6.67	4
	DPM	-7.15	-2.44	-0.33	1.56	2.87
1.6%	Non-NSP(DM1)	-3.52	-0.37	1.28	3.13	2.08
	DPM	-3.17	1.57	3.63	5.41	3.45
2%	Non-NSP(DM1)	-1.18	1.48	2.76	4.36	2.45
	DPM	-2.48	1.66	3.38	4.93	3.11

Figure 3.6a shows wall and mean temperatures along the tube axis for Re = 1600, the nanoparticle volume fractions of 0%−2% and $q'' = 2000$ W/m^2 for non-NSP DM 1 and DPM models. As could be expected, as the nanoparticle volume fraction increases the wall and the mean temperature decrease. It can also be observed that the wall and balk temperature profiles for the nanofluid in comparison with the base fluid are diverged with the x-coordinate. For a volume fraction of 0.6%, wall temperature for DPM is higher than the one for non-NSP DM 1, whereas the mean temperature for both models are very similar. However, by increasing the volume fraction to 2%, both models predict the same wall and mean temperatures. In Figure 3.6b, the radial temperature is displayed at $X/D = 173$ for the same boundary conditions and for both models. It is found that the temperature is strongly dependent upon the nanoparticle volume fraction. When the volume fraction increases, fluid temperature decreases quickly, especially near the tube wall. Moreover, the difference between temperature values, for the host liquid and nanofluid, increases with *r* increment. This means that higher heat transfer rate is obtained by use of the nanoparticles. For φ = 0.6%, DPM and non-NSP DM 1 give the same temperature profile. However, for φ = 2%, non-NSP DM 1 gives a higher temperature profile than DPM, expect for $r = 0$ and $r = 2.25$ mm where the same temperature values are observed by employing the both models.

University of Malaya

(a)

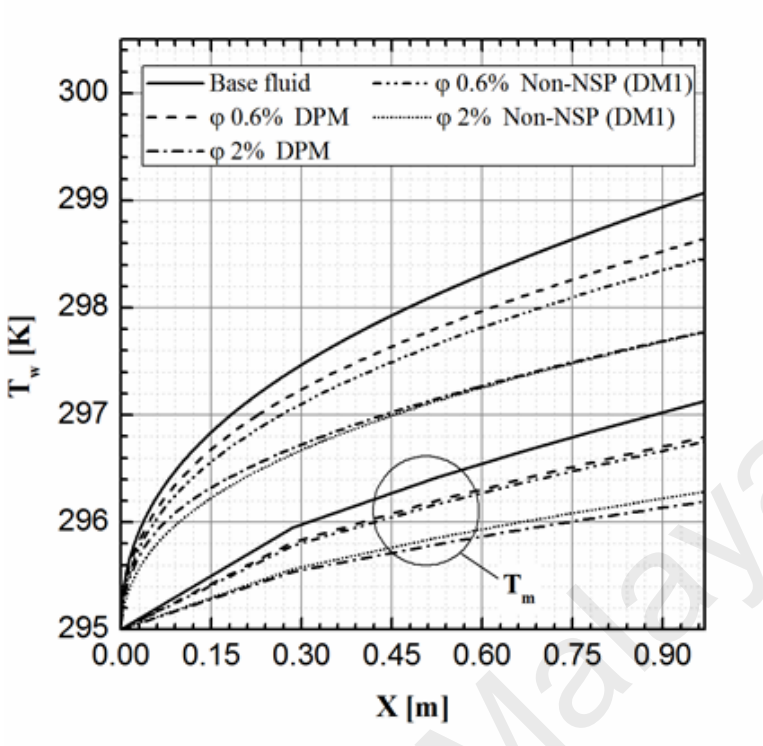

(b)

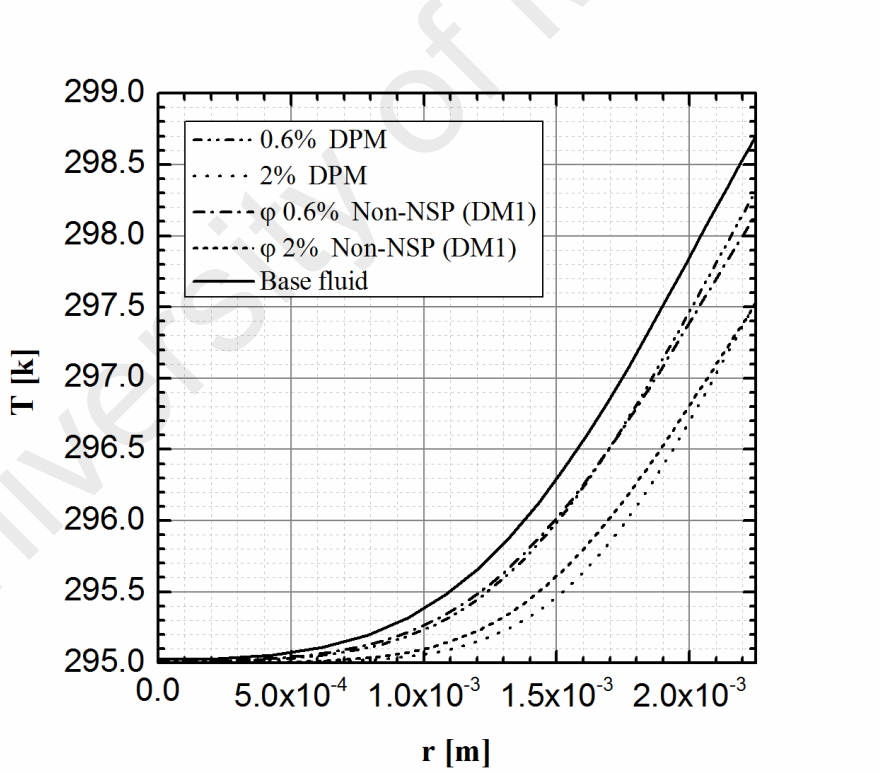

Figure 3.6: Effect of particle loading, for Re=1600, on: (a) the axial development of wall and bulk temperature and (b) on the radial temperature at X/D=173.

University of Malaya

Table 3.8 shows the local Nusselt number predicted by non-NSP DM 1 and DPM models at different axial positions and different Re numbers (e.g. 745, 1200 and 1600) for the nanofluid volume fraction of 1.6%. Totally, the average error of Non-NSP DM 1 is less than DPM at all Re numbers. In addition, the error values decrease with the raise of Re number in almost all positions.

Table 3.8: Error in local Nusselt number using Non-NSP (DM1) and DPM for 1.6% Al_2O_3/water nanofluid at different Reynolds numbers of 745, 1200 and1600

Re	Model	X/D=63	X/D=116	X/D=146	X/D=173	Ave_Error
745	Non-NSP(DM1)	-2.66	3.48	6.50	9.23	5.47
	DPM	-1.48	4.59	7.44	9.97	5.87
1200	Non-NSP(DM1)	-3.84	0.50	2.63	4.53	2.88
	DPM	-2.20	3.20	5.52	5.52	4.11
1600	Non-NSP(DM1)	-3.52	-0.37	1.28	3.13	2.08
	DPM	-3.17	1.57	3.63	5.41	3.45

3.4 Conclusions

In the present paper, a steady state laminar convection of water/Al_2O_3 nanofluid inside a circular tube was investigated numerically using the commercial Ansys-Fluent codes. Different single- and two-phase CFD models were taken into account for the simulation cases. Several UDF codes are written to define the thermal conductivity model, the dynamic viscosity model, the dispersion models and the non-Newtonian rheology for the nanofluids. The UDF codes are incorporated with the single- and two-phase CFD models. The validity of the CFD models was assessed by the correlation given in Ref. (Velagapudi et al., 2008). The conclusions of this study are drawn as follows:

- Both NSP and Non-NSP models underpredict the Nu number.
- The non-NSP model predicts a more accurate Nusselt number than NSP, with the average errors of 5.98% and 4.84% respectively.

University of Malaya

- Employing the dispersion models, the average error decreased from 4.84% to 2.07% and 3.33%, for DM1 and DM2 respectively.
- Both mixture1 and mixture2 underestimate Nusselt number values; Mixture 1 shows the largest prediction error and the predicted Nusselt number by this model is even less than that of water, while mixture2 behaves similar to the NSP model in prediction of the Nusselt number.
- The Eulerian model shows the average error of 2.79%., whereas DPM model has the least average error of 2.73%.
- Heat transfer increased with the particles volume concentration and Reynolds number.
- The results, in terms of wall and mean temperature, given by non-NSP (DM1) and DPM were approximately similar.

University of Malaya

4 CHAPTER 4: MODELLING ON TURBULENT FORCED CONVECTION OF NANOFLUID

4.1 Introduction

CFD analysis of various modeling approaches is presented in this chapter to investigate the turbulent forced convection flow of Cu-water nanofluid in a heated tube. The CFD results will be benchmarked against those from the experimental investigations of Xuan and Li (2003) for the same testing fluid and conditions. The deviation in the Nusselt number will be reported for each and every model which gives insight to strengths and weaknesses of each approach. This study benefits when comes to selecting a suitable model for a similar type case study. Further investigations are also done to probe the accuracy improvement of the Eulerian CFD model in prediction of the nanofluid heat transfer.

4.2 Methodology

At the first step, a comprehensive comparison of CFD analysis of various modeling approaches, including two types of single-phase modelling approaches (i.e., Newtonian and non-Newtonian) and three types of the two-phase models (i.e. Eulerian-Eulerian, mixture and Eulerian-Lagrangian), will be done. The effect of the different interphase interactions (i.e. the drag force, Brownian motion, lift force, virtual mass and heat transfer) between the base fluid, and the solidus phase (nanoparticles) is considered in the two-phase CFD models (Section 4.3.1).

Modifications to the single-phase model have been suggested by many researchers (Corcione, 2011; Kumar et al., 2010; Masoumi et al., 2009; Özerinç et al., 2010) through developed effective thermo-physical properties. However, this is not the case for the two-phase model. Therefore, in the next step, the present study will focus on the E-E two-phase model improvements for an accurate prediction of the Nusselt number. The parameters which play the crucial role in the nanofluid heat transfer

University of Malaya

prediction in the E-E two-phase model will be identified. So, the accuracy of the existing formulations from the literature for viscosity and effective particle conductivity of the solidus phase in E-E two-phase models will be assessed (Section 4.3.2).

4.2.1 Geometry Structure

A cylindrical tube in a horizontal position of dimensions of 0.01m in diameter and 1m in length is considered in the current study. A constant heat flux is applied to the tube wall (Figure 3.1). The two-dimensional (2D) axisymmetric geometry has been taken into consideration. Therefore, the simulation domain is limited to a rectangle with dimensions of 0.005×1 m^2.

4.2.2 Governing Equations

In turbulent forced convection the general form of governing equations are similar to the laminar ones (see Section 3.2.3). However, the parameters of turbulent viscosity μ_t and turbulent conductivity k_t must be added to the dynamic viscosity in the momentum equation and to the thermal conductivity in energy equation respectively. These parameters are calculated by the standard *k*-ε model is employed according to Launder and Spalding (1974), which is

$$\nabla.(\rho k V) = \nabla.[(\frac{\mu_t}{\sigma_k})\nabla(k)] + G_k - \rho\varepsilon \tag{4.1}$$

$$\nabla.(\rho \varepsilon V) = \nabla.[\frac{\mu_t}{\sigma_\varepsilon}\nabla\varepsilon] + \frac{\varepsilon}{k}(C_{1\varepsilon}G_k - C_{2\varepsilon}\rho\varepsilon) \tag{4.2}$$

$$G_k = \mu_t(\nabla V + (\nabla V)^T),\ \mu_t = \rho C_\mu \frac{k^2}{\varepsilon} \tag{4.3}$$

$$C_\mu = 0.09, \sigma_k = 1.00, \sigma_\varepsilon = 1.30, C_{1\varepsilon} = 1.44, C_{2\varepsilon} = 1.92 \tag{4.4}$$

$$k_t = \frac{C_p \mu_t}{\mathrm{Pr}_t},\ \mathrm{Pr}_t = 0.8 \tag{4.5}$$

University of Malaya

4.2.3 Nanofluids Thermophysical Properties

The effective thermal conductivity of fluid has been determined by the temperature dependent model proposed by Patel et al. (2006) and used by the literature (Santra et al., 2008, 2009). The details of the correlation are given as follows;

$$\frac{k_{eff}}{k_f} = 1 + \left(\frac{k_s A_p}{k_f A_f}\right)(1 + c.Pe) \tag{4.6}$$

where $\frac{A_p}{A_f} = \frac{d_f}{d_p}\frac{\phi}{(1-\phi)}$, $Pe = \frac{u_b d_p}{\alpha_f}$ and c =25,000. α_f is the thermal diffusivity of base fluid. u_b indicates the Brownian motion velocity of the nanoparticles which is given by

$$u_b = \frac{2k_b T}{\pi \mu_f d_p{}^2} \tag{4.7}$$

where K_b is the Boltzmann constant. For temperature dependent viscosity, the correlation purposed by Masoumi et.al (2009) has been used in this study. The details of the correlation are given as follows;

$$\mu_{nf} = \mu_f + \frac{\rho_p V_B d_p^2}{72C\delta} \tag{4.8}$$

where V_B , δ and C are Brownian velocity, distance between the nanoparticles and correction factor respectively. In addition V_B , C and δ are defined as follows:

$$C = \mu_{bf}^{-1}[(c_1 d_p + c_2)\varphi + (c_3 d_p + c_4)] \tag{4.9}$$

$$c_1 = -0.000001133,\ c_2 = -0.000002771$$
$$c_3 = 0.00000009,\quad c_4 = -0.000000393$$

$$V_B = \frac{1}{d_p}\sqrt{\frac{18k_B T}{\pi \rho_p d_p}} \tag{4.10}$$

$$\delta = \sqrt[3]{\frac{\pi}{6\phi}}\, d_p \tag{4.11}$$

where k_B represents Boltzmann constant. The nanofluid viscosity is predicted by this model as a function of temperature, mean particle diameter, particle volume fraction,

University of Malaya

density of particle and the base fluid physical properties. The thermal conductivity and dynamic viscosity calculated by the above correlations at ambient temperature show less than 1 % deviation from the experimental data from literature (Xuan & Li, 2003). User Define Function (UDF) codes are written to define Equations (4.6) – (4.7) and Equations (4.8) – (4.11) for the effective thermal conductivity and the effective dynamic viscosity of the nanofluid respectively. The UDF codes are incorporated with the commercial CFD codes of Ansys-Fluent.

In turbulent flows, the turbulent mechanism caused by turbulent motion of the fluid is so much stronger than the perturbation induced by nanoparticles motion. As a result, unlike the laminar flows, the thermal dispersion conductivity can be neglected in this regime.

In the single-phase model, the effective dynamic viscosity of Cu/water nanofluid is calculated based on two general fluid behaviors, i.e. Newtonian and non-Newtonian models, which are considered for the nanofluid. The details of each rheology can be found in Chapter 2 (see Sections 3.2.3.1.1 and 3.2.3.1.1). For the nano-Newtonian rheology, the values of m and n parameters for different φ have been given in Table **3.2**. Since the rate of change of shear stress with a shear rate for Cu/water nanofluid is not available, these data of Al_2O_3/water nanofluid has been adopted for Cu/water nanofluid to observe the nature of the heat transfer. This approach has already been used in some previous studies (Santra et al., 2008, 2009) for modelling of cu/water laminar forced convection. UDF codes are written to define the non-Newtonian rheology. The UDF codes are incorporated with the commercial CFD codes of Ansys-Fluent.

For the E-E two-phase model, it should be noted that Equations (3.31) to (3.37) (see Section 3.2.3.2.1) are originally developed to estimate the effective radial thermal conductivity in pack beds according to (Kuipers et al., 1992). Since there are no correlation for calculation of effective nanoparticle conductivity, Kuipers correlations,

University of Malaya

which were already used by Kalteh et al. (2011) for modeling of forced convection of cu/water nanofluid through a channel, are utilized in the current investigation at first calculations. In the E-E two phase model, the viscosity of the second phase, i.e., solid viscosity is required. A value of 1.38×10^{-3} Pa.s as suggested by Kalteh et al. (2011) is adopted in this study. However, we have carried out a sensitivity study to investigate the effect of the solid viscosity on heat transfer, and this will be discussed in the Results and Discussion section (see Section 4.3.2).

4.2.4 Boundary Condition

A constant heat flux of 35000w/m^2 is applied at the tube wall. The effects of Cu nanoparticle volume concentration (φ) ranging from 0 to 2% in the base water and the effect Reynolds number (Re) ranging from 10,000 to 25,000 are investigated. Thus, the uniform axial velocity of flow at the inlet and the constant and uniform heat flux on the wall are defined as the boundary conditions of the problem. At the tube inlet section, a uniform axial velocity (V_0) based on Reynolds number and the profile temperature of $T_0 = 295$ K, are assumed. The no-sleep boundary condition is also considered on the wall for the based fluid and the nanoparticles. For the two-phase flow, the velocity of particles is assumed the same as that of the base fluid at the pipe inlet.

4.2.5 Numerical Method and Validation

All numerical methods are the same as those which have been selected for laminar flow in the previous study (see Section 3.2.4.). The meshing tool available in Ansys is used to construct the computational mesh. A structured mesh based on a rectangular grid is used throughout the domain (Figure 3.2). While the radial lengths of the domain are divided into 34 mesh elements with a bias towards the top of the domain, the axial lengths are divided to 699 elements without any bias. The model typically has about 23766 cells. The mesh needs to be dense near the wall where the effect of viscosity is high, but the turbulent mechanism is low. The accuracy of the

University of Malaya

enhanced wall treatment model is assessed and the y^+ value for most of the cells near the wall are less than 1. Several grid distributions have been tested to ensure that the calculated results are grid independent. Figure 4.1 draws the comparisons for the Nusselt numbers versus the Reynolds numbers based on the water for three different grid distributions. It is shown that all of these results are independent of the number of grid points. Considering the computational time and effort, the selected grid consists of 600 and 35 nodes in the axial and radial directions, respectively.

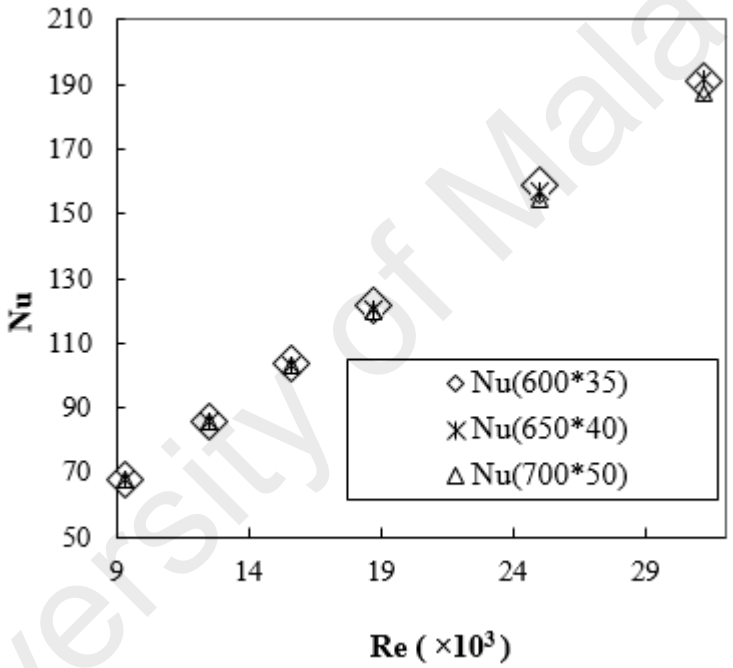

Figure 4.1: Grid-dependency results by Nusselt number calculation based on turbulent forced convection of pure water (φ=0%)

The numerical single-phase and two-phase approaches (Eulerian-Eulerian, mixture and Eulerian-Lagrangian models) are used in this study to investigate the turbulence forced convection flow through a cylindrical pipe. For validation assessment of the single-phase approach, pure water (φ=0) flow is simulated under different high Reynolds numbers with a constant wall heat flux. Similarly, for validation of two-phase approaches, a very dilute Cu/water nanofluid (φ=0.00001%) flow is simulated under the same condition. There are two commonly-used correlations offered by Dittus-Boelter

University of Malaya

(Xuan & Li, 2003) and Gnielinski (Bergman et al., 2011) to calculate the Nusselt number for fully developed (hydrodynamically and thermally) turbulent flow in a smooth circular tube. The error of Dittus-Boelter correlation is as large as 25%, and this error may be reduced to less than 10% through the use of Gnielinski correlation. The results of the simulation are then compared with Gnielinski's correlation (Figure 4.2). A good agreement was achieved between the simulation results and the correlation with deviations less than 5%.

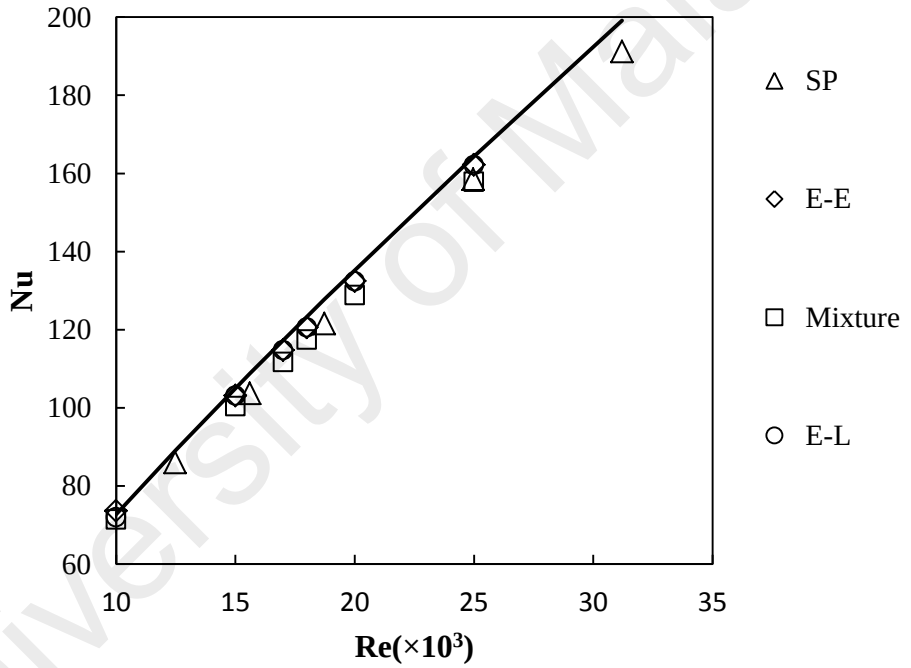

Figure 4.2: The CFD prediction of Nusselt number for very dilute Cu-water nanofluid (φ=0.00001%) using Single-Phase (SP), Eulerian-Eulerian (E-E), Mixture and Eulerian-Lagrangian (E-L) models. The comparison has been made with the Gnielinski correlation (Bergman et al., 2011)

University of Malaya

4.2.6 Simulation Cases

Table 4.1 (a)-(b) show different simulation cases which have been investigated in the present study. The turbulent forced convection of Cu/water nanofluid of different Re numbers and Cu nanoparticle volume fractions in a heated tube were investigated using the single phase models (i.e. Newtonian and non-Newtonian) and two-phase models (i.e. mixture, Eulerian-Eulerian and Eulerian-Lagrangian). This investigation has been done in two steps. First, a comprehensive comparison between different single-phase and two-phase CFD models has been made to find the accuracy of the each individual model in predicting the thermal characteristics of the nanofluids (Table 4.1 (a)).

In the next step, the study was focused just on the Eulerian-Eulerian (E-E) two-phase model Table 4.1 (b)). An improvement of the E-E model was investigated to find and recover the weak points of the model in heat transfer prediction of the nanofluid (Cases 1-36). The improved two-phase model was used to simulate the cu-water nanofluid heat transfer through the heated pipe at different Re numbers and the nanoparticle volume fractions (Cases 37-54). The results were benchmarked against the experimental data from the literature.

University of Malaya

Table 4.1: Table of simulation cases

(a)

Simulation Cases	Model		Changing Parameters	Purpose
1-16	Single-Phase	NSP	Re=10000-25000 φ =0.5%-2%	validation
17-32		Non-NSP		
33-48		Mixture		
49-64	Two-Phase	E-E		
65-80		E-L		

NSP=Newtonian Single-Phase, Non-NSP=Non-Newtonian Single-Phase, E- E=Eulerian-Eulerian, E-L=Eulerian-Lagrangian

(b)

Simulation Cases	Model	Changing Parameters	Purpose
1-36	Two-Phase	Re=10000-25000	Model
37-54	E-E	φ =0.3% –1.5%	correction

University of Malaya

4.3 Results and Discussion

4.3.1 A Comprehensive Comparison between the Models

For comparison, the CFD results have been benchmarked against the Xuan and Li empirical correlation (Xuan & Li, 2003) at different Re numbers (10,000-25,000). The details of the correlation are given as follows;

$$Nu_{nf} = 0.0059\left(1+7.6286\phi^{0.6886}Pe_d^{0.001}\right)\mathrm{Re}_{nf}^{0.9238}\,\mathrm{Pr}_{nf}^{0.4} \quad (4.12)$$

The errors in the predicted Nusselt number by the CFD models are displayed in Table 4.2 (a) – (d), which are presented for φ=0.5, 1, 1.5 and 2%, respectively.

Table 4.2: The error of Newtonian Single-Phase (NSP), Non-Newtonian Single-Phase (Non-NSP), Mixture and Eulerian-Eulerian (E-E) two-phase models in prediction of Nusselt number

(a)

Re	Nu (φ=0.5%)	Error (%)				
(×10^3)	Xuan & Li	NSP	Non-NSP	Mixture	E-E	E-L
10	72.74	12.37	11.98	14.39	9.41	12.92
15	105.79	8.69	13.83	10.88	4.48	9.20
20	138.01	7.87	17.72	9.82	1.54	8.20
25	169.61	7.05	16.07	9.09	0.39	7.50

(b)

Re	Nu (φ=1%)	Error (%)				
(×10^3)	Xuan & Li	NSP	Non-NSP	Mixture	E-E	E-L
10	80.82	6.29	0.21	9.78	-5.49	5.75
15	117.55	3.07	5.54	6.71	-9.94	2.47
20	153.35	3.44	10.94	5.94	-12.79	1.73
25	188.46	2.36	8.26	4.31	-14.42	0.65

University of Malaya

(c)

Re	Nu (φ=1.5%)	Error (%)				
($\times 10^3$)	Xuan & Li	NSP	Non-NSP	Mixture	E-E	E-L
10	88.28	7.07	-0.47	10.47	-13.10	3.80
15	128.41	4.15	5.29	7.00	-17.28	1.02
20	167.51	3.36	8.88	7.15	-19.92	0.49
25	205.88	-0.17	4.85	3.26	-21.67	-1.90

(d)

Re	Nu (φ=2%)	Error (%)				
($\times 10^3$)	Xuan & Li	NSP	Non-NSP	Mixture	E-E	E-L
10	94.66	6.88	-1.17	14.13	-18.23	3.04
15	137.69	4.60	6.56	12.25	-22.20	0.74
20	179.62	3.19	6.96	10.33	-24.66	0.09
25	220.76	-2.73	19.41	3.25	-26.48	-4.05

Referring to Table 4.2 (a), which is for φ=0.5%, the E-E model predicts the Nu number with the smallest error (0.3%-9%). This is followed by the E-L and NSP models, and these models have almost the same errors (7%-13%). The mixture (9%-15%) and non-NSP (12%-18%) models have the largest errors. Except for the non-NSP model, the errors of the other models decrease with the increase of the Re number. All models overpredict the Nu number (positive errors).

Increasing φ to 1%, as given in Table 4.2 (b), E-L and NSP models in general predicted well the Nu numbers with a maximum of 6%; the errors reduce with the increase of Re numbers. Relatively, E-L is a better model than NSP model. Mixture and non-NSP models have errors of 4%-10% and 0.2%-11%, respectively. E-E model

University of Malaya

significantly underpredict (negative value) the Nu number (6%-15% errors), and the error increases with the increase of the Re number.

For φ= 1.5%, as given in Table 4.2 (c), the trend of the error is the same as that for φ=1% (Table **4.2** (b)). The E-L model shows the smallest errors (0%-4%). This is followed by the NSP model with 0%-7% error, mixture model with 3%-11% error and non-NSP model with 0%-9% error. The E-E model has the largest errors of 13%-25%.

For φ= 2%, as given in Table 4.2 (d)**,** the E-L model shows the smallest errors (0%-4%). The NSP model has 3%-7% error. The error for the non-NSP model is less than 7% for Re up to 20,000 but it significantly increased to 19% for Re=25000. The mixture model has the error of 3%-14%, and the error decreases with the increase of Re number. The E-E model has the largest errors of 18%-27%, and it is higher than that for φ= 1%.

Comparing Table 4.2 (a) to (d), the E-L and NSP model show the smallest errors overall for all φ except for φ=0.5% (maximum errors of 6% and 7% respectively). This is followed by the mixture model with maximum error of 15%. The E-E model only predicted well for φ=0.5% (less than 10% error). The non-NSP model shows random errors, with a maximum of 20%, and the errors do not follow any specific trend with changing φ and Re numbers.

The error in the non-NSP model may have resulted from the values of *m* and *n* used in Equations (3.13) – (3.17), and these values represent fluid behavior and adopted from Putra et al. (2003), which were developed for Al_2O_3/water nanofluid. Santra et al. (2009) showed the importance of the non-NSP model for laminar flow Cu/water nanofluid. However, the non-NSP may not be suitable for turbulent flow of Cu/water nanofluid. The prediction of the non-NSP may be improved by using different values of *m* and *n*. As a result, experimental studies may be needed to find the values of the fluid behavior parameters of Cu/water nanofluid for different nanoparticle volume fractions.

University of Malaya

NSP, E-L and mixture models which consider Brownian motion in most of the cases predict well the Nu numbers. This shows the importance of considering the Brownian motion, especially for larger volume fractions of the nanoparticle. Although the E-E model shows the smallest error for φ= 0.5%, the error begins to increase and the predicted Nu numbers by the model have the most deviations from the experiment data for φ= 1% to 2%. The error of Eulerian model may be caused by adoption of improper effective nanoparticle conductivity used in the model. The details of investigation on the E-E model are discussed in the next section (see Section 4.3.2).

4.3.2 Two-phase Model Improvement

Due to some shortcomings of the E-E two-phase model in predicting the heat transfer for the Cu-water nanofluid, we attempted to improve the model. To this end, the most sensitive parameter affecting the heat transfer is investigated. First, the interphase interaction forces with the phases were investigated. The effect of the virtual mass and the lift force are considered negligible due to a very dilute fluid (Fluent, 2009; Kalteh et al., 2011). The velocity and temperature of the primary phase (the base fluid) and the solidus phase (nanoparticles) are plotted in Figure 4.3 and Figure 4.4, respectively.

University of Malaya

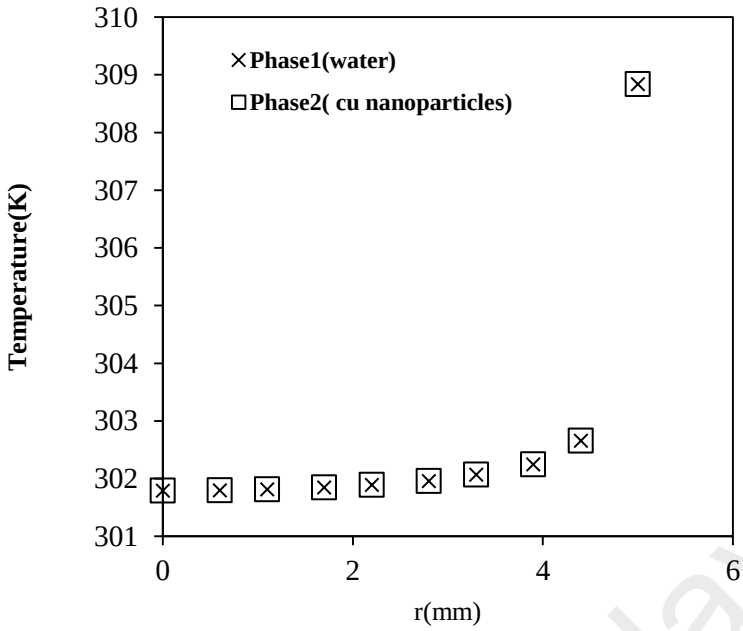

Figure 4.3 : Temperature distribution at different points of pipe cross section for both fluid and solid particles phases at Z/D=70, φ=0.8% and Re=11000.

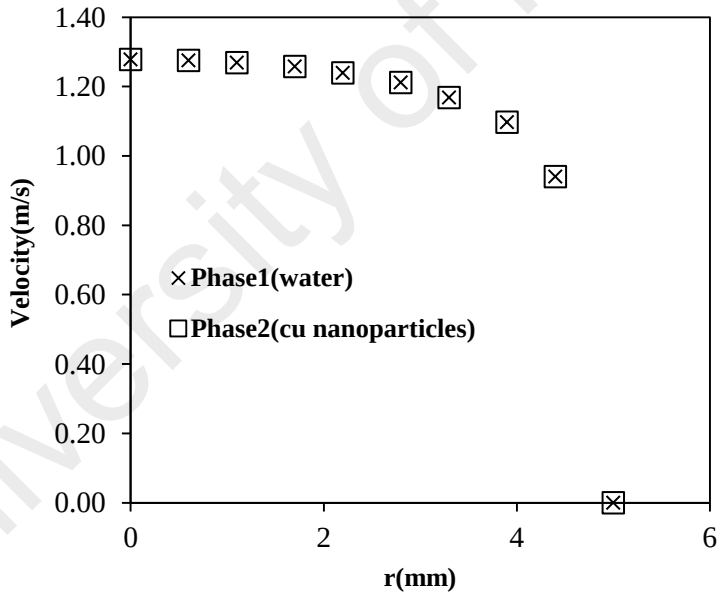

Figure 4.4: Velocity distribution at different points of pipe cross section for both fluid and solid particles phases at Z/D=70, φ=0.8% and Re=11000.

The velocity and temperature differences between the phases are negligible. This suggests that the interphase drag force and heat transfer are not significant and can be neglected. Second, the thermo-physical properties of each phase are checked. The thermo-physical properties of water are known, whereas the viscosity of the solidus

University of Malaya

phase (i.e., representing nanoparticle) was calculated based on the study of Kalteh et al.(2011) and the particle conductivity was calculated using Kuipers correlations (Kuipers et al., 1992) (see Equations (3.31) to (3.37)). The viscosity of the secondary phase (nanoparticle phase) needs to be specified. However, an exact viscosity data of the solidus phase (nanoparticles) is not available. The value of the 1.38×10^{-3} Pa.s suggested by Kalteh et al. (2011) for laminar flow of the E–E two-phase model was used. Further checking was carried out to investigate the effects of the use of such a value on the turbulent flow in the cases of this study. For that, the corresponding pressure drop and the local Nusselt number of a highly dilute nanofluid with volumetric concentration of 0.00001 (which is quite close to pure water) was compared with that of pure water for a flow with Re = 11000. The differences in the pressure drop and the Nusselt number between those two fluids are negligible, i.e., <0.04%. This test was repeated for the highest Re number in our case, which is 25,000, and the differences are less than 2%. In addition, a sensitivity study was carried out to investigate the effect of the value of the solidus viscosity on the heat transfer of the two phase flow model. Table 4.3 shows the Nusselt number of the flow with Re=10,000, nano-particle fraction, φ_p of 0.3% and d_p =100 nm at the location of z/D= 70 using solid viscosities from 0.00001 to 0.01 Pa.s. The Nusselt number is about the same for all the solidus viscosities. Therefore, the value of the solidus viscosity is not critical in the context of our investigations, and the particle viscosity of 1.38×10^{-3} Pa s is used in the present study.

University of Malaya

Table 4.3: Sensitivity study of the Nusselt number on the particle phase viscosity for Re= 10,000, φ_p=0.3% and d_p =100 nm at z/D= 70

Particle viscosity (Pas)	Nusselt number
0.01	82.4786
0.005	82.3120
0.002	82.2037
0.00138	82.1800
0.001	82.1652
0.0008	82.1557
0.0002	82.1271
0.00005	82.1175
0.00001	82.1147

The Kuipers et al. (Kuipers et al., 1992) model for the particle conductivity was originally developed to estimate the effective radial thermal conductivity in pack beds, and the use of the model for a dilute case of nanofluid may not be suitable. For example, Table 4.4 shows the calculation of the effective conductivity using the Kuipers model for the different nanoparticle volume fractions. The results show that the effective nanoparticle conductivities decrease as the nanoparticles volume fractions increase. In contrast, the nanofluid conductivity is actually found to increase with the increase of the particle volume fractions (Q. Li et al., 2003; Özerinç et al., 2010). We also found that the effective conductivity is a sensitive parameter affecting the heat transfer prediction of the nanofluid according to Equation (3.29), and therefore this parameter is selected for further modification in the CFD model for a better heat transfer prediction.

Table 4.4: The values of effective nanoparticle conductivity based on Kuipers correlations (Kuipers et al., 1992)

φ(%)	$K_{eff,p}$(W/m.^{0}C)
0.3%	64.50
0.5%	50.22
0.8%	40.00
1%	35.96
1.2%	32.99
1.5%	29.73

University of Malaya

The accuracy of the results predicted by the CFD models of the two-phase model are improved by modifying the value of the effective conductivity of the solidus phase ($k_{eff,p}$) representing the conductivity of copper nanoparticle in Equation (3.29). This is done using a trial and error method, and the effective conductivity is estimated to predict an accurate Nusselt number according to the Xuan and Li (2003) experimental correlation for the Reynolds number ranging from 10,000 to 25,000 and volume fractions ranging from 0.3% to 1.5 %. Figure 4.5 illustrates the method for finding the proper effective nanoparticle conductivity. The prediction of the Nusselt number for each case is repeated until the difference of that calculated from Xuan and Li's correlation (Xuan & Li, 2003) is less than 1%. Figure 4.6 (a) and (b) show the estimated effective conductivities as a function of the Re number for the Cu nanoparticle with the volume fractions, ranging from 0.3% to 1.5%. For each volume fraction, the effective conductivity is found to increase almost linearly with the increase of the Re number. A possible explanation for this may be due to the effect of the Re number on the size of particle clusters and their Brownian motion. As the Re increases, the bigger clusters break up, their Brownian velocity increases, and they therefore transport more heat (Akbari et al., 2012). This means that, in general, the nanoparticle conductivity increases with the increase in the Re number. For a particular Re number, the effective conductivity increases with the increase of the particle volume fraction. The increase in the nanoparticle volume fraction leads to the increase of the interaction and collision of the nanoparticles. This has an effect on the diffusion and relative movement of the particles, especially near the wall. In general, this means that the decrease of the thermal boundary layer thickness is due to the presence more nanoparticles and the more random motion within the base fluid (Daungthongsuk & Wongwises, 2007; Haghshenas Fard et al., 2010; Trisaksri & Wongwises, 2007). For example, the effective conductivity is the lowest for the lowest particle volume fraction in the current study

University of Malaya

(i.e., 0.3%) and vice versa. A linear regression line is plotted for the distribution of the conductivity data versus the Re number for each of the particle volume fractions (Figure 4.6). This, consequently, allows us to develop a linear correlation for each of the particle volume fractions. The correlation for the 0.3% volume fraction is given as y=0.0007x - 5.24, for 0.5% is =0.0016x +4.8871, for 0.8% is =0.0014x + 21.458, for 1% is =0.0015x +21.833, for 1.2% is =0.0015x +22.936 and for 1.5% is =0.0012x -30.317. Note that y represents the effective conductivity while x represents the Re number. The slope of the line which indicates the rate of change of the particle conductivity versus the Reynolds number is quite close to one another (i.e., 0.0012-0.0016) for the 0.5-1.5% volume fractions. However, this is not the case for the 0.3% volume fraction where the slope is not as steep as in the other cases.

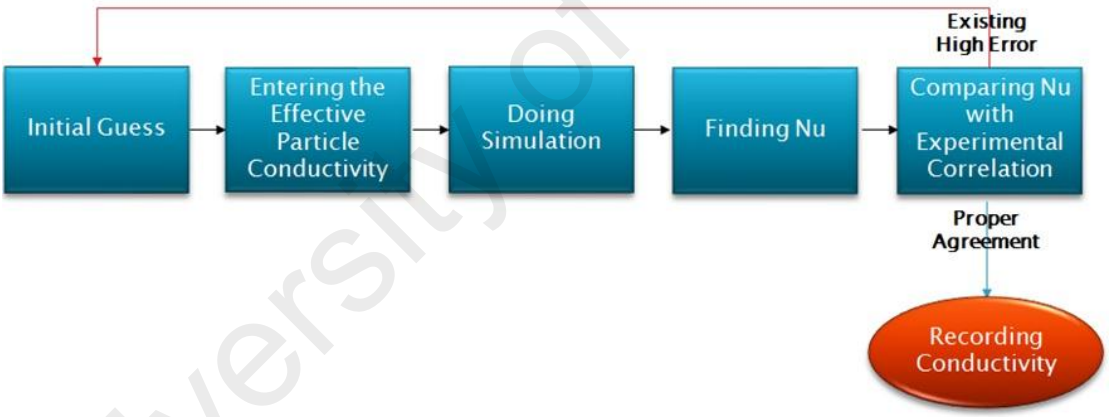

Figure 4.5: A schematic flowchart of the trial and error procedure for finding a proper effective nanoparticle conductivity

University of Malaya

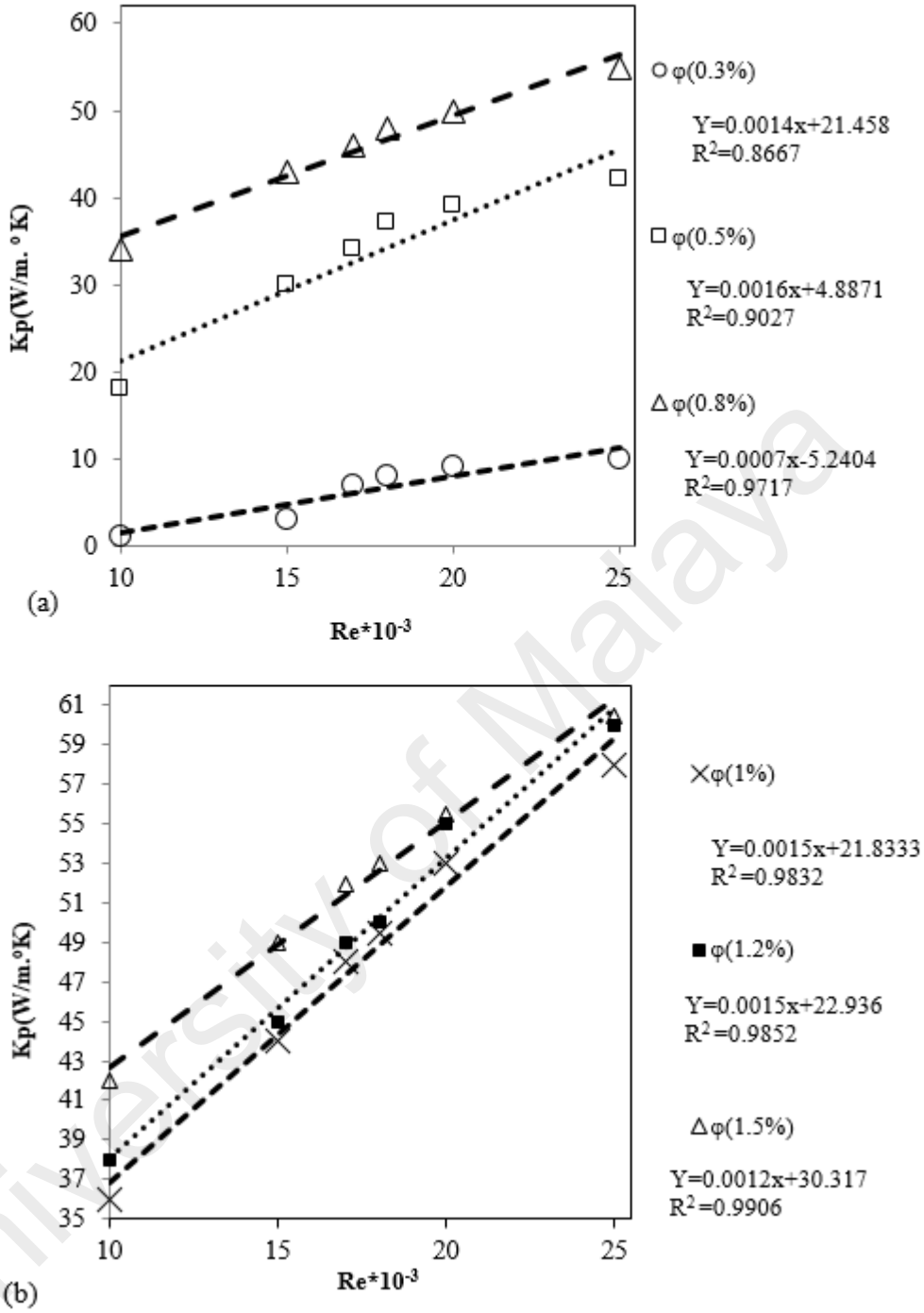

Figure 4.6 (a) - (b): The effective Cu nanoparticle conductivities versus Reynolds numbers at different volume fractions according trial and error.

Based on the different effective nanoparticle conductivity correlations (linear regression lines) already calculated in this study that correspond to the several values of the Reynolds number (10,000 to 25,000) in some of the nanoparticle volume fractions (0.3% to 1.5%) according to Figure 4.6, a general correlation can be developed to relate the effective particle conductivities as a function of the Reynolds number and the

University of Malaya

nanoparticle volume fraction. So, using the mathematical surface fitting technique in MATLAB software (Hanselman & Littlefield, 1997), a general equation is developed as follows:

$$\frac{k_{eff,p}}{k_s} = -0.1207 - (5.243\cdot10^{-6})\,\mathrm{Re} + (29.13)\varphi + (-7.342\cdot10^{-11})\,\mathrm{Re}^2 + (6.894\cdot10^{-5})\varphi\cdot\mathrm{Re} - (1.24\cdot10^{3})\varphi^2 \quad (4.6)$$

$$10^4 \le \mathrm{Re} \le 2.5\times10^4$$
$$0.3\% \le \varphi \le 1.5\%$$

where $k_{eff,p}$ and k_s are the effective nanoparticle conductivities and the conventional values of conductivity for the particle materials, respectively. Note that the use of the above suggested equation is limited to the volume fractions (from 0.3% to 1.5%), Re (from 10,000 to 25,000) and Cu-water nanofluid. Figure 4.7 shows a two-degree surface fitted to the data points in a three-coordinate system.

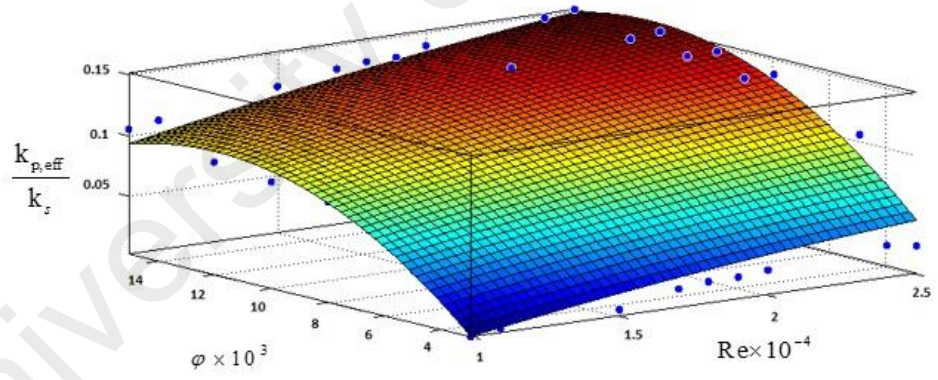

Figure 4.7: Surface fitting interpolation technique to correlate the dimensionless conductivities versus nanoparticle volume fraction and Reynolds number. The surface is in degree of two; the regression value (R) is equal 0.9427.

In the next step, the developed correlations have been checked again. First, the effective particle conductivities were calculated for the 0.3, 0.5, 0.8, 1.0, 1.2 and 1.5 percentage volume fractions at three typical Reynolds numbers, 11,000, 19,000, and 24,000. Then CFD simulations were carried out using the E-E two-phase model and the calculated effective particle conductivities. The comparison of the Nusselt number from

University of Malaya

the simulations and from Xuan and Li's experimental investigations is shown in Figure 4.8; According to this figure, there is a good agreement between the results of the Eulerian-Eulerian two-phase model and that of the experiment.

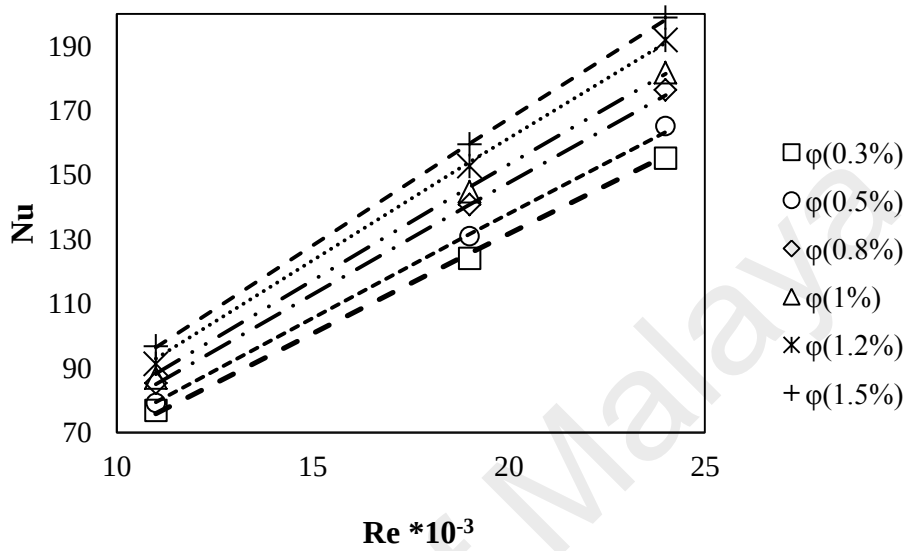

Figure 4.8 : Validation of effective Cu nanoparticle conductivity correlations at different volume fractions and Reynolds numbers.

4.4 Conclusions

Forced convection heat transfer of cu-water nanofluid in a pipe with a constant wall heat flux has been investigated numerically for Reynolds numbers of 10,000 to 25,000 and particle volume fractions of 0.3% to 2% using the commercial CFD package of Ansys-Fluent. Several UDF codes are written to define the thermal conductivity model, the dynamic viscosity model and the non-Newtonian rheology for the nanofluids. The UDF codes are incorporated with the single- and two-phase CFD models.The CFD results of different single- and two-phase models have been checked against the experimental findings from the literature. The conclusions of this study are as follows:

- Non-NSP, the single-phase model, in general, does not show a good agreement with Xuan and Li's correlation in prediction of the Nu number.

University of Malaya

- E-E model gives inaccurate results except for φ=0.5%.
- In the E-E model, the effect of the interphase drag force is negligible because of the insignificant velocity difference between the base fluid and the nanoparticles in our cases. Similarly, the effect of the interphase heat transfer is negligible because of the insignificant temperature differences between the base fluid and the nanoparticles.
- The use of the Kuipers correlations from our literature, to calculate the effective nanoparticle conductivity for the use in the E-E model, resulted in inaccurate Nusselt number predictions for the Cu-water nanofluids.
- In the E-E model, the value of the effective nanoparticle conductivity was found to be a sensitive parameter for heat transfer calculations. A new correlation has been suggested to calculate the effective nanoparticle conductivity of the Cu-water nanofluids as a function of the Reynolds number and nanoparticle fractions for use in the E-E model.
- For each volume fraction, the effective nanoparticle conductivity was found to increase almost linearly with the increase of the Re number. A possible explanation for this may be due to the effect of the Re number on the size of particle clusters and their Brownian motion.
- The mixture model gives a maximum error of 15%.
- NSP, the single phase model and E-L, the two-phase model, overall, are the recommended models.

University of Malaya

5 CHAPTER 5: MODELLING ON SUBCOOLED FLOW BOILING OF NANOFLUIDS

5.1 Introduction

The subcooled flow boiling of two types of nanofluids (i.e. Al_2O_3/water and Cu/water nanofluids) in a vertical heated pipe is numerically investigated. For this purpose, the Eulerian-Eulerian (E-E) two-phase CFD model is used. Initially, for a strong validation of the CFD model, water subcooled flow boiling is modeled under different nucleate boiling parameters (i.e. nucleate site density, bubble frequency, and bubble departure diameter), boundary conditions (i.e. fluid mass flux, inlet subcooled temperature and wall heat flux) and bubble dynamic mechanisms (i.e. non-drag forces, turbulence interaction resource and interfacial area concentration). The predicted heat transfer coefficients are benchmarked against the empirical correlation of Chen (S. J. Kim et al., 2010). According to the findings of the validation tests, the most accurate combination of the boiling properties is used in the E-E approach to model the nanofluids subcooled flow boiling. The effect of interphase interactions (i.e. interactions of the nanoparticles and the base liquid) and nonhomogeneous nanoparticles distribution on heat transfer predictions are also investigated. For this purpose, the Eulerian-Lagrangian CFD model is selected to be incorporated with the E-E model. The surface wettability improvement induced by the nanoparticles deposition is considered in the CFD model to find out how the heat transfer predictions are affected by such wettability improvement.

University of Malaya

5.2 Methodology

5.2.1 Geometry Structure

A cylindrical tube in a vertical position and with dimensions of 0.0154 m diameter, 5mm thickness and 2m length is considered in the current study (Figure 5.1). A constant heat flux is applied to the tube wall. The two-dimensional (2D) axisymmetric geometry has been considered and as a result, a rectangular domain with dimensions of 0.0077m × 2 m is created.

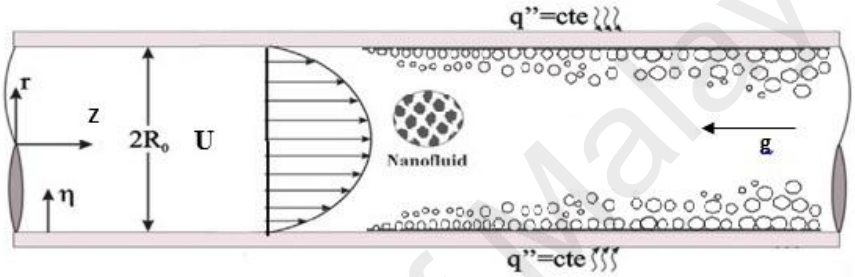

Figure 5.1: The geometry structure of the physical model

5.2.2 Governing Equations

Since the boiling is a two-phase phenomenon, the Eulerian-Eulerian two-phase CFD model has been widely used by many studies (Aminfar et al., 2013; Chen et al., 2009; Cheung et al., 2014; Krepper et al., 2007; Yeoh et al., 2014) for modelling of the boiling of conventional fluids. In case of nanofluid subcooled boiling, two strategies would be selected. At the first point of view, the nanofluid is supposed to behave hydro-dynamically like its pure base liquid and theoretically can be treated as a single liquid in spite of the presence of two distinct phases (X. Li et al., 2014). In this way, the hydrodynamic and thermal interphase interactions between the solid nanoparticles and fluid are neglected. It is also supposed that the suspension of the nanoparticles in the base liquid is homogeneous and this nanoparticles distribution remains homogeneous in each position through the heated pipe. Thus, the conventional Eulerian-Eulerian two-

University of Malaya

phase model can be used for modelling of the nanofluid subcooled flow boiling. In the second approach, the nanofluid is considered as a two-phase or the nanofluid subcooled flow boiling is considered as a three-phase flow (i.e. base liquid, nanoparticles and vapor). In this way, the subcooled flow boiling of the base liquid is modeled by the Eulerian-Eulerian (E-E) frame work, while the effects of nanoparticles are tracked as a discrete phase by Eulerian-Lagrangian (E-L) frame work. Thus, the nanofluid subcooled flow boiling is model by a three-phase CFD model (E-E plus E-L). Figure 5.2 shows the CFD models are used in this study. The details of the both CFD models are given in the following sections.

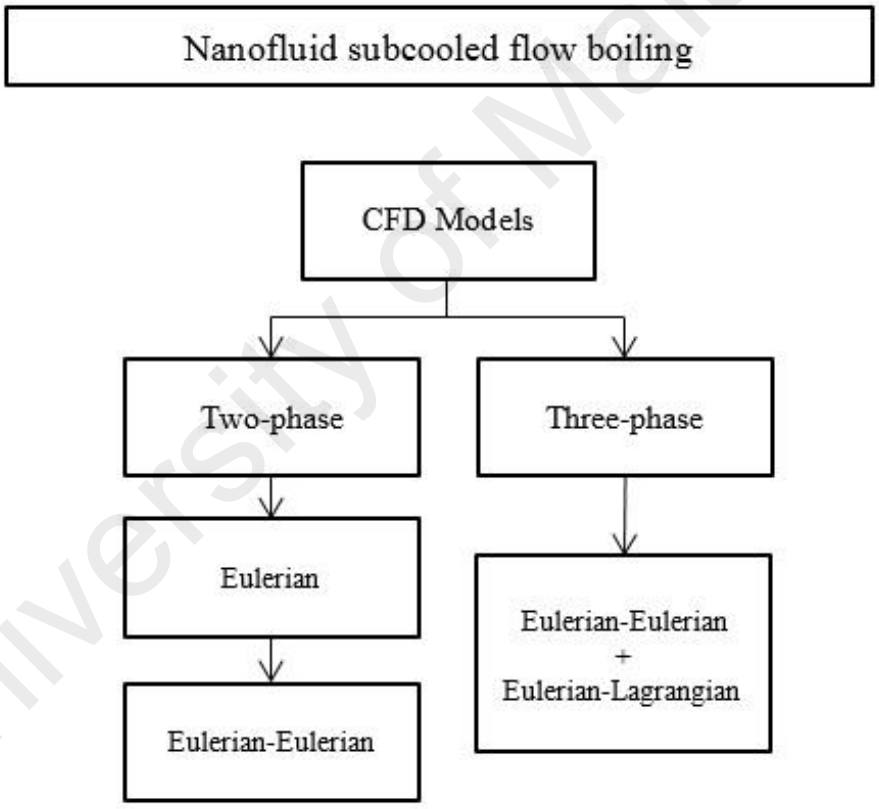

Figure 5.2: Different CFD approaches for modelling of nanofluids subcooled flow boiling

University of Malaya

5.2.2.1 Two-phase Model for Nanofluid Subcooled Flow Boiling

Ensemble-averaged of mass, momentum and energy transport equations are considered for each phase in the Eulerian–Eulerian modelling framework. The liquid phase (α_l) is the continuum and the vapour phase (bubbles) is the disperse phase (α_g). These equations can be written as (Cheung et al., 2014):

Continuity equation of liquid phase

$$\frac{\partial \rho_{l,eff}\,\alpha_l}{\partial t} + \nabla.\left(\rho_l \alpha_l \overrightarrow{u_l}\right) = \Gamma_{lg} \tag{5.1}$$

Continuity equation of vapour phase

$$\frac{\partial \rho_g \alpha_g}{\partial t} + \nabla.\left(\rho_g \alpha_g \overrightarrow{u_g}\right) = \Gamma_{gl} \tag{5.2}$$

Momentum equation of liquid phase

$$\begin{aligned}&\frac{\partial \rho_{l,eff}\,\alpha_l \overrightarrow{u_l}}{\partial t} + \nabla.\left(\rho_{l,eff}\,\alpha_l \overrightarrow{u_l}\overrightarrow{u_l}\right) = -\alpha_l \nabla p + \rho_{l,eff}\,\alpha_l \vec{g} + \\ &\nabla\left[\alpha_l \mu_{e,l}\left(\nabla\overrightarrow{u_l} + \left(\nabla\overrightarrow{u_l}\right)^T\right)\right] + \left(\Gamma_{lg}\overrightarrow{u_g} - \Gamma_{gl}\overrightarrow{u_l}\right) + F_{lg}\end{aligned} \tag{5.3}$$

Momentum equation of vapour phase

$$\begin{aligned}&\frac{\partial \rho_g \alpha_g \overrightarrow{u_g}}{\partial t} + \nabla.\left(\rho_g \alpha_g \overrightarrow{u_g}\overrightarrow{u_g}\right) = -\alpha_g \nabla p + \rho_g \alpha_g \vec{g} + \nabla\left[\alpha_g \mu_g \left(\nabla\overrightarrow{u_g}\right)\right] \\ &+\left(\Gamma_{gl}\overrightarrow{u_l} - \Gamma_{lg}\overrightarrow{u_g}\right) + F_{gl}\end{aligned} \tag{5.4}$$

Energy equation of liquid phase

$$\frac{\partial \rho_{l,eff}\,\alpha_l H_l}{\partial t} + \nabla.\left(\rho_{l,eff}\,\alpha_l \overrightarrow{u_l} H_l\right) = \nabla\left[\alpha_l \mathrm{k}_{e,l}\left(\nabla T_l\right)\right] + \left(\Gamma_{gl} H_l - \Gamma_{lg} H_g\right) \tag{5.5}$$

Energy equation of vapour phase

$$\frac{\partial \rho_g \alpha_g H_g}{\partial t} + \nabla.\left(\rho_g \alpha_g \overrightarrow{u_g} H_g\right) = \nabla\left[\alpha_g \mathrm{k}_g\left(\nabla T_g\right)\right] + \left(\Gamma_{lg} H_g - \Gamma_{gl} H_l\right) \tag{5.6}$$

University of Malaya

5.2.2.1.1 Effective Thermo-physical Properties

The effective properties of nanofluids at two different temperatures of 360 ^{o}k and 373.15 ^{o}k were calculated using the widely accepted correlations in the literature: The effective mass density of the nanofluid, $\rho_{l,eff}$ is calculated using

$$\rho_{l,eff} = (1-\varphi)\rho_l + \varphi\,\rho_{NP} \tag{5.7}$$

The effective specific heat at constant pressure of the nanofluid, $c_{p,eff}$ is calculated as

$$c_{p\ l,eff} = \frac{(1-\varphi)(\rho\ c_p)_l + \varphi(\rho\ c_p)_{NP}}{(1-\varphi)\rho_l + \varphi\ \rho_{NP}} \tag{5.8}$$

The effective thermal conductivity of fluid has been determined by the model proposed by Maxwell (1881) and used by Li et al. (2014) for modelling of nanofluid pool boiling.

$$\frac{\mathrm{k}_{l,eff}}{\mathrm{k}_l} = \frac{(1-\varphi)(\mathrm{k}_{\mathrm{NP}} + 2\mathrm{k}_{\mathrm{l}}) + 3\varphi\mathrm{k}_{NP}}{(1-\varphi)(\mathrm{k}_{\mathrm{NP}} + 2\mathrm{k}_{\mathrm{l}}) + 3\varphi\mathrm{k}_l} \tag{5.9}$$

The effective dynamic viscosity of nanofluids is calculated based on the correlation suggested by Maiga et al. (2004)

$$\mu_{l,eff} = \left(123\varphi^2 + 7.3\varphi + 1\right)\mu_l \tag{5.10}$$

where the subscript NP represents nanoparticles and φ is volumetric concentration of nanoparticles in the liquid. An option of linear temperature dependent has been selected in Ansys-Fluent for each kind of the properties based on the above calculations.

5.2.2.1.2 Interfacial Force

The interfacial force F_{lg} appearing in Equation (5.3) is formulated through appropriate consideration of different sub-forces affecting the interface between each phase. For the liquid phase, the interfacial force comprises the sum of the sub-forces, such as drag, lift, wall lubrication and turbulent dispersion respectively. Note that for the gas phase, $F_{gl} = -F_{lg}$ (Cheung et al., 2014). Interphase momentum transfer between gas and liquid due to drag force is given by (Cheung et al., 2014)

University of Malaya

$$F_d = \frac{1}{8} C_D a_{if} \rho_{l,eff} \left| \overrightarrow{u_g} - \overrightarrow{u_l} \right| \left(\overrightarrow{u_g} - \overrightarrow{u_l} \right) \tag{5.11}$$

where a_{if} is the interfacial area per unit volume. The drag coefficient C_D has been correlated for several distinct Reynolds number regions for individual bubbles according to Ishii and Zuber (Cheung et al., 2014; Mamoru Ishii & Zuber, 1979). Lift force in terms of the slip velocity and the curl of the liquid phase velocity is described by (Cheung et al., 2014)

$$F_L = \alpha_g \rho_{l,eff} C_L \left(\overrightarrow{u_g} - \overrightarrow{u_l} \right) \times \left(\nabla \times \overrightarrow{u_l} \right) \tag{5.12}$$

The lift coefficient C_L is given by Tomiyama (1998). Wall lubrication force, which is in the normal direction away from the heated wall and decays with distance from the wall, is expressed by (Cheung et al., 2014)

$$F_{\text{lub}} = -\frac{\alpha_g \rho_g \left(\overrightarrow{u_g} - \overrightarrow{u_l} \right)}{D_s} \max \left(0, C_{w1} + C_{w2} \frac{D_s}{y_w} \right) \vec{n} \tag{5.13}$$

The wall lubrication constants C_{w1} and C_{w2} as suggested by Antal et al. (1991) are -0.01 and 0.05 respectively. Turbulence dispersion taken as a function of turbulent kinetic energy and gradient of the void fraction of the liquid yields in the form of (Cheung et al., 2014)

$$F_{turb} = -C_{TD} \rho_{l,eff} k \nabla \alpha_l \tag{5.14}$$

The recommended value for C_{TD} according to Kurul and Podowski (1990) of 0.1 is used for the turbulent dispersion force.

University of Malaya

5.2.2.1.3 Interfacial Mass

The interfacial mass transfer rate due to condensation in the bulk subcooled liquid in Equation (5.1) can be expressed as (Cheung et al., 2014):

$$\Gamma_{\lg} = \frac{h a_{if} T_{sub}}{h_{fg}} \tag{5.15}$$

where h represents the inter-phase heat transfer coefficient modelled by widely used Ranz-Marshall's correlation (Ranz & Marshall, 1952). The wall vapor generation rate is modelled in a mechanistic manner by considering the total mass of bubbles detaching from the heated surface as (Cheung et al., 2014)

$$\Gamma_{gl} = \frac{q_e}{h_{fg}} \tag{5.16}$$

5.2.2.1.4 Interfacial Area

Interfacial area concentration is defined as the interfacial area between two phases per unit mixture volume. The interfacial area can be calculated in one of two ways (Kataoka et al., 2012):

- Use an algebraic relationship between a specified bubble diameter (d_b) and the interfacial area concentration (a_{if}). The algebraic interfacial area models are derived from the surface area to volume ratio, $A_{b,}$ of a spherical bubble:

$$A_b = \frac{\pi d_b^2}{\frac{1}{6}\pi d_b^3} = \frac{6}{d_b} \tag{5.17}$$

For a dispersed phase, g, with volume fraction, α_g, the particle model estimates the interfacial area concentration, (a_{if}) as

$$a_{if} = \alpha_g A_b = \frac{6\alpha_g}{d_b} \tag{5.18}$$

where d_b is calculated based on Sauter mean diameter (Zeitoun & Shoukri, 1996)

University of Malaya

$$\frac{d_b}{\sqrt{\sigma / g\Delta\rho}} = \frac{0.0683\left(\rho_l / \rho_g\right)^{1.326}}{\mathrm{Re}^{0.324}\left(Ja + \left(\frac{149.2\left(\rho_l / \rho_g\right)^{1.326}}{Bo^{0.487}\,\mathrm{Re}^{1.6}}\right)\right)} \tag{5.19}$$

Here Re is the flow Reynolds number, Bo the boiling number and Ja the Jakob number based on liquid subcooling.

- Use a transport equation for interfacial area concentration (IAC). This allows for a distribution of bubble diameters and coalescence/breakage effects.

$$\frac{\partial a_{if}}{\partial t} + \nabla.\left(a_{if} u_g\right) = \frac{2}{3}\frac{a_{if}}{\alpha_g \rho_g}\left[\Gamma_{\mathrm{lg}} - \alpha_g \frac{d\rho_g}{dt}\right] + S_{co} + S_{bk} + S_{ph} \tag{5.20}$$

where S_{co}, S_{bk}, and S_{ph} mean the variance source terms of IAC by a coalescence, breakup and nucleation, respectively (Bae et al., 2010). Detail descriptions of these source terms can be found in (M Ishii et al., 2002), (Hibiki & Ishii, 2002), and (Yao & Morel, 2004).

5.2.2.1.5 Turbulence Modelling

Due to the lower density of vapour, it is commonly assumed that, in subcooled flow boiling, the motion of the dispersed vapour phase follows the fluctuations in the continuous liquid phase (Kurul & Podowski, 1990). Accordingly, the turbulence stresses are modelled only for the liquid phase, whereas the vapour phase is assumed to be laminar (Končar et al., 2004). In the present work, the following option from the Ansys-Fluent V.15 code was applied: turbulence in the liquid phase is modelled using the standard k–ε model according to Launder and Spalding (1974) with additional source terms describing the bubble-induced turbulence. So, the k–ε model is given as

$$\frac{\partial}{\partial t}\left(\alpha_l \rho_{l,eff} k_l\right) + \nabla.(\alpha_l \rho_{l,eff} k_l \overrightarrow{u_l}) = \nabla.[(\frac{\mu_l^t}{\sigma_k})\nabla(k_l)] + G_l - \rho_{l,eff}\,\varepsilon_l + S_l^k \tag{5.21}$$

$$\begin{aligned}\frac{\partial}{\partial t}\left(\alpha_l \rho_{l,eff} \varepsilon_l\right) + \nabla.(\rho_{l,eff} \varepsilon_l \overrightarrow{u_l}) &= \nabla.[\frac{\mu_l^t}{\sigma_\varepsilon}\nabla\varepsilon_l] \\ + \frac{\varepsilon_l}{k_l}(C_{1\varepsilon}G_k - C_{2\varepsilon}\rho_{l,eff}\,\varepsilon_l) &+ S_l^\varepsilon\end{aligned} \tag{5.22}$$

University of Malaya

$$G_l = \mu_{l,t}(\nabla\overrightarrow{u_l} + (\nabla\overrightarrow{u_l})^T) \tag{5.23}$$

$$\mu_t = \rho_{l,eff} C_\mu \frac{k^2}{\varepsilon} \tag{5.24}$$

$$C_\mu = 0.09, \sigma_k = 1.00, \sigma_\varepsilon = 1.30, C_{1\varepsilon} = 1.44, C_{2\varepsilon} = 1.92$$

where G_l is the production of turbulence due to the liquid shear stress. Two additional source terms corresponding to the bubble induced turbulence are (Končar et al., 2005):

$$S_l^k = -F_{\lg}^{drag}.\left(\overrightarrow{u_g} - \overrightarrow{u_l}\right), \tag{5.25}$$

$$S_l^\varepsilon = C_{3\varepsilon}\frac{S_l^k}{\tau} \tag{5.26}$$

τ is a characteristic time for bubble induced turbulence and this parameter is calculated by Troshko and Hassan (2001) as follows:

$$\tau = \frac{2C_{vm}d_b}{3C_D\left|\overrightarrow{u_g} - \overrightarrow{u_l}\right|} \tag{5.27}$$

where C_{vm} and $C_{3\varepsilon}$ are equal 0.5 and 0.45 respectively. Shear and bubble-induced turbulence are linearly superimposed, according to an assumption from Sato et al. (1981), where the effective viscosity of the continuous liquid phase is expressed as (Končar et al., 2004):

$$\mu_{eff,l} = \mu_l + \mu_{t,l} + \mu_b \tag{5.28}$$

The bubble-induced turbulence viscosity μ_l^b in the liquid phase is given by

$$\mu_b = C_{\mu b}\rho_l\alpha_g d_b\left|\overrightarrow{u_g} - \overrightarrow{u_l}\right| \tag{5.29}$$

where the coefficient $C_{\mu b}$ is equal to 0.6, as recommended by Sato et al. (1981).

University of Malaya

5.2.2.1.6 Heat Flux Partitioning Model

For engineering calculations, currently the most widely used CFD approach to model subcooled flow boiling is the Eulerian two-fluid framework (see references (Drew & Passman, 2006; Mamoru Ishii, 1975; JY Tu & Yeoh, 2002)). The heat transfer during subcooled flow boiling is modeled by consideration of two separate regions: (i) heat transfer from heated wall and (ii) heat transfer in two-phase flow away from the wall (Cheung et al., 2014). The heat transfer rate from the wall is modeled by partitioning the wall heat flux in three components: surface quenching or transient conduction, evaporation and single-phase turbulent convection. Transient conduction (surface quenching heat flux component) occurs over the area of the heater surface under the influence of bubbles while it is assumed that single-phase turbulent convection persists in areas of the heated surface which are unaffected by the presence of bubbles (see Figure 5.3) (Cheung et al., 2014). During subcooled flow boiling, bubble nucleation at the heater surface is the source of void in the bulk liquid (X. Li et al., 2014). The wall heat flux partition model requires the evaluation of three important parameters: active nucleation site density (Na), bubble departure diameter (D_{bd}) and bubble departure frequency (f) (Cheung et al., 2014). The first and most well-known wall partitioning boiling model is the RPI model, which was formulated by Kurul and Podowski (1991) of the Rensselaer Polytechnic Institute. The Eulerian two-phase model and RPI wall boiling model have been used by many researchers (Aminfar et al., 2013; Chen et al., 2009; Cheung et al., 2014; Končar et al., 2004; Končar & Mavko, 2003; Krepper et al., 2007; JY Tu & Yeoh, 2002; Yeoh et al., 2014) to investigate the subcooled flow boiling of a pure base fluid numerically. The total wall heat flux is calculated as follows (E Abedini et al., 2013; Cheung et al., 2014; X. Li et al., 2014):

$$q = q_e + q_q + q_c \tag{5.30}$$

University of Malaya

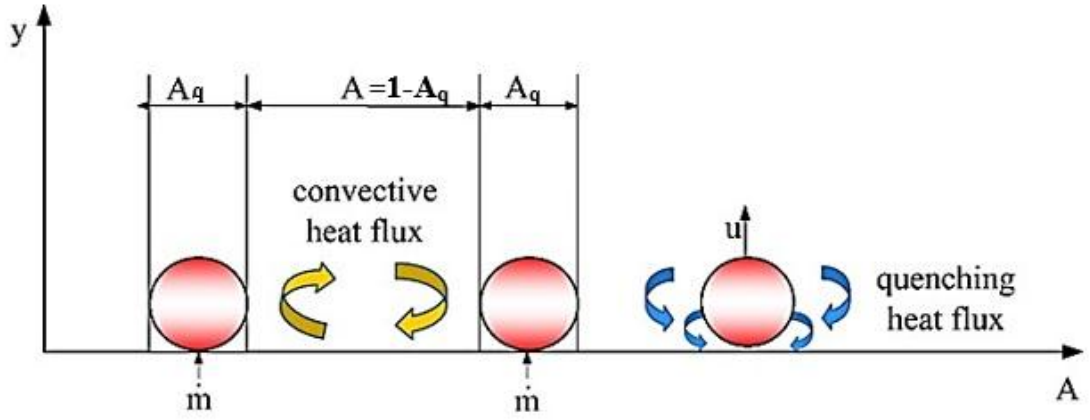

Figure 5.3: Heat flux partition of wall boiling model.

The wall heat flux component due to evaporation which occurs at the nucleate boiling region can be determined from (Cheung et al., 2014)

$$q_e = N_a f \left(\frac{\pi D_d^3}{6} \right) \rho_g h_{fg} \tag{5.31}$$

where N_a, f, D_d and h_{fg} are the active nucleation site density, the bubble frequency, departing bubble diameter and the latent heat, respectively. The wall heat flux component contributed by surface quenching is formulated accordingly. As liquid comes in contact with the hot surface, the heat is transferred to liquid mainly based on transient conduction which can be determined from (Cheung et al., 2014)

$$q_q = \left(\frac{2}{\sqrt{\pi}} \sqrt{\mathrm{k}_l \rho_l C_{p,l} f} \right) A_q \left(T_w - T_l \right) \tag{5.32}$$

where A_q denotes the fraction of the wall area that is in contact with the fresh liquid and is cooled down by transient conduction. This area is calculated from (Cheung et al., 2014)

$$A_q = N_a \left(K \frac{\pi D_d^2}{4} \right) \tag{5.33}$$

Heat transfer due to turbulent convection can be defined based on local Stanton number as (Cheung et al., 2014)

$$q_c = St \rho_l C_{p,l} u_l \left(1 - A_q \right) \left(T_w - T_l \right) \tag{5.34}$$

University of Malaya

where u_l is adjacent liquid velocity and

$$St = \frac{Nu}{\mathrm{Re}\,\mathrm{Pr}} \tag{5.35}$$

where Nu, Re and Pr are the local Nusselt, Reynolds and Prandtl numbers.

There are a number of correlations for the nucleate boiling parameters (i.e. N_a and D_d) available in the literature (E Abedini et al., 2013; Cheung et al., 2014; X. Li et al., 2014). At the heated wall, only some of the nucleation sites will be activated as the temperature of the surface exceeds the saturation liquid temperature at the local pressure. The active nucleation site density (N_a) depends on the distributions of cavities on the wall surface, heater and liquid properties, and contact angle between liquid and the wall (Cheung et al., 2014). The empirical correlations of the bubble departure diameter have been defined as a function of bubble contact angle, Jacob number, or other thermo-hydraulic parameters. In this study, a sensitivity test will be done on some widely used correlations in order to select the most proper combination for the simulation of water subcooled flow boiling (see Section 5.2.2.1). The correlations for calculations of the active nucleation site density and the bubble departure diameter are given in Table 5.1 and Table 5.2 respectively. Since the models of Fritz (Fritz, 1935), Cole-Shulman (Cole & Shulman, 1966) and Cole-Rohsenow (Cole & Rohsenow, 1969) for bubble departure diameters are not available in the commercial CFD codes of Ansys-Fluent, UDF codes are written to define Equations (5.42), (5.43) and (5.44). The most proper correlations are selected to use in the E-E CFD model for the rest of the investigation. Since these correlations were originally developed for conventional fluids like water, the applicability of them is open to question. So, the recently suggested correlations by Li et al. (2014) for calculation of N_a and D_d of nucleate boiling of very dilute nanofluids ($\leq$ 0.1% vol. nanofluids) are also used in the E-E CFD model to show how the model predictions are changed by such new correlations (see Section 5.2.4). Li

University of Malaya

et al. (2014) consider the changes of the nucleation site density and the bubble departure diameter because of the nanoparticles deposition in these correlations as follows

$$N_a = 1.206\times10^4\left(1-\cos\theta\right)\left(T_w - T_{sat}\right)^{2.06} \tag{5.36}$$

$$D_{bd} = 0.626977\frac{2+3\cos\theta-\cos^3\theta}{4}\left[\sigma/\mathrm{g}\left(\rho_l-\rho_g\right)\right]^{0.5} \tag{5.37}$$

where θ is the liquid contact angle with the heater surface. UDF codes are written to define Equations (5.36) and (5.37).

Table 5.1: Empirical correlations for nucleation site density (Cheung et al., 2014).

Name	Correlation	Details
Lemmert & Chawla(1977)	$N_a = \left[m\left(T_w - T_{sat}\right)\right]^n$ (5.38)	m=210, n=1.805
Kocamustafaogullari &Ishii (1983)	$N_a = \frac{1}{D_{bd}^2}\left[\left(\frac{2\sigma T_{sat}}{\Delta T_{eff}\,\rho_g h_{fg}}\right)/\left(0.5\times D_{db}\right)\right]^{-4.4} f(\rho^*)$ (5.39)	Kurul and Podowski $\rho^* = \left(\rho_l-\rho_g\right)/\rho_g$, $f(\rho^*) = 2.157e-7\rho^{*-3.2}(1+0.0049\rho^*)^{4.13}$, $\Delta T_{eff} = ST_{\sup}$

University of Malaya

Table 5.2: Empirical correlations for bubble departure diameter (Cheung et al., 2014).

Name	Correlation	Details
Unal (1976)	$D_{bd} = \dfrac{2.42\times10^{-5} p^{0.709} a}{\sqrt{b\phi}}$ (5.40)	$a = \dfrac{\left(Q_w - h_l T_{sub}\right)^{1/3} \mathrm{k}_l}{2C^{1/3} h_{fg} \sqrt{\pi \mathrm{k}_l / \rho_l C_{p,l} \rho_g}} \sqrt{\dfrac{\mathrm{k}_w \rho_w C_w}{\mathrm{k}_l \rho_l C_{p,l}}}$, $b = \dfrac{T_{sub}}{2\left(1 - \rho_g / \rho_l\right)}$, $C = \dfrac{h_{fg} \mu_l \left[C_{p,l} / \left(0.013 h_{fg} \mathrm{Pr}^{1.7}\right)\right]}{\left[\sigma / \left(\rho_l - \rho_g\right) g\right]^{0.5}}$, $\phi = \begin{cases} \left(\dfrac{u_l}{0.061}\right)^{0.47} & \text{for} \quad u_l \geq 0.61 \text{ m/s} \\ 1 & \text{for} \quad u_l < 0.61 \text{ m/s} \end{cases}$
Kocamustafaogullari & Ishii (1983)	$D_{bd} = 0.0012\left(\dfrac{\rho_l - \rho_g}{\rho_l}\right)^{0.9} D_{LF}$ (5.41)	D_{LF} is equal to D_{bd} suggested by Fritz et al. (1935)
Fritz (1935)	$D_{bd} = 0.0208\theta[\sigma / \mathrm{g}\left(\rho_l - \rho_g\right)]^{0.5}$ (5.42)	
Cole & Shulman (1966)	$D_{bd} = [\sigma / \mathrm{g}\left(\rho_l - \rho_g\right)]^{0.5} P^{-1}$ (5.43)	
Cole & Rohsenow (1969)	$D_{bd} = 1.5e-4[\sigma / \mathrm{g}\left(\rho_l - \rho_g\right)]^{0.5} \times \left(\dfrac{\rho_l C_{p,l} T_{sat} h_{fg}}{\rho_g}\right)^{1.25}$ (5.44)	
Tolubinsky & Kostanchuk (1970)	$D_{bd} = D_{ref} \exp\left(-T_{sub} / \Delta T_{refd}\right)$ (5.45)	D_{ref}=1.3mm is suggested by (Bartolomei & Chanturiya, 1967) ΔT_{refd}=53 ^{o}k is suggested by (Krepper & Rzehak, 2011)

University of Malaya

The Cole correlation (Cole, 1960) for bubble departure frequency is calculated as

$$f = \sqrt{\frac{4g\left(\rho_l - \rho_g\right)}{3D_d \rho_l}} \tag{5.46}$$

5.2.2.2 Three-phase Model for Nanofluid Subcooled Flow Boiling

In the three-phase CFD model, the E-L model (DPM) is added to the E-E model to track the effects of nanoparticles as a discrete third phase on subcooled flow boiling heat transfer. Considering the momentum and heat exchanges between the nanoparticle phase and the continuous phase, the sink/source terms S_m and S_e are added to the conservation of momentum and energy equations respectively (Bianco et al., 2009; Fluent, 2009). The commercial Ansys-Fluent V.15 codes predict the trajectory of a discrete phase particle by integrating the force balance on the particle, which is written in a Lagrangian reference frame. The details of the equations are found in Section 3.2.3.2.3.

5.2.3 Boundary Conditions

The boundary conditions at the inlet are specified from the known inflow conditions. A constant heat flux is considered around the outer side of the wall of the pipe (conjugate boiling heat transfer). Because of the uniform wall heat flux and vertical flow direction, this phenomenon can be solved as axis-symmetric model. A no-slip condition is applied for liquid and vapour phase velocity on the inner pipe surface. For the three-phase CFD model, the no-sleep boundary condition is also considered for the nanoparticles on the wall of the pipe. In this model, the velocity of particles is assumed the same as that of the base liquid at the pipe inlet. Due to the constraints of axis-symmetry, along the centreline of the pipe, gradient of axial velocity, temperature and volume fraction are equal to zero whereas the radial velocity is equal to zero.

University of Malaya

5.2.4 Numerical Methods

The numerical methods available in the commercial CFD package of Ansys-Fluent V.15 has been used for the current study. Fluent uses a finite volume approach to convert the governing partial differential equations into a system of discrete algebraic equations. As discretization methods, a first-order upwind scheme is selected for the momentum, volume fraction, turbulent kinetic energy and turbulent dissipation rate equations whereas the first order upwind for energy equation is selected. The coupled algorithm is selected as the pressure-velocity coupling scheme. All these conditions are the same for governing equations of both two and three-phase models. For nucleate site density and bubble departure diameter, codes are developed to incorporate the Ansys-Fluent case file using User Defined Function (UDF). The scaled residuals for the velocity components and energy are set equal to 10^{-8} and 10^{-9}, respectively.

5.2.5 Simulation Cases

Table 5.3 shows different simulation cases which have been investigated in the present study. Initially, in order to establish a reliable numerical model, the validation part is focused on an accurate prediction of water subcooled flow boiling. A sensitivity test is done considering 12 combinations of the different correlations of nucleation boiling parameters in the E-E CFD model to simulate water subcooled flow boiling (cases 1-12). The predicted boiling heat transfer coefficient (BHTC) is benchmarked against the empirical correlation from literature in order to select the most accurate combination of nucleate boiling parameters. Then the repeatability and the consistency of this combination are checked for the other boundary conditions (cases 13-18). It should be noted that the selected boundary conditions keeps the nanofluid flow in subcooled condition. Selecting the boundary condition from the outside of this range causes that the other convective flows such as the saturated flow boiling and the forced convection flows are appeared.The influences of interfacial area transport (IAT)

University of Malaya

equation, non-drag forces and turbulence interaction resources on the E-E CFD model prediction are assessed (cases 19, 20-21 and 22 respectively). The validated E-E two-phase model is used to investigate Al_2O_3-water and Cu-water nanofluids subcooled flow boiling (cases 23-26 and 27-30 respectively) for different volume fractions and the given boundary condition. The investigation is repeated using the E-E plus E-L three-phase model (cases 31- 34 and 35-38 for Al_2O_3-water and Cu-water nanofluids respectively). Finally the changes of the nanofluids nucleate boiling parameters induced by the nanoparticles deposition is considered in the CFD model to investigate how the heat transfer predictions are affected (cases 39- 41).

University of Malaya

Table 5.3: The simulation table for different cases changing in working fluids, CFD model, boiling properties and boundary conditions (B.C.).

Simulation Cases	Model	Fluid	B.C.	Investigated parameters	Purpose
1-12	Two-Phase E-E model	water	G= 1445 (kg/m^{2}s), ΔT_{sub}=10 (^{o}K) q″= 60 (KW/m^2)	Nucleate boiling parameters	validation
13-18			G= 1445-2408 (kg/m^{2}s), ΔT_{sub}=10-20 (^{o}K) q″= 70-110 (KW/m^2)	Boundary conditions (i.e. G, ΔT_{sub} and q″)	
19			G= 1445 (kg/m^{2}s), ΔT_{sub}=10 (^{o}K) q″= 60 (KW/m^2)	IAT equation	
20-22			G= 1445 (kg/m^{2}s), ΔT_{sub}=10 (^{o}K) q″= 50 (KW/m^2)	Non-drag forces and turbulence interaction resources	
23-26 27-30	Two-Phase E-E model	Al_2O_3-water Cu-water	G= 1927 (kg/m2s), ΔT_{sub} =10(^{o}K) q″= 70 (KW/m^2) φ= 0.5%-2%	The two- and three-phase CFD models	Heat transfer prediction of nanofluids subcooled flow boiling
31-34 35-38	Three-Phase model: E-E model + E-L model (DPM)	Al_2O_3-water Cu-water			
39-41		Al_2O_3-water	G= 1927 (kg/m2s), ΔT_{sub} =10(^{o}K) q″= 70 (KW/m^2) φ= 0.1%	nucleation site parameters	

E-E=Eulerian-Eulerian, E-L=Eulerian-Lagrangian, DPM= Discrete Phase Model

University of Malaya

5.3 Results and Discussion

5.3.1 Mesh Dependency Test

The meshing tool available in Ansys is used to construct the computational mesh. A structured mesh based on a rectangular grid is used throughout the domain (Figure 5.4). A grid independence test was performed for the tube using water as working fluid to analyse the effects of grid size on the results. Four sets of mesh are considered, which are 8,872 nodes, 11,368 nodes, 13,846 nodes, and 15,306 nodes at G=1445 kg/m^{2}s, ΔT_{sub}=10^{o}K and q″=60 KW/m^2. By comparing the mesh configurations, in terms of average heat transfer coefficient, the corresponding changes are less than 1%. Therefore, the first grid case has been adopted to obtain an acceptable compromise between the computational time and the results accuracy.

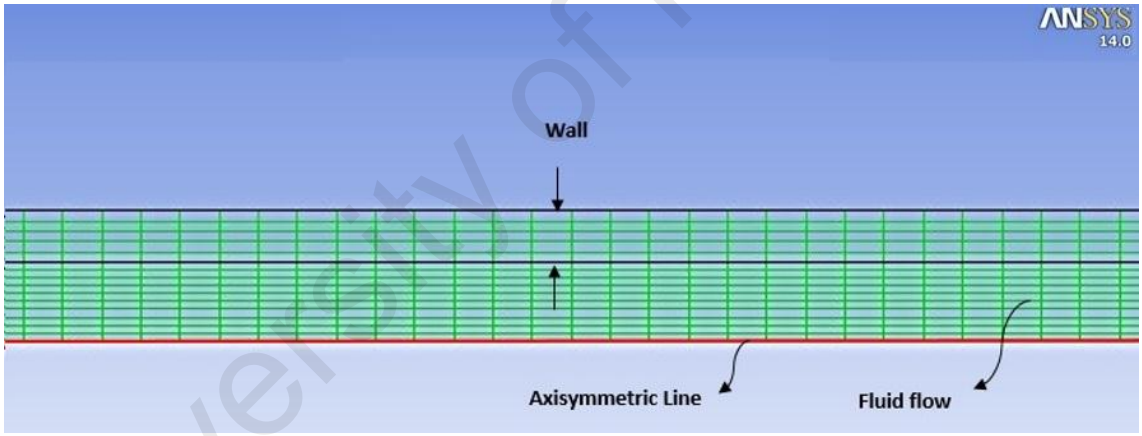

Figure 5.4: A sample mesh structure for modelling of subcooled flow boiling

5.3.2 Validation

In order to establish accuracy and reliability of the numerical model, the predicted local heat transfer coefficient for subcooled boiling of water flow inside a tube with constant wall heat flux has been compared against Chen's correlation (S. J. Kim et al., 2010). This correlation is given as follows:

$$q'' = h_{FC}(T_W - T_b) + h_{NB}(T_W - T_{sat}) \quad (5.47)$$

University of Malaya

where h_{FC} and h_{NB} are the heat transfer coefficients due to forced convection and nucleate boiling, respectively:

$$h_{FC} = 0.023\left(\frac{\mathrm{k}_l}{D_i}\right)\left(\frac{G\left(1-X\right)D_i}{\mu_l}\right)^{0.8}\left(\frac{\mu_l C_{p,l}}{\mathrm{k}_l}\right)^{0.4} F \qquad (5.48)$$

where X is the flow quality and F is the forced convection enhancement factor. At subcooled conditions, X and F must be set equal to zero and one, respectively, as recommended by Collier and Thome (1994).

$$h_{NB} = 0.00122\left[\frac{\mathrm{k}_f^{0.79} C_{p,f}^{0.45} \rho_f^{0.49}}{\sigma^{0.5} \mu_f^{0.29} h_{fg}^{0.24} \rho_g^{0.24}}\right]\left(T_W - T_{sat}\right)^{0.24} \times \left[P_{sat}(T_W) - P\right]^{0.75} S \qquad (5.49)$$

where k_f, μ_f, ρ_f, ρ_g, and σ are thermal conductivity, dynamic viscosity, liquid and vapor density, and surface tension of saturated water, respectively; $P = 1.0\times10^5$ Pa and $P_{sat}(T_w)$ are the pressure at operating condition, and the saturation pressure (in Pa) corresponding to the local wall temperature, respectively. The nucleate boiling suppression parameter, S, is (S. J. Kim et al., 2010):

$$S = \frac{1}{1+2.53\times10^{-6}\left(\left(\mathrm{G}(1-\mathrm{X})\mathrm{D}_i/\mu_l\right)F^{1.25}\right)^{1.17}} \qquad (5.50)$$

5.3.2.1 Sensitivity Tests on Nucleation Boiling Parameters

A sensitivity test has been done on the E-E CFD model prediction of water subcooled flow boiling using twelve different combinations of empirical correlations of nucleate boiling parameters (i.e. active nucleation site density (N_a), bubble departure diameter (D_{bd}) and bubble frequency (f)). The average wall temperature ($\mathrm{T_w}$) and the boiling heat transfer coefficient (BHTC) or $\mathrm{h_{sim}}$ are predicted by the CFD model. The predicted BHTCs are compared against the Chen's correlation (S. J. Kim et al., 2010). The results of this sensitivity test are shown in Table 5.4. For the given boundary condition (G=1445 kg/m^{2}s, $\Delta\mathrm{T_{sub}}$=10^{o}K and q″=60 KW/m^2), the CFD model using the combination of Lemmert-Chawla's correlation (Lemmert & Chawla, 1977) for active

University of Malaya

nucleation site density, Unal's correlation (Ünal, 1976) for bubble departure diameter and Cole's correlation (Cole, 1960) for bubble frequency gives the least deviation of -2.84% from Chen's correlation. The repeatability and the consistency of this combination are checked for the other boundary conditions (e.g. q''= 70 –110 (KW/m^2), G= 1445 – 2408 (kg/m^{2}s) and ΔT_{sub}= 10 – 20 (^{o}K)).

Table 5.4: CFD model results of water subcooled flow boiling; the sensitivity tests on different combinations of nucleate boiling parameters

	f	Na	D_{bd}	T_{wall} (^{o}K)	h_{sim} (w/m^2. ^{o}K)	Error (%)
G=1445 (kg/m^{2}s), ΔT_{sub}=10 (^{o}K), q=60 (Kw/m^2)	Cole	Koca-Ishii*	Unal	377.64	9265.15	-16.41
			Koca-Ishii*	377.64	9265.82	-16.41
			Fritz	377.65	9264.25	-16.42
			Cole-Shulman	377.65	9264.25	-16.42
			Cole-Rohsenow	377.63	9278.62	-16.26
			Tolub-Kostan*	377.65	9264.25	-16.42
		Lemmert -Chawla	Unal	376.54	10470.43	-2.84
			Koca-Ishii*	375.57	11648.42	10.06
			Fritz	377.57	9329.72	-15.68
			Cole-Shulman	377.65	9264.25	-16.42
			Cole-Rohsenow	374.96	12668.33	21.02
			Tolub-Kostan*	376.62	10309.16	-4.67

* Koca-Ishii= Kocamustafaogullari & Ishii, Tolub-Kostan= Tolubinsky & Kostanchuk

Table 5.5 shows the results of the CFD modeling of water subcooled boiling for different wall heat flux (e.g. q''= 70, 90 and 110 KW/m^2) at a constant mass flux (G= 2408 kg/m^{2}s) and inlet subcooled temperature (ΔT_{sub}= 10 ^{o}K). The predicted BHTCs show a maximum deviation of 12% from Chen's correlation (S. J. Kim et al., 2010). For all cases, the local wall temperature (T_w) increases by a maximum of 3 ^{o}K, as the axial position (Z) increases from 0.4 m to 1.6 m. Unlike forced convection regime, the

University of Malaya

local heat transfer coefficient increases by increasing the axial wall temperature. This increase of the heat transfer coefficient may be justified due to the presence of nucleate boiling heat transfer mechanism at higher axial positions (Z > 0.4 m) where the temperature is higher than the saturated temperature (> 373.15 ^{o}K). For example, in each case, the heat transfer coefficient is predicted to increase by 1 KW/m^2.^{o}K as the axil position increases from o.4 m to 1.6 m. The increase of wall heat flux from 70 KW/m^2 to 110 KW/m^2 causes the increase of the local wall temperature and the local wall heat flux by maximum 5 ^{o}K and 2 KW/m^2.^{o}K respectively. Increasing the wall heat flux, the onset of the nucleate boiling happens closer to the pipe inlet (Z_{ONB}= 1.07 m and 0.01 m for q″=70 KW/m^2 and 110 KW/m^2 respectively). The outlet vapor volume fraction (α_{out}) also increases to a maximum of 0.772 as the wall heat flux increases to a maximum of 110 KW/m^2.

University of Malaya

Table 5.5: CFD model results of water subcooled flow boiling; assessing the effect of wall heat flux on local wall temperature, local heat transfer coefficient, onset of nucleate boiling length and outlet vapor volume fraction

	q'' (KW/m^2)	Z (m)	T_{wall} (^oK)	h_{sim} ($W/m^2.{}^oK$)	h_{Chen} ($W/m^2.{}^oK$)	Error (%)	Z_{ONB} (m)	α_{out}
G=2408 (kg/m^2s) ΔT_{sub}=10 (^oK)	70	Z_1=0.4	372.43	13578.10	15250.53	-10.97	1.07	5.52×10^{-4}
		Z_2=0.8	373.37	14115.97	15253.47	-7.46		
		Z_3=1.2	374.50	14192.32	15313.38	-7.32		
		Z_4=1.6	375.56	14390.45	15443.24	-6.82		
	90	Z_1=0.4	375.06	13672.43	15528.88	-11.95	0.15	3.89×10^{-2}
		Z_2=0.8	376.14	14364.39	15665.16	-8.30		
		Z_3=1.2	377.34	14816.01	15868.42	-6.63		
		Z_4=1.6	378.48	15401.70	16202.10	-4.94		
	110	Z_1=0.4	377.32	14115.66	15803.30	-10.68	0.01	3.77×10^{-1}
		Z_2=0.8	378.42	15129.133	16164.76	-6.41		
		Z_3=1.2	379.85	15683.66	16450.72	-4.67		
		Z_4=1.6	380.85	16916.42	16734.66	1.09		

Similarly, the sensitivity test results for different inlet subcooled temperatures and different mass fluxes have been shown in Table 5.6 and Table 5.7 respectively. The predicted BHTCs show maximum$\pm$ 17% deviation from the Chen correlation (S. J. Kim et al., 2010).

University of Malaya

Table 5.6: CFD model results of water subcooled flow boiling; assessing the effect of inlet subcooled temperature on local wall temperature, local heat transfer coefficient, onset of nucleate boiling length and outlet vapor volume fraction

	ΔT_{sub} (^oK)	Z (m)	T_{wall} (^oK)	h_{sim} ($W/m^2.{}^oK$)	h_{Chen} ($W/m^2.{}^oK$)	Error (%)	Z_{ONB} (m)	α_{out}
G=1445 (kg/m^2s) q''=70 (KW/m^2)	10	Z_1=0.4	376.66	9575.73	10677.89	-10.32	0.05	4.31×10^{-1}
		Z_2=0.8	377.35	10797.21	10848.93	-0.48		
		Z_3=1.2	377.83	12541.23	11182.39	12.15		
		Z_4=1.6	378.95	13756.05	11775.40	16.82		
	15	Z_1=0.4	372.94	8671.01	10002.69	-13.31	0.72	1.99×10^{-3}
		Z_2=0.8	374.51	9015.66	10063.84	-10.42		
		Z_3=1.2	376.02	9334.186	10266.66	-9.08		
		Z_4=1.6	377.06	10090.42	10523.31	-4.11		
	20	Z_1=0.4	368.35	8415.06	9746.22	-13.66	1.72	5.88×10^{-6}
		Z_2=0.8	369.95	8712.90	9746.22	-10.60		
		Z_3=1.2	371.77	8805.26	9746.22	-9.65		
		Z_4=1.6	373.59	8911.97	9758.02	-8.67		

University of Malaya

Table 5.7: CFD model results of water subcooled flow boiling; assessing the effect of inlet mass flux on local wall temperature, local heat transfer coefficient, onset of nucleate boiling length and outlet vapor volume fraction

	G (kg/m^2s)	Z (m)	T_{wall} (^oK)	h_{sim} ($W/m^2.{}^oK$)	h_{Chen} ($W/m^2.{}^oK$)	Error (%)	Z_{ONB} (m)	α_{out}
ΔT_{sub}=10 (^oK) q''=70 (KW/m^2)	1445	Z_1=0.4	376.66	9575.73	10677.89	-10.32	0.05	4.31×10^{-1}
		Z_2=0.8	377.35	10797.21	10848.93	-0.48		
		Z_3=1.2	377.83	12541.23	11182.39	12.15		
		Z_4=1.6	378.95	13756.05	11775.40	16.82		
	1927	Z_1=0.4	372.77	13387.59	12919.53	3.62	0.84	9.06×10^{-3}
		Z_2=0.8	373.97	13994.49	12949.86	8.07		
		Z_3=1.2	375.37	14112.52	13087.92	7.83		
		Z_4=1.6	376.63	14495.24	13391.45	8.24		
	2408	Z_1=0.4	372.43	13578.10	15250.53	-10.97	1.07	5.52×10^{-4}
		Z_2=0.8	373.37	14115.97	15253.47	-7.46		
		Z_3=1.2	374.50	14192.32	15313.38	-7.32		
		Z_4=1.6	375.56	14390.45	15443.24	-6.82		

According to Table 5.6, the increase of the inlet subcooled temperature at the constant wall heat flux (q''= 70 KW/m^2) and the constant inlet mass flux (G= 1445 kg/m^2s) has a converse effect on subcooled flow boiling. For example, a 10 ^oK increase of the inlet subcooled temperature shows the maximum 8 ^oK and 5 $KW/m^2.{}^oK$ decrease of the local wall temperature and the local heat transfer coefficient respectively. Increasing the inlet subcooled boiling from 10 ^oK to 20 ^oK, the length of the onset of the nucleate boiling increases to a maximum of 1.72 m while, the outlet vapor volume fraction decreases to a minimum of 6×10^{-6}. Table 5.7 also shows the converse effect of mass flux increment on the heat transfer of the water subcooled flow boiling. The increase of the mass flux shows the decrease of the local wall temperature, the local heat

University of Malaya

transfer coefficient and the outlet vapor volume fraction. However, the length of the onset of nucleate boiling increases by increasing the mass flux.

5.3.2.2 Sensitivity test on interfacial area concentration

Table 5.8 shows the E-E CFD model predictions of water subcooled flow boiling with and without the implementation of an interfacial area transport (IAT) equation. Incorporation of the IAT equation with the E-E CFD model does not show any effect on the predicted values of average wall temperature, average heat transfer coefficient and the length of the onset of nucleate boiling.

Table 5.8: CFD model results of water subcooled flow boiling; assessing the CFD model predictions with and without the implementation of an interfacial area transport (IAT) equation.

	a_{if}	T_{wall} (^oK)	h_{sim} ($w/m^2.{}^oK$)	Error (%)	Z_{ONB} (m)	α_{out}
G=1445 (kg/m^2s), ΔT_{sub}=10 (^oK), q''=60 (KW/m^2)	Algebraic relationship	376.54	10470.43	-2.84	0.115	6.23×10^{-2}
	IAT equation	376.53	10473.88	-2.76	0.111	1.22×10^{-1}

However, the exception is seen for the prediction of the outlet vapor volume fraction. The E-E CFD model predicts $\alpha_{out}= 6.23\times10^{-2}$. This value is predicted to be 1.22×10^{-1}, with a two-fold increase, where the IAT equation is included in the E-E CFD model. Since the average volume fraction of vapor is so low (in order of 0.01), the changes in prediction of vapor volume fraction have no significant effect on the other parameters, such as wall temperature and the average heat transfer coefficient.

University of Malaya

5.3.2.3 Sensitivity Test on Non-drag Forces and Turbulence Resource

The effect of non-drag forces (i.e. lift, wall lubrication and turbulent dispersion forces) and turbulence interaction resource on average wall temperature, average heat transfer coefficient, length of the onset of the nucleate boiling and outlet vapor volume fraction are assessed. According to Table 5.9, the prediction of the average wall temperature, the average heat transfer coefficient, and the length of the onset of the nucleate boiling are not sensitive to the non-drag forces and turbulence interaction resource. However, considering the non-drag forces and turbulence interaction resource in the CFD model shows a significant decrease in the predicted value of the outlet vapor volume fraction by 20%. Since the average volume fraction of vapor is so low (in order of 0.001), the changes in the prediction of the vapor volume fraction have no significant effect on the other parameters, such as wall temperature, the average heat transfer coefficient and the length of the onset of nucleate boiling.

Table 5.9: CFD model results of water subcooled flow boiling; sensitivity tests on the effects of non-drag forces and turbulence interaction resource on the CFD model prediction

	Interphase interaction effect	T_{wall} (^oK)	h_{sim} ($w/m^2.{}^oK$)	Error (%)	Z_{ONB} (m)	α_{out}
G=1445 (kg/m^2s), ΔT_{sub}=10 (^oK), q''=50 (Kw/m^2)	-	375.090	9398.411	-10.05	0.614	5.30×10^{-3}
	Non-drag forces	375.087	9402.267	-10.01	0.614	4.14×10^{-3}
	Turbulence interaction resource	375.087	9401.957	-10.01	0.614	4.03×10^{-3}

University of Malaya

5.3.3 CFD Models Comparison for Nanofluids

CFD modeling of the nanofluids subcooled flow boiling through a vertical heated pipe is investigated in this section. The heat transfer predictions of Al_2O_3-water and Cu-water nanofluid subcooled flow boiling using the Eulerian-Eulerian two-phase model are given in **Table 5.10**. In this investigation, the nanofluids are considered as a single-phase liquid.

Table 5.10: Heat transfer prediction of Al_2O_3-water and Cu-water nanofluid subcooled flow boiling using Eulerian-Eulerian two-phase CFD model

B.C.	Fluid	φ (%)	T_{wall} (^oK)	h_{sim} ($w/m^2.{}^oK$)	h_{NF}/h_{BF}	Error (%)	Z_{ONB} (m)	α_{out}
G=1927 (kg/m^2s), ΔT_{sub}=10 (^oK), q″=70 (KW/m^2)	Water	0	374.69	13997.46	1	6.96	0.84	9.06×10^{-3}
	Al_2O_3-water	0.5	374.85	13830.73	0.99	10.41	0.80	1.20×10^{-2}
		1	375.01	13668.26	0.98	10.50	0.75	1.54×10^{-2}
		1.5	375.17	13511.59	0.97	10.75	0.71	1.94×10^{-2}
		2	375.34	13349.95	0.95	11.01	0.66	2.40×10^{-2}
	Cu-water	0.5	375.00	13726.54	0.98	10.52	0.76	1.81×10^{-2}
		1	375.32	13456.80	0.96	10.29	0.67	3.28×10^{-2}
		1.5	375.61	13251.54	0.95	10.73	0.58	5.80×10^{-2}
		2	375.89	13075.66	0.93	11.37	0.48	1.02×10^{-1}

According to Table 5.10, for 0.5 vol. % Al_2O_3-water nanofluid, the heat transfer predictions are as much as pure water. However, a minor heat transfer degradation is seen as the nanoparticle volume fraction increases. For example, the average wall temperature (T_w) increases from 374.69 ^oK for pure water to 375.34 ^oK for 2 vol.% Al_2O_3-water nanofluid. This minor increase of wall temperature (less than 1 ^oK) effects the heat transfer coefficient (h_{sim} or h_{NF}/h_w), the length of the onset of nucleate boiling (Z_{ONB}) and the vapor fraction at the pipe outlet (α_{out}) remarkably. For example, the

University of Malaya

addition of 2 vol.% Al_2O_3 nanoparticles in the pure water causes a maximum 5% decrease in the heat transfer coefficient; Z_{ONB} decreases from 0.84m for pure water to 0.66 m for 2 vol.% Al_2O_3-water nanofluid, while α_{out} increases from 0.00906 to 0.024. This heat transfer degradation can be justified due to the decrease of the inlet velocity in the case of constant inlet mass flux. Increasing the nanoparticle volume fraction, the effective density of the nanofluid also increases. So, the inlet velocity decreases at a constant inlet mass flux. Decreasing the velocity leads to more bubbles generation or more quenching and evaporation heat transfers. However, the forced convection heat transfer decreases as the inlet velocity decreases. Since, in the given cases, the volume fraction of vapour is low (in order of 0.01), the effect of quenching and evaporation heat transfers on total BHTC is less than that of forced convection. Therefore, as the nanoparticle volume fraction increases, more BHTC degradation is resulted by more reduction of the forced convection heat transfer. The predicted heat transfer coefficients are underestimated by Chen's correlation (S. J. Kim et al., 2010) with a maximum of 12% deviation. The trends of the predicted results for Al_2O_3-water nanofluid are repeated for Cu-water nanofluid. According to **Table 5.10**, Cu-water nanofluid shows a little more heat transfer deterioration than Al_2O_3-water nanofluid. For example, increasing the Cu nanoparticle volume fraction to 2%, the temperature increases to a maximum 375.89 ^oK; the average heat transfer coefficient decreases by a maximum of 7%. The onset of the nucleate boiling of 2 vol.% Cu-water subcooled flow boiling happens closer to the pipe inlet (Z_{ONB} = 0.48 m) than that of 2% Al_2O_3-water nanofluid (Z_{ONB} = 0.66 m). The outlet vapor fraction of 2vol.% Cu-water (α_{out}=0.102) is about four times higher than that of 2 vol.% Al_2O_3-water nanofluid (α_{out}=0.024).

Table 5.11 shows the heat transfer predictions of Al_2O_3-water and Cu-water nanofluid subcooled flow boiling using Eulerian-Eulerian plus DPM three-phase CFD model. Unlike the previous investigation, in this way, the nanofluid is taken into

University of Malaya

account as a two-phase fluid. The interphase interactions between the nanoparticles (i.e. Al_2O_3 and Cu) and the base liquid (i.e. water) are also considered in the CFD model.

Table 5.11: Heat transfer prediction of Al_2O_3-water and Cu-water nanofluid subcooled flow boiling using Eulerian-Eulerian plus DPM three-phase CFD model

B.C.	Fluid	φ (%)	T_{wall} (^oK)	h_{sim} ($w/m^2.{}^oK$)	h_{NF}/h_{BF}	Error (%)	Z_{ONB} (m)	α_{out}
G=1927 (kg/m^2s), ΔT_{sub}=10 (^oK), q″=70 (KW/m^2)	Water	0	374.69	13997.46	1	6.96	0.84	9.06×10^{-3}
	Al_2O_3-water	0.5	375.16	13235.13	0.95	5.53	0.48	1.17×10^{-2}
		1	375.35	13038.26	0.93	5.24	0.45	1.45×10^{-2}
		1.5	375.53	12851.86	0.92	5.12	0.42	1.77×10^{-2}
		2	375.69	12689.96	0.91	5.26	0.39	2.13×10^{-2}
	Cu-water	0.5	375.38	13054.91	0.93	4.78	0.45	1.78×10^{-2}
		1	375.78	12710.11	0.91	3.81	0.37	3.19×10^{-2}
		1.5	376.12	12456.77	0.89	3.58	0.30	5.54×10^{-2}
		2	376.44	12263.57	0.88	3.82	0.25	9.65×10^{-2}

According to Table 5.10 and Table 5.11, the average wall temperatures predicted by the three-phase model are a bit higher than those predicted by the two-phase model (less than 1 ^oK difference). The three-phase CFD model predicts the average heat transfer coefficients with a maximum of 6% deviation from Chen's correlation (S. J. Kim et al., 2010). This deviation is less than that of the two-phase model prediction (maximum 9% and 12 % for Al_2O_3-water and Cu-water respectively). For a small fraction of the nanoparticles (0.5%) in the base fluid, the two-phase CFD model predicts a minor decrease in heat transfer coefficient (~ 2%). However, this decrease of heat transfer coefficient becomes more significant as predicted by the three-phase CFD model (5% and 7 % decreases for Al_2O_3-water and Cu-water respectively). As the nanoparticle volume fraction increases, the BHTC degradation predicted by the three-

University of Malaya

phase model is more than that predicted by the two-phase model (maximum 7% and 12 % decreases in BHTC predicted by the two-phase and three-phase models respectively). Z_{ONB} predicted by the three-phase model is less than Z_{ONB} predicted by the two-phase. For example, for 2 vol.% Al_2O_3-water, the two-phase model predicts Z_{ONB} = 0.66 m while this value is equal to 0.39 m as predicted by the three-phase model. The two-phase and three-phase CFD models predict the same outlet vapor volume fraction (α_{out}) in almost all cases (maximum difference of 0.0235).

5.3.4 Effects of Nanoparticle Deposition

As stated previously in sections 2.3 and 5.1, the nanoparticles deposition plays an important role in the wettability improvement of the heater surface. This wettability improvement decreases the contact angle of the base liquid droplet with the heated surface. This is followed by a decrease in the active nucleate site density and an increase in the bubble departure diameter. All these changes are considered in Equations (5.36)-(5.37), suggested by Li et al. (2014), to incorporate the CFD model. Since Equations (5.36)-(5.37) are suggested for very dilute nanofluids (≤0.1% volume fraction) and the data for contact angle of droplet with the surface is just available for Al_2O_3-water nanofluid, this study is limited to the simulation of 0.1 vol.% Al_2O_3-water nanofluid subcooled flow boiling. This CFD modeling is carried out for both clean and nanofluid boiled surfaces. For more comparison, the CFD modeling is repeated using the Equations (5.38) and (5.40). Table 5.12 shows the results of this investigation. Replacing the previously used Equations of (5.38) and (5.40) with Equations (5.36)-(5.37) shows an invisible effect on the CFD model predictions of T_w, h_{sim} or BHTC and Z_{ONB}. The contact angle of the droplet of 0.1 vol.% Al_2O_3-water nanofluid on stainless steel (SS) surface decreases from 71^o for clean surfaces to 41^o for nanofluid boiled surfaces (S. Kim et al., 2007). However, this decrease of droplets contact angle does not show any significant changes in the CFD model predictions. The exception is seen

University of Malaya

regarding the outlet vapor volume fraction where the difference between the predicted values is significant. The CFD model using Equations (5.36)-(5.37) predicts the α_{out} = 9.79×10^{-3} for the clean surface. The α_{out} is predicted to increase to 1.24×10^{-2} for the nanofluid boiled surfaces. These both predictions are lower than the CFD model prediction using Equations (5.38) and (5.40) (α_{out} =1.66×10^{-2}).

Table 5.12: Heat transfer prediction of 0.1 vol. % Al_2O_3-water nanofluid subcooled flow boiling using the three-phase CFD model with and without considering the nanoparticle deposition

B.C.	Wall status	Boiling properties	T_{wall} (^oK)	h_{sim} ($W/m^2.{}^oK$)	h_{NF}/h_{BF}	Error (%)	Z_{ONB} (m)	α_{out}
G=1927 (kg/m^2s), ΔT_{sub}=10 (^oK), q″=70 (KW/m^2)	Clean surface	D_{bd}: Unal (1976) *Na*: Lemmert-Chawla (1977)	374.95	13519.79	0.97	6.94	0.51	1.66×10^{-2}
		D_{bd} & *Na*: Li et al. (2014)	375.00	13417.82	0.96	6.05	0.51	9.79×10^{-3}
	Nanofluid boiled surface	D_{bd} & *Na*: Li et al. (2014)	375.02	13393.23	0.96	5.82	0.51	1.24×10^{-2}

5.4 Conclusions

The subcooled flow boiling of Al_2O_3/water and Cu/water nanofluids in a vertical heated pipe has been investigated numerically using the commercial Ansys-Fluent CFD codes. For this purpose, the Eulerian-Eulerian (E-E) two-phase CFD model was selected. Initially, for a strong validation of the CFD model, water subcooled flow boiling was modeled under different nucleate boiling parameters (i.e. nucleate site density, bubble frequency, and bubble departure diameter), boundary conditions (i.e. fluid mass flux, inlet subcooled temperature and wall heat flux) and bubble dynamic mechanisms (i.e. non-drag forces, turbulence interaction resource and interfacial area

University of Malaya

concentration). According to the findings of the sensitivity tests, the most accurate combination of the boiling properties was used in the E-E approach to model the nanofluids subcooled flow boiling. The effect of interphase interactions (i.e. interactions of the nanoparticles and the base liquid) and nonhomogeneous nanoparticles distribution on heat transfer predictions were also investigated. For this purpose, the Eulerian-Lagrangian CFD model was selected to be incorporated with the E-E model. The surface wettability improvement induced by the nanoparticles deposition has been considered in the CFD model to find out how the heat transfer predictions are affected by such wettability improvement. Since some models of nucleate boiling parameters are not available in Ansys-Fluent CFD codes, several UDF codes were written to define the nucleate site density and the bubble departure diameter for the nanofluids. The UDF codes were incorporated with the commercial CFD codes of Ansys-Fluent.The conclusions of this study are summarized as follows:

- The E-E two-phase CFD model using the combination of Lemmert-Chawla' s correlation (Lemmert & Chawla, 1977) for active nucleation site density, Unal' s correlation (Ünal, 1976) for bubble departure diameter and Cole' s correlation (Cole, 1960) for bubble frequency show a good agreement with Chen's correlation in prediction of BHTC of water subcooled flow boiling.
- Considering the interfacial transport equation, non-drag forces and turbulence interaction resource in the E-E two-phase CFD model show no effect on prediction of BHTC of water subcooled flow boiling.
- The E-E two-phase CFD model predicts heat transfer degradation for both Al_2O_3/water and Cu/water nanofluids subcooled flow boiling. As the nanoparticles volume fraction increases T_w and α_{out} increase; however, BHTC and Z_{ONB} decreases. The predicted BHTCs are underestimated by Chen's correlation with a maximum 12% deviation.

University of Malaya

- The E-E plus E-L three-phase CFD model predicts more heat transfer degradation than the E-E two-phase CFD model for the nanofluids subcooled flow boiling. Using the three-phase CFD model, the deviation of the predicted BHTC from Chen correlation decreases to 6%.
- Considering the wettability improvement in the CFD model shows no effect on prediction of BHTC of 0.1 vol.% Al_2O_3/water subcooled flow boiling.

University of Malaya

6 CHAPTER 6: CONCLUSION AND FUTURE WORK

6.1 Conclusions

The aims of this study were to obtain a detailed understanding of the modeling of the nanofluids convective heat transfer. For this purpose, the study was focused on CFD modeling of nanofluid heat transfer during forced convection and convective flow boiling through a heated pipe. In case of the forced convection heat transfer, the research was limited to laminar and turbulent flows. Depending on whether the nanofluid was assumed as a homogeneous single-phase liquid or a colloidal mixture of nanoparticles and the base liquid, the nanofluid flows were modelled by either single-phase or two-phase approaches. There are various single- and two-phase models that have been incorporated in the numerical studies from the literature in order to improve the prediction of heat transfer of various nanofluids. The different single-phase models (i.e. Newtonian and non-Newtonian) and two-phase models (i.e. Eulerian-Eulerian, mixture and Eulerian-Lagrangian) were used to simulate nanofluid forced convection through a heated pipe. Different fluid rheology, effective conductivity models and effective viscosity models were used in the single-phase approach to achieve the most accurate prediction of nanofluid heat transfer.

In case of the convective flow boiling, the research was focused on subcooled flow boiling through a vertical heated pipe. Different sensitivity tests are carried out to present the effects of nucleate boiling parameters (i.e. nucleate site density, bubble frequency, and bubble departure diameter), boundary conditions (i.e. fluid mass flux, inlet subcooled temperature and wall heat flux) and bubble dynamic mechanisms (i.e. non-drag forces, turbulence interaction resource and interfacial area concentration) on the heat transfer predictions of water subcooled flow boiling. The Eulerian-Eulerian two-phase model and a three-phase model (i.e. Eulerian-Eulerian plus Eulerian-Lagrangian) were used for the first time to model the nanofluids' heat transfer during

University of Malaya

subcooled flow boiling regime in a vertical heated tube. The surface wettability improvement induced by the nanoparticles deposition was considered in the CFD model to find out how the heat transfer predictions were effected by such wettability improvement. All the simulation results are benchmarked against the experimental ones from literature. The following provides a summary of the main conclusions of this study:

- Single-phase CFD model is able to predict the nanofluid heat transfer accurately, if the effective properties of nanofluid and nanofluid rheology are determined accurately; it needs less computational effort than two-phase models.
- Eulerian-Eulerian CFD model needs an accurate correlation for calculation of the particle conductivity for accurate prediction; this model is not recommended for nanofluid heat transfer especially during turbulent regime.
- Mixture CFD model is able to predict the nanofluid heat transfer accurately. The efficiency of this model is less than the single-phase model; it needs more computational effort than the single-phase model, whereas the accuracy of mixture model is less than that of the single-phase model.
- Eulerian-Lagrangian CFD model is the most accurate two-phase model in prediction of nanofluid heat transfer. This model does not need the determination of nanofluid effective properties and the determination of nanofluid rheology.
- A proper selection of nucleate boiling parameters is needed for an accurate prediction of heat transfer during nanofluid subcooled flow boiling.

University of Malaya

6.2 Contribution of study

Accurate prediction of the nanofluid heat transfer is a fundamental requirement for safe operation and optimal design of thermal systems. This thesis contributes to numerically investigate a number of single and multiphase CFD models in accurate prediction of the forced convection and the subcooled boiling of the nanofluids. An appropriate use of the CFD models and the quantitative error involved in the prediction of heat transfer of various nanofluids during the forced convection have been found very much unclear through the literature. The results of this study show that the single-phase CFD model is capable of predicting the nanofluid forced convection accurately, if the proper thermo-physical properties and nanofluid rheology are selected. The two-phase CFD models under the Eulerian frame-works (i.e. Eulerian-Eulerian and mixture models) predict the nanofluid heat transfer inaccurately. The lack of the experimental data for the calculation of the solidus viscosity and the nanoparticle conductivity has been known as the main weak points of the Eulerian models. However, the Eulerian-Lagrangian two-phase CFD model predicts the nanofluid heat transfer accurately. The accuracy of the single-phase and the Eulerian-Lagrangian two-phase models are similar in laminar flows. But the Eulerian-Lagrangian two-phase model predicts more accurate results than the single-phase in the turbulent flows. So, this study contributes to be used as a reference for the selection of the proper CFD model in the other similar cases. In case of subcooled flow boiling, it was clarified that the proper selection of nucleate boiling parameters (i.e. active nucleate site density, bubble departure diameter and bubble frequency) are important in the accurate prediction of the boiling heat transfer coefficient (BHTC). However, the bubble dynamic mechanisms (i.e. non-drag forces, turbulence interaction resource and interfacial area concentration) have an invisible effects on BHTC during subcooled flow boiling. So, neglecting the bubble dynamic mechanisms saves the computational efforts, while the reasonable prediction of BHTC

University of Malaya

is achieved. It was also, found that the Eulerian-Eulerian (two-fluid) CFD model gives a roughly accurate prediction of the BHTC of the nanofluids and combination of the Eulerian-Eulerian and the Eulerian-Lagrangian models improves the accuracy of BHTC prediction significantly. It was observed that the nanoparticle deposition or wettability improvement of the heated surface have no effect on BHTC of the nanofluids. The different UDF codes have been created to define the different models of fluid rheology, thermo-physical properties, nucleate site density and bubble departure diameter. All the UDF codes, developed in this study, can be used and incorporated Ansys-Fluent software for modelling of the other similar cases for academic and industrial purposes.

6.3 Recommendation for future work

The results presented here have demonstrated the effectiveness of the different CFD approaches in heat transfer prediction of nanofluids during forced convention and subcooled flow boiling. This research could be further developed in a number of ways:

6.3.1 Mixed convection flow of nanofluids

The transfer of heat by combined forced and natural convection (mixed convection) in inclined tubes is significant in many industrial applications such as solar energy collectors, supercritical boilers and nuclear reactors (Allahyari et al., 2011). The contribution of natural convection may enhance the rate of heat transfer to a fluid in laminar flow through a horizontal tube by a factor of three or four. The irregular motion of nanoparticles may increase the secondary flow strength so as to increase the heat transfer by natural convection (Mirmasoumi & Behzadmehr, 2008a, 2008b). The efficiency of the different CFD approaches in heat transfer prediction of the nanofluid forced convection has been investigated in this study. It is recommended to investigate how the results of this study are affected by the presence of the secondary flow (natural convention). Further studies are needed to develop the different single- and two-phase CFD models for analysing the nanofluid heat transfer during mixed convection.

University of Malaya

6.3.2 Critical heat flux

The heat flux at which the boiling crisis occurs is named the critical heat flux (CHF). Basically, the boiling process changes from efficient nucleate boiling to lesser efficient annular film boiling at the CHF point. In general, thermal performance improvements are highly desirable and it is therefore needed to predict CHF accurately at the earliest stages of a new product design. In terms of boiling regimes, nucleate boiling is an efficient heat-transfer mechanism. However, for the incorporation of nucleate boiling in most practical applications, it is imperative that the CHF is not exceeded. CHF phenomenon is the thermal limit during a heat-transfer phase change. At the CHF point the heat transfer is maximized, followed by a drastic degradation after the CHF point. The occurrence of CHF is accompanied by localized overheating at the heated surface, and a decrease in the heat-transfer rate. An increase in the CHF of the boiling system would therefore allow for more compact and effective cooling systems for nuclear reactors, air-conditioning units, etc.(Le Corre et al., 2010). The CHF enhancement by using the nanofluids has been reported by experimental studies (Bang & Chang, 2004; Barber et al., 2011). The nanoparticle deposition has been known as the most important factor for such enhancement (Kim, 2007). In this study the subcooled nucleate flow boiling was numerically investigated. The nanoparticle deposition effects have been considered in the CFD model. Further numerical studies are recommended to be carried out for assessing the efficiency of the CFD model in prediction of the CHF of the nanofluids.

University of Malaya

REFERENCES

Abedini, E., Behzadmehr, A., Rajabnia, H., Sarvari, S., & Mansouri, S. (2013). Experimental investigation and comparison of subcooled flow boiling of TiO_2 nanofluid in a vertical and horizontal tube. *Proceedings of the Institution of Mechanical Engineers, Part C: Journal of Mechanical Engineering Science, 227*(8), 1742-1753.

Abedini, E., Behzadmehr, A., Sarvari, S., & Mansouri, S. (2013). Numerical investigation of subcooled flow boiling of a nanofluid. *International Journal of Thermal Sciences, 64*, 232-239.

Abu-Nada, E. (2009). Effects of variable viscosity and thermal conductivity of Al_2O_3–water nanofluid on heat transfer enhancement in natural convection. *International Journal of Heat and Fluid Flow, 30*(4), 679-690.

Abu-Nada, E., Masoud, Z., & Hijazi, A. (2008). Natural convection heat transfer enhancement in horizontal concentric annuli using nanofluids. *International Communications in Heat and Mass Transfer, 35*(5), 657-665.

Akbari, M., Galanis, N., & Behzadmehr, A. (2012). Comparative assessment of single and two-phase models for numerical studies of nanofluid turbulent forced convection. *International Journal of Heat and Fluid Flow, 37*, 136-146.

Allahyari, S., Behzadmehr, A., & Sarvari, S. H. (2011). Conjugate heat transfer of laminar mixed convection of a nanofluid through a horizontal tube with circumferentially non-uniform heating. *International Journal of Thermal Sciences, 50*(10), 1963-1972.

Aminfar, H., Mohammadporfard, M., & Maroofiazar, R. (2013). Eulerian simulation of subcooled boiling flow in straight and curved annuli. *Journal of Mechanical Science and Technology, 27*(5), 1295-1304.

Aminfar, H., & Motallebzadeh, R. (2011). Numerical Investigation of the Effects of Nanoparticle Diameter on Velocity Field and Nanoparticle Distribution of Nanofluid Using Lagrangian-Eulerian Approach. *Journal of Dispersion Science and Technology, 32*(9), 1311-1317.

Anoop, K., Sundararajan, T., & Das, S. K. (2009). Effect of particle size on the convective heat transfer in nanofluid in the developing region. *International Journal of Heat and Mass Transfer, 52*(9), 2189-2195.

Antal, S., Lahey Jr, R., & Flaherty, J. (1991). Analysis of phase distribution and turbulence in dispersed particle/liquid flows. *Chem. Eng. Commun, 174*, 85-113.

Bae, B.-U., Yun, B.-J., Yoon, H.-Y., Song, C.-H., & Park, G.-C. (2010). Analysis of subcooled boiling flow with one-group interfacial area transport equation and bubble lift-off model. *Nuclear Engineering and Design, 240*(9), 2281-2294.

Bahiraei, M., & Hosseinalipour, S. M. (2013a). A Comprehensive Review on Different Numerical Approaches for Simulation in Nanofluids: Traditional and Novel Techniques. *Journal of Dispersion Science and Technology*.

University of Malaya

Bahiraei, M., & Hosseinalipour, S. M. (2013b). Effects of various forces on particle distribution and thermal features of suspensions containing alumina nanoparticles. *Journal of Dispersion Science and Technology*.

Bang, I. C., & Chang, S. H. (2004). Boiling heat transfer performance and phenomena of Al_2O_3-water nano-fluids from a plain surface in a pool: American Nuclear Society, 555 North Kensington Avenue, La Grange Park, IL 60526 (United States).

Barber, J., Brutin, D., & Tadrist, L. (2011). A review on boiling heat transfer enhancement with nanofluids. *Nanoscale research letters, 6*(1), 1-16.

Bartolomei, G., & Chanturiya, V. (1967). Experimental study of true void fraction when boiling subcooled water in vertical tubes. *Thermal Engineering, 14*(2), 123-128.

Batchelor, G. (1977). The effect of Brownian motion on the bulk stress in a suspension of spherical particles. *Journal of Fluid Mechanics, 83*(01), 97-117.

Behroyan, I., Ganesan, P., He, S., & Sivasankaran, S. (2015). Turbulent forced convection of Cu–water nanofluid: CFD model comparison. *International Communications in Heat and Mass Transfer*.

Behroyan, I., Vanaki, S. M., Ganesan, P., & Saidur, R. (2015). A comprehensive comparison of various CFD models for convective heat transfer of Al_2O_3 nanofluid inside a heated tube. *International Communications in Heat and Mass Transfer*.

Behzadmehr, A., Saffar-Avval, M., & Galanis, N. (2007). Prediction of turbulent forced convection of a nanofluid in a tube with uniform heat flux using a two phase approach. *International Journal of Heat and Fluid Flow, 28*(2), 211-219.

Bejan, A., & Kraus, A. D. (2003). *Heat transfer handbook* (Vol. 1): John Wiley & Sons.

Bergman, T. L., Incropera, F. P., Lavine, A. S., & DeWitt, D. P. (2011). *Fundamentals of heat and mass transfer*: John Wiley & Sons.

Bianco, V., Chiacchio, F., Manca, O., & Nardini, S. (2009). Numerical investigation of nanofluids forced convection in circular tubes. *Applied Thermal Engineering, 29*(17), 3632-3642.

Bird, R. B., Stewart, W. E., & Lightfoot, E. N. (2007). *Transport phenomena*: John Wiley & Sons.

Brinkman, H. (1952). The viscosity of concentrated suspensions and solutions. *The Journal of Chemical Physics, 20*, 571.

Chang, H., Jwo, C., Lo, C., Tsung, T., Kao, M., & Lin, H. (2005). Rheology of CuO nanoparticle suspension prepared by ASNSS. *Rev. Adv. Mater. Sci, 10*(2), 128-132.

Chen, E., Li, Y., Cheng, X., & Wang, L. (2009). Modeling of low-pressure subcooled boiling flow of water via the homogeneous MUSIG approach. *Nuclear Engineering and Design, 239*(10), 1733-1743.

University of Malaya

Cheung, S., Vahaji, S., Yeoh, G., & Tu, J. (2014). Modeling subcooled flow boiling in vertical channels at low pressures–Part 1: Assessment of empirical correlations. *International Journal of Heat and Mass Transfer, 75*, 736-753.

Choi, S. U., & Eastman, J. (1995). Enhancing thermal conductivity of fluids with nanoparticles: Argonne National Lab., IL (United States).

Chon, C. H., Kihm, K. D., Lee, S. P., & Choi, S. U. (2005). Empirical correlation finding the role of temperature and particle size for nanofluid (Al_2O_3) thermal conductivity enhancement. *Applied Physics Letters, 87*(15), 153107-153107-153103.

Cole, R. (1960). A photographic study of pool boiling in the region of the critical heat flux. *AIChE Journal, 6*(4), 533-538.

Cole, R., & Rohsenow, W. (1969). *Correlation of bubble departure diameters for boiling of saturated liquids.* Paper presented at the Chem. Eng. Prog. Symp. Ser.

Cole, R., & Shulman, H. (1966). *Bubble departure diameters at subatmospheric pressures.* Paper presented at the Chemical Engineers Progress Symposium Series.

Collier, J. G., & Thome, J. R. (1994). *Convective boiling and condensation*: Oxford University Press.

Corcione, M. (2011). Empirical correlating equations for predicting the effective thermal conductivity and dynamic viscosity of nanofluids. *Energy Conversion and Management, 52*(1), 789-793.

Corcione, M., Cianfrini, M., & Quintino, A. (2012). Heat transfer of nanofluids in turbulent pipe flow. *International Journal of Thermal Sciences, 56*, 58-69.

Das, S. K., Choi, S. U. S., Yu, W., & Pradeep, T. (2008). *Nanofluids: science and technology*: Wiley-Interscience Hoboken, NJ.

Das, S. K., Putra, N., & Roetzel, W. (2003). Pool boiling characteristics of nano-fluids. *International Journal of Heat and Mass Transfer, 46*(5), 851-862.

Daungthongsuk, W., & Wongwises, S. (2007). A critical review of convective heat transfer of nanofluids. *Renewable and Sustainable Energy Reviews, 11*(5), 797-817.

Ding, Y., Alias, H., Wen, D., & Williams, R. A. (2006). Heat transfer of aqueous suspensions of carbon nanotubes (CNT nanofluids). *International Journal of Heat and Mass Transfer, 49*(1), 240-250.

Ding, Y., & Wen, D. (2005). Particle migration in a flow of nanoparticle suspensions. *Powder Technology, 149*(2), 84-92.

Drew, D. A., & Passman, S. L. (2006). *Theory of multicomponent fluids* (Vol. 135): Springer Science & Business Media.

Eastman, J. A., Phillpot, S., Choi, S., & Keblinski, P. (2004). Thermal transport in nanofluids 1. *Annu. Rev. Mater. Res., 34*, 219-246.

University of Malaya

Edel, Z. J., & Mukherjee, A. (2011). Experimental investigation of vapor bubble growth during flow boiling in a microchannel. *International Journal of Multiphase Flow, 37*(10), 1257-1265.

Einstein, A. (1956). *Investigations on the Theory of the Brownian Movement*: Courier Dover Publications.

Evans, W., Fish, J., & Keblinski, P. (2006). Role of Brownian motion hydrodynamics on nanofluid thermal conductivity. *Applied Physics Letters, 88*(9), 093116.

Fluent, A. (2009). 12.0 Theory Guide. *Ansys Inc, 5*.

Fritz, W. (1935). Maximum volume of vapor bubbles. *Phys. Z, 36*(11), 379-384.

Ganesan, P., Behroyan, I., He, S., Sivasankaran, S., & Sandaran, S. C. (2015). Turbulent forced convection of Cu–water nanofluid in a heated tube: Improvement of the two-phase model. *Numerical Heat Transfer, Part A: Applications*, 1-20.

Göktepe, S., Atalık, K., & Ertürk, H. (2014). Comparison of single and two-phase models for nanofluid convection at the entrance of a uniformly heated tube. *International Journal of Thermal Sciences, 80*, 83-92.

Haghshenas Fard, M., Esfahany, M. N., & Talaie, M. (2010). Numerical study of convective heat transfer of nanofluids in a circular tube two-phase model versus single-phase model. *International Communications in Heat and Mass Transfer, 37*(1), 91-97.

Hamilton, R., & Crosser, O. (1962). Thermal conductivity of heterogeneous two-component systems. *Industrial & Engineering chemistry fundamentals, 1*(3), 187-191.

Hanselman, D., & Littlefield, B. C. (1997). *Mastering MATLAB 5: A comprehensive tutorial and reference*: Prentice Hall PTR.

Hejazian, M., Moraveji, M. K., & Beheshti, A. (2014a). Comparative Numerical Investigation on TiO2/Water Nanofluid Turbulent Flow by Implementation of Single Phase and Two Phase Approaches. *Numerical Heat Transfer, Part A: Applications, 66*(3), 330-348.

Hejazian, M., Moraveji, M. K., & Beheshti, A. (2014b). Comparative study of Euler and mixture models for turbulent flow of Al_2O_3 nanofluid inside a horizontal tube. *International Communications in Heat and Mass Transfer*.

Heris, S. Z., Esfahany, M. N., & Etemad, G. (2007). Numerical investigation of nanofluid laminar convective heat transfer through a circular tube. *Numerical Heat Transfer, Part A: Applications, 52*(11), 1043-1058.

Hibiki, T., & Ishii, M. (2002). Development of one-group interfacial area transport equation in bubbly flow systems. *International Journal of Heat and Mass Transfer, 45*(11), 2351-2372.

Ishii, M. (1975). Thermo-fluid dynamic theory of two-phase flow. *NASA STI/Recon Technical Report A, 75*, 29657.

University of Malaya

Ishii, M., Kim, S., & Uhle, J. (2002). Interfacial area transport equation: model development and benchmark experiments. *International Journal of Heat and Mass Transfer, 45*(15), 3111-3123.

Ishii, M., & Zuber, N. (1979). Drag coefficient and relative velocity in bubbly, droplet or particulate flows. *AIChE Journal, 25*(5), 843-855.

Jang, S. P., & Choi, S. U. (2004). Role of Brownian motion in the enhanced thermal conductivity of nanofluids. *Applied Physics Letters, 84*(21), 4316-4318.

Jang, S. P., & Choi, S. U. (2007). Effects of various parameters on nanofluid thermal conductivity. *Journal of Heat Transfer, 129*(5), 617-623.

Kakaç, S., & Pramuanjaroenkij, A. (2009). Review of convective heat transfer enhancement with nanofluids. *International Journal of Heat and Mass Transfer, 52*(13), 3187-3196.

Kalteh, M., Abbassi, A., Saffar-Avval, M., Frijns, A., Darhuber, A., & Harting, J. (2012). Experimental and numerical investigation of nanofluid forced convection inside a wide microchannel heat sink. *Applied Thermal Engineering, 36*, 260-268.

Kalteh, M., Abbassi, A., Saffar-Avval, M., & Harting, J. (2011). Eulerian–Eulerian two-phase numerical simulation of nanofluid laminar forced convection in a microchannel. *International Journal of Heat and Fluid Flow, 32*(1), 107-116.

Kamyar, A., Saidur, R., & Hasanuzzaman, M. (2012). Application of computational fluid dynamics (CFD) for nanofluids. *International Journal of Heat and Mass Transfer, 55*(15), 4104-4115.

Kandlikar, S. G. (2003). *Heat transfer mechanisms during flow boiling in microchannels.* Paper presented at the ASME 2003 1st International Conference on Microchannels and Minichannels.

Kataoka, I., Okada, H., Yoshida, K., Naitoh, M., & Morii, T. (2012). *Transport of Interfacial Area Concentration in Two-Phase Flow*: INTECH Open Access Publisher.

Keblinski, P., Phillpot, S., Choi, S., & Eastman, J. (2002). Mechanisms of heat flow in suspensions of nano-sized particles (nanofluids). *International Journal of Heat and Mass Transfer, 45*(4), 855-863.

Keshavarz Moraveji, M., & Esmaeili, E. (2012). Comparison between single-phase and two-phases CFD modeling of laminar forced convection flow of nanofluids in a circular tube under constant heat flux. *International Communications in Heat and Mass Transfer, 39*(8), 1297-1302.

Kim, S., Bang, I. C., Buongiorno, J., & Hu, L. (2006). Effects of nanoparticle deposition on surface wettability influencing boiling heat transfer in nanofluids. *Applied Physics Letters, 89*(15), 153107.

Kim, S., Bang, I. C., Buongiorno, J., & Hu, L. (2007). Surface wettability change during pool boiling of nanofluids and its effect on critical heat flux. *International Journal of Heat and Mass Transfer, 50*(19), 4105-4116.

University of Malaya

Kim, S. J. (2007). *Pool boiling heat transfer characteristics of nanofluids.* Massachusetts Institute of Technology.

Kim, S. J., McKrell, T., Buongiorno, J., & Hu, L.-w. (2010). Subcooled flow boiling heat transfer of dilute alumina, zinc oxide, and diamond nanofluids at atmospheric pressure. *Nuclear Engineering and Design, 240*(5), 1186-1194.

Kocamustafaogullari, G., & Ishii, M. (1983). Interfacial area and nucleation site density in boiling systems. *International Journal of Heat and Mass Transfer, 26*(9), 1377-1387.

Končar, B., Kljenak, I., & Mavko, B. (2004). Modelling of local two-phase flow parameters in upward subcooled flow boiling at low pressure. *International Journal of Heat and Mass Transfer, 47*(6), 1499-1513.

Končar, B., Krepper, E., & Egorov, Y. (2005). *CFD modelling of subcooled flow boiling for nuclear engineering applications.* Paper presented at the International Conference "Nuclear Energy for New Europe" Bled, Slovenia.

Končar, B., & Mavko, B. (2003). Modelling of low-pressure subcooled flow boiling using the RELAP5 code. *Nuclear Engineering and Design, 220*(3), 255-273.

Koo, J., & Kleinstreuer, C. (2004). A new thermal conductivity model for nanofluids. *Journal of Nanoparticle Research, 6*(6), 577-588.

Koo, J., & Kleinstreuer, C. (2005). Laminar nanofluid flow in microheat-sinks. *International Journal of Heat and Mass Transfer, 48*(13), 2652-2661.

Krepper, E., Končar, B., & Egorov, Y. (2007). CFD modelling of subcooled boiling concept, validation and application to fuel assembly design. *Nuclear Engineering and Design, 237*(7), 716-731.

Krepper, E., & Rzehak, R. (2011). CFD for subcooled flow boiling: Simulation of DEBORA experiments. *Nuclear Engineering and Design, 241*(9), 3851-3866.

Kuipers, J., Prins, W., & Van Swaaij, W. (1992). Numerical calculation of wall-to-bed heat-transfer coefficients in gas-fluidized beds. *AIChE Journal, 38*(7), 1079-1091.

Kulkarni, D. P., Das, D. K., & Chukwu, G. A. (2006). Temperature dependent rheological property of copper oxide nanoparticles suspension (nanofluid). *Journal of nanoscience and nanotechnology, 6*(4), 1150-1154.

Kumar, P. M., Kumar, J., & Sendhilnathan, S. (2010). Theoretical model to determine the thermal conductivity of nanofluids. *International Journal of Engineering Science and Technology, 2*(7), 2846-2852.

Kurul, N., & Podowski, M. (1991). *On the modeling of multidimensional effects in boiling channels.* Paper presented at the ANS Proceeding of the 27th National Heat Transfer Conference.

Kurul, N., & Podowski, M. Z. (1990). *Multidimensional effects in forced convection subcooled boiling.* Paper presented at the Proceedings of the Ninth International Heat Transfer Conference.

University of Malaya

Kwark, S. M., Kumar, R., Moreno, G., Yoo, J., & You, S. M. (2010). Pool boiling characteristics of low concentration nanofluids. *International Journal of Heat and Mass Transfer, 53*(5), 972-981.

Lai, F. H., & Yang, Y.T. (2011). Lattice Boltzmann simulation of natural convection heat transfer of Al_2O_3/water nanofluids in a square enclosure. *International Journal of Thermal Sciences, 50*(10), 1930-1941.

Launder, B. E., & Spalding, D. (1974). The numerical computation of turbulent flows. *Computer methods in applied mechanics and engineering, 3*(2), 269-289.

Le Corre, J.-M., Yao, S.-C., & Amon, C. H. (2010). Two-phase flow regimes and mechanisms of critical heat flux under subcooled flow boiling conditions. Nuclear Engineering and Design, 240(2), 245-251.

Lemmert, M., & Chawla, J. (1977). Influence of flow velocity on surface boiling heat transfer coefficient. *Heat Transfer in Boiling, 237*, 247.

Leong, K., Yang, C., & Murshed, S. (2006). A model for the thermal conductivity of nanofluids–the effect of interfacial layer. *Journal of Nanoparticle Research, 8*(2), 245-254.

Li, C., Wang, B., & Peng, X. (2003). *Experimental investigations on boiling of nano-particle suspensions.* Paper presented at the 2003 Boiling heat transfer conference, Jamica, USA.

Li, C. H., & Peterson, G. P. (2007). Mixing effect on the enhancement of the effective thermal conductivity of nanoparticle suspensions (nanofluids). *International Journal of Heat and Mass Transfer, 50*(23–24), 4668-4677.2007.03.015

Li, C. H., Williams, W., Buongiorno, J., Hu, L.-W., & Peterson, G. (2008). Transient and steady-state experimental comparison study of effective thermal conductivity of Al_2O_3/water nanofluids. *Journal of Heat Transfer, 130*(4), 040301.040301-044503.040304.

Li, Q., & Xuan, Y. (2002). Convective heat transfer and flow characteristics of Cu-water nanofluid. *Science in China Series E: Technolgical Science, 45*(4), 408-416.

Li, Q., Xuan, Y., & Wang, J. (2003). Investigation on convective heat transfer and flow features of nanofluids. *Journal of Heat Transfer, 125*, 151-155.

Li, X., Li, K., Tu, J., & Buongiorno, J. (2014). On two-fluid modeling of nucleate boiling of dilute nanofluids. *International Journal of Heat and Mass Transfer, 69*, 443-450.

Liu, S., & Sakr, M. (2013). A comprehensive review on passive heat transfer enhancements in pipe exchangers. *Renewable and Sustainable Energy Reviews, 19*, 64-81.

Liu, Z.-H., Yang, X.-F., & Xiong, J.-G. (2010). Boiling characteristics of carbon nanotube suspensions under sub-atmospheric pressures. *International Journal of Thermal Sciences, 49*(7), 1156-1164.

University of Malaya

Lotfi, R., Saboohi, Y., & Rashidi, A. (2010). Numerical study of forced convective heat transfer of nanofluids: comparison of different approaches. *International Communications in Heat and Mass Transfer, 37*(1), 74-78.

Lun-Chun, L., & Zhen-Hua, L. (2008). Boiling characteristics in small vertical tubes with closed bottom for nanofluids and nanoparticle-suspensions. *Heat and Mass Transfer, 45*(1), 1-9.

Lundgren, T. S. (1972). Slow flow through stationary random beds and suspensions of spheres. *Journal of Fluid Mechanics, 51*(02), 273-299.

Maïga, S. E. B., Nguyen, C. T., Galanis, N., & Roy, G. (2004). Heat transfer behaviours of nanofluids in a uniformly heated tube. *Superlattices and Microstructures, 35*(3), 543-557.

Manninen, M., Taivassalo, V., & Kallio, S. (1996). On the mixture model for multiphase flow.

Masoumi, N., Sohrabi, N., & Behzadmehr, A. (2009). A new model for calculating the effective viscosity of nanofluids. *Journal of Physics D: Applied Physics, 42*(5), 055501.

Maxwell, J. C. (1881). *A treatise on electricity and magnetism* (Vol. 1): Clarendon press.

Miller, A., & Gidaspow, D. (1992). Dense, vertical gas-solid flow in a pipe. *AIChE Journal, 38*(11), 1801-1815.

Mirmasoumi, S., & Behzadmehr, A. (2008a). Effect of nanoparticles mean diameter on mixed convection heat transfer of a nanofluid in a horizontal tube. International Journal of Heat and Fluid Flow, 29(2), 557-566.

Mirmasoumi, S., & Behzadmehr, A. (2008b). Numerical study of laminar mixed convection of a nanofluid in a horizontal tube using two-phase mixture model. Applied Thermal Engineering, 28(7), 717-727.

Mirzaei, M., Saffar-Avval, M., & Naderan, H. (2014). Heat transfer investigation of laminar developing flow of nanofluids in a microchannel based on Eulerian–Lagrangian approach. *The Canadian Journal of Chemical Engineering, 92*(6), 1139-1149.

Moghari, R. (2011). Two phase mixed convection Al_2O_3-water nanofluid flow in an elliptical tube. *Int J. of Multiphase Flow, 3*, 585-595.

Mojarrad, M. S., Keshavarz, A., & Shokouhi, A. (2013). Nanofluids thermal behavior analysis using a new dispersion model along with single-phase. *Heat and Mass Transfer, 49*(9), 1333-1343.

Mokmeli, A., & Saffar-Avval, M. (2010). Prediction of nanofluid convective heat transfer using the dispersion model. *International Journal of Thermal Sciences, 49*(3), 471-478.

Mooney, M. (1951). The viscosity of a concentrated suspension of spherical particles. *Journal of Colloid Science, 6*(2), 162-170.

University of Malaya

Moraveji, M. K., & Ardehali, R. M. (2013). CFD modeling (comparing single and two-phase approaches) on thermal performance of Al_2O_3/water nanofluid in mini-channel heat sink. *International Communications in Heat and Mass Transfer, 44*, 157-164.

Moraveji, M. K., Darabi, M., Haddad, S. M. H., & Davarnejad, R. (2011). Modeling of convective heat transfer of a nanofluid in the developing region of tube flow with computational fluid dynamics. *International Communications in Heat and Mass Transfer, 38*(9), 1291-1295.

Moraveji, M. K., Haddad, S. M. H., & Darabi, M. (2012). Modeling of forced convective heat transfer of a non-Newtonian nanofluid in the horizontal tube under constant heat flux with computational fluid dynamics. *International Communications in Heat and Mass Transfer, 39*(7), 995-999.

Murshed, S., Leong, K., & Yang, C. (2008). Thermophysical and electrokinetic properties of nanofluids–a critical review. *Applied Thermal Engineering, 28*(17), 2109-2125.

Murshed, S., Leong, K., & Yang, C. (2009). A combined model for the effective thermal conductivity of nanofluids. *Applied Thermal Engineering, 29*(11), 2477-2483.

Namburu, P., Kulkarni, D., Dandekar, A., & Das, D. (2007). Experimental investigation of viscosity and specific heat of silicon dioxide nanofluids. *Micro & Nano Letters, IET, 2*(3), 67-71.

Namburu, P. K., Das, D. K., Tanguturi, K. M., & Vajjha, R. S. (2009). Numerical study of turbulent flow and heat transfer characteristics of nanofluids considering variable properties. *International Journal of Thermal Sciences, 48*(2), 290-302.

Namburu, P. K., Kulkarni, D. P., Misra, D., & Das, D. K. (2007). Viscosity of copper oxide nanoparticles dispersed in ethylene glycol and water mixture. *Experimental Thermal and Fluid Science, 32*(2), 397-402.

Niu, J., Fu, C., & Tan, W. (2012). Slip-flow and heat transfer of a non-Newtonian nanofluid in a microtube. *PLoS one, 7*(5), e37274.

Nuim Labib, M., Nine, M. J., Afrianto, H., Chung, H., & Jeong, H. (2013). Numerical investigation on effect of base fluids and hybrid nanofluid in forced convective heat transfer. *International Journal of Thermal Sciences, 71*, 163-171.

Özerinç, S., Kakaç, S., & Yazıcıoğlu, A. G. (2010). Enhanced thermal conductivity of nanofluids: a state-of-the-art review. *Microfluidics and Nanofluidics, 8*(2), 145-170.

Pak, B. C., & Cho, Y. I. (1998). Hydrodynamic and heat transfer study of dispersed fluids with submicron metallic oxide particles. *Experimental Heat Transfer An International Journal, 11*(2), 151-170.

Palm, S. J., Roy, G., & Nguyen, C. T. (2006). Heat transfer enhancement with the use of nanofluids in radial flow cooling systems considering temperature-dependent properties. *Applied Thermal Engineering, 26*(17), 2209-2218.

University of Malaya

Patel, H. E., Anoop, K., Sundararajan, T., & Das, S. K. (2006). *A micro-convection model for thermal conductivity of nanofluids.* Paper presented at the International Heat Transfer Conference 13.

Prakash, M., & Giannelis, E. (2007). Mechanism of heat transport in nanofluids. *Journal of computer-aided materials design, 14*(1), 109-117.

Prasher, R., Bhattacharya, P., & Phelan, P. E. (2006). Brownian-motion-based convective-conductive model for the effective thermal conductivity of nanofluids. *Journal of Heat Transfer, 128*(6), 588-595.

Putra, N., Roetzel, W., & Das, S. K. (2003). Natural convection of nano-fluids. *Heat and Mass Transfer, 39*(8-9), 775-784.

Qu, W., & Mudawar, I. (2003). Flow boiling heat transfer in two-phase micro-channel heat sinks—I. Experimental investigation and assessment of correlation methods. *International Journal of Heat and Mass Transfer, 46*(15), 2755-2771.

Ranz, W., & Marshall, W. (1952). Evaporation from drops. *Chem. Eng. Prog, 48*(3), 141-146.

Rashidi, F., & Nezamabad, N. M. (2011). *Experimental investigation of convective heat transfer coefficient of CNTs nanofluid under constant heat flux.* Paper presented at the Proceedings of the World Congress on Engineering.

Roy, G., Nguyen, C. T., & Lajoie, P.-R. (2004). Numerical investigation of laminar flow and heat transfer in a radial flow cooling system with the use of nanofluids. *Superlattices and Microstructures, 35*(3), 497-511.

Rzehak, R., & Krepper, E. (2013). CFD for subcooled flow boiling: Parametric variations. *Science and Technology of Nuclear Installations, 2013*.

Saberi, M., Kalbasi, M., & Alipourzade, A. (2013). Numerical study of forced convective heat transfer of nanofluids inside a vertical tube. *Int. J. of Thermal Technologies, 3*(1), 10-15.

Salman, B., Mohammed, H., & Kherbeet, A. (2014). Numerical Study of Three Different Approaches to Simulate Nanofluids Flow and Heat Transfer in a Microtube. *Heat Transfer—Asian Research*.

Santra, A. K., Sen, S., & Chakraborty, N. (2008). Study of heat transfer augmentation in a differentially heated square cavity using copper–water nanofluid. *International Journal of Thermal Sciences, 47*(9), 1113-1122.

Santra, A. K., Sen, S., & Chakraborty, N. (2009). Study of heat transfer due to laminar flow of copper–water nanofluid through two isothermally heated parallel plates. *International Journal of Thermal Sciences, 48*(2), 391-400.

Sarafraz, M., & Hormozi, F. (2014). Scale formation and subcooled flow boiling heat transfer of CuO–water nanofluid inside the vertical annulus. *Experimental Thermal and Fluid Science, 52*, 205-214.

University of Malaya

Sarafraz, M., Hormozi, F., & Kamalgharibi, M. (2014). Sedimentation and convective boiling heat transfer of CuO-water/ethylene glycol nanofluids. *Heat and Mass Transfer, 50*(9), 1237-1249.

Sarafraz, M. M., & Hormozi, F. (2013). Forced Convective and Nucleate Flow Boiling Heat Transfer to Alumnia Nanofluids. *Periodica Polytechnica Chemical Engineering, 58*(1), 37-46.

Sato, Y., Sadatomi, M., & Sekoguchi, K. (1981). Momentum and heat transfer in two-phase bubble flow—I. Theory. *International Journal of Multiphase Flow, 7*(2), 167-177.

Schiller, L., & Naumann, A. (1935). A drag coefficient correlation. *Vdi Zeitung, 77*, 318-320.

Setoodeh, H., Keshavarz, A., Ghasemian, A., & Nasouhi, A. (2015). Subcooled flow boiling of alumina/water nanofluid in a channel with a hot spot: An experimental study. *Applied Thermal Engineering, 90*, 384-394.

Shah, M. (1979). A general correlation for heat transfer during film condensation inside pipes. *International Journal of Heat and Mass Transfer, 22*(4), 547-556.

Shahriar, A., Amin, B., & Seyed, S. Conjugate heat transfer of laminar mixed convection of a nanofluid through an inclined tube with circumferentially non-uniform heating. *Nanoscale research letters, 6*.

Siddique, M., Khaled, A.-R., Abdulhafiz, N., & Boukhary, A. (2010). Recent advances in heat transfer enhancements: a review report. *International Journal of Chemical Engineering, 2010*.

Suriyawong, A., & Wongwises, S. (2010). Nucleate pool boiling heat transfer characteristics of TiO_2–water nanofluids at very low concentrations. *Experimental Thermal and Fluid Science, 34*(8), 992-999.

Tavman, I., Turgut, A., Chirtoc, M., Schuchmann, H., & Tavman, S. (2008). Experimental investigation of viscosity and thermal conductivity of suspensions containing nanosized ceramic particles. *Archives of Materials Science, 100*, 100.

Tolubinsky, V., & Kostanchuk, D. (1970). *Vapour bubbles growth rate and heat transfer intensity at subcooled water boiling.* Paper presented at the Proceedings of the 4th international heat transfer conference.

Tomiyama, A. (1998). Struggle with computational bubble dynamics. *Multiphase Science and Technology, 10*(4), 369-405.

Trisaksri, V., & Wongwises, S. (2007). Critical review of heat transfer characteristics of nanofluids. *Renewable and Sustainable Energy Reviews, 11*(3), 512-523.

Troshko, A., & Hassan, Y. (2001). A two-equation turbulence model of turbulent bubbly flows. *International Journal of Multiphase Flow, 27*(11), 1965-2000.

Tu, J., Dinh, N., & Theofanous, T. (2004). *An experimental study of nanofluid boiling heat transfer.* Paper presented at the Proceedings of 6th international symposium on heat transfer, Beijing, China.

University of Malaya

Tu, J., & Yeoh, G. (2002). On numerical modelling of low-pressure subcooled boiling flows. *International Journal of Heat and Mass Transfer, 45*(6), 1197-1209.

Turgut, A., Tavman, I., Chirtoc, M., Schuchmann, H., Sauter, C., & Tavman, S. (2009). Thermal conductivity and viscosity measurements of water-based TiO2 nanofluids. *International Journal of Thermophysics, 30*(4), 1213-1226.

Ünal, H. (1976). Maximum bubble diameter, maximum bubble-growth time and bubble-growth rate during the subcooled nucleate flow boiling of water up to 17.7 MN/m 2. *International Journal of Heat and Mass Transfer, 19*(6), 643-649.

Vafaei, S., & Borca-Tasciuc, T. (2014). Role of nanoparticles on nanofluid boiling phenomenon: Nanoparticle deposition. *Chemical Engineering Research and Design, 92*(5), 842-856.

Vanaki, S. M., Ganesan, P., & Mohammed, H. (2016). Numerical study of convective heat transfer of nanofluids: A review. Renewable and Sustainable Energy Reviews, 54, 1212-1239.

Vassallo, P., Kumar, R., & D'Amico, S. (2004). Pool boiling heat transfer experiments in silica–water nano-fluids. *International Journal of Heat and Mass Transfer, 47*(2), 407-411.

Velagapudi, V., Konijeti, K. R., & Aduru, K. S. C. (2008). Empirical correlations to predict thermophysical and heat transfer characteristics of nanofluids. *Thermal Science, 12*(2), 27-37.

Wang, X., Xu, X., & S. Choi, S. U. (1999). Thermal conductivity of nanoparticle-fluid mixture. *Journal of thermophysics and heat transfer, 13*(4), 474-480.

Wen, D., & Ding, Y. (2004). Experimental investigation into convective heat transfer of nanofluids at the entrance region under laminar flow conditions. *International Journal of Heat and Mass Transfer, 47*(24), 5181-5188.

Wen, D., & Ding, Y. (2005). Experimental investigation into the pool boiling heat transfer of aqueous based γ-alumina nanofluids. *Journal of Nanoparticle Research, 7*(2-3), 265-274.

Xie, H., Fujii, M., & Zhang, X. (2005). Effect of interfacial nanolayer on the effective thermal conductivity of nanoparticle-fluid mixture. *International Journal of Heat and Mass Transfer, 48*(14), 2926-2932.

Xuan, Y., & Li, Q. (2000). Heat transfer enhancement of nanofluids. *International Journal of Heat and Fluid Flow, 21*(1), 58-64.

Xuan, Y., & Li, Q. (2003). Investigation on convective heat transfer and flow features of nanofluids. *Journal of Heat transfer, 125*(1), 151-155.

Xuan, Y., & Roetzel, W. (2000). Conceptions for heat transfer correlation of nanofluids. *International Journal of Heat and Mass Transfer, 43*(19), 3701-3707.

Xue, Q.-Z. (2003). Model for effective thermal conductivity of nanofluids. *Physics letters A, 307*(5), 313-317.

University of Malaya

Yang, Y., Zhang, Z. G., Grulke, E. A., Anderson, W. B., & Wu, G. (2005). Heat transfer properties of nanoparticle-in-fluid dispersions (nanofluids) in laminar flow. *International Journal of Heat and Mass Transfer, 48*(6), 1107-1116.

Yao, W., & Morel, C. (2004). Volumetric interfacial area prediction in upward bubbly two-phase flow. *International Journal of Heat and Mass Transfer, 47*(2), 307-328.

Yarmand, H., Ahmadi, G., Gharehkhani, S., Kazi, S. N., Safaei, M. R., Alehashem, M. S., & Mahat, A. B. (2014). Entropy Generation during Turbulent Flow of Zirconia-water and Other Nanofluids in a Square Cross Section Tube with a Constant Heat Flux. *Entropy, 16*(11), 6116-6132.

Yarmand, H., Gharehkhani, S., Kazi, S. N., Sadeghinezhad, E., & Safaei, M. R. (2014). Numerical investigation of heat transfer enhancement in a rectangular heated pipe for turbulent nanofluid. *The Scientific World Journal, 2014*.

Yeoh, G., Vahaji, S., Cheung, S., & Tu, J. (2014). Modeling subcooled flow boiling in vertical channels at low pressures–Part 2: Evaluation of mechanistic approach. *International Journal of Heat and Mass Transfer, 75*, 754-768.

You, S., Kim, J., & Kim, K. (2003). Effect of nanoparticles on critical heat flux of water in pool boiling heat transfer. *Applied Physics Letters, 83*(16), 3374-3376.

Yu, W., & Choi, S. (2003). The role of interfacial layers in the enhanced thermal conductivity of nanofluids: a renovated Maxwell model. *Journal of Nanoparticle Research, 5*(1-2), 167-171.

Zeinali Heris, S., Etemad, S. G., & Nasr Esfahany, M. (2006). Experimental investigation of oxide nanofluids laminar flow convective heat transfer. *International Communications in Heat and Mass Transfer, 33*(4), 529-535.

Zeitoun, O., & Shoukri, M. (1996). Bubble behavior and mean diameter in subcooled flow boiling. *Journal of Heat Transfer, 118*(1), 110-116.

Zhu, D., & Wang, X. (2009). Experimental investigation on viscosity of Cu-H_2O nanofluids. *Journal of Wuhan University of Technology-Mater. Sci. Ed., 24*(1), 48-52.

Zhuan, R., & Wang, W. (2012). Flow pattern of boiling in micro-channel by numerical simulation. *International Journal of Heat and Mass Transfer, 55*(5), 1741-1753.

Zou, L. (2011). *Experimental study on subcooled flow boiling on heating surfaces with different thermal conductivities.* University of Illinois at Urbana-Champaign.

Zu, Y., Yan, Y., Gedupudi, S., Karayiannis, T., & Kenning, D. (2011). Confined bubble growth during flow boiling in a mini-/micro-channel of rectangular cross-section part II: Approximate 3-D numerical simulation. *International Journal of Thermal Sciences, 50*(3), 267-273.

University of Malaya

LIST OF PUBLICATIONS

Published paper:

- I. Behroyan, P. Ganesan, S. He, S. Sivasankaran, Turbulent forced convection of Cu–water nanofluid: CFD model comparison, International Communications in Heat and Mass Transfer, 2015. 67: p. 163-172.
- Ganesan P, Behroyan I, He S, Sivasankaran S, Sandaran SC. Turbulent forced convection of Cu–water nanofluid in a heated tube: Improvement of the two-phase model. Numerical Heat Transfer, Part A: Applications. 2015 Nov 19: p.1-20.
- I. Behroyan, Sh M. Vanaki, P. Ganesan, and R. Saidur. A comprehensive comparison of various CFD models for convective heat transfer of Al_2O_3 nanofluid inside a heated tube, International Communications in Heat and Mass Transfer, 2016. 70: p. 27-37.

Under review papers

- I. Behroyan, P. Ganesan, "Modelling of subcooled flow boiling heat transfer of Al_2O_3-water and Cu-water nanofluids through a vertical heated pipe", International Communications in Heat and Mass Transfer. (ISI-Cited).

Conference proceedings

- I. Behroyan, P. Ganesan, "Modelling of subcooled flow boiling heat transfer of water through a vertical heated pipe", 16th International Conference on Applied Physics and Mathematics (ICAPM) 2016, held at Kuala Lumpur, Malaysia on January 10, 2016,

University of Malaya

APPENDIX

List of UDF codes

The list of UDF codes using in this study is given as follows:

1. UDF codes for conductivity:
    a. Chon et al. (Chon et al., 2005) model (Equations (2.5)-(2.6))
    b. Patel et al. (Patel et al., 2006) model (Equations (2.7)-(2.8))
    c. Dispersion model 1 (Equation (3.22))
    d. Dispersion model 2 (Equation (3.23))
2. UDF codes for viscosity:
    a. Masoumi et al.(Masoumi et al., 2009) model (Equations (2.18)-(2.21))
    b. Chon et al. (Chon et al., 2005) model plus Pak and Cho (Pak & Cho, 1998) model (Equations (3.11)-(3.12))
3. UDF codes for non-Newtonian rheology (Equations (3.13)-(3.17))
4. UDF codes for nucleate site density:
    a. Lemmert and Chawla (Lemmert & Chawla, 1977) model (Equation (5.38))
    b. Kocamustafaogullari and Ishii (Kocamustafaogullari & Ishii, 1983) model (Equation (5.39))
    c. Li et al. (X. Li et al., 2014) model (Equation (5.36))
5. UDF codes for bubble departure diameter:
    a. Fritz (Fritz, 1935) model (Equation (5.42))
    b. Cole and Shulman (Cole & Shulman, 1966) model (Equation (5.43))

University of Malaya

c. Cole and Rohsenow (Cole & Rohsenow, 1969) model (Equation (5.44))

d. Li et al. (X. Li et al., 2014) model (Equation (5.37))

University of Malaya

University of Malaya